

博士論文

**Self-Assembly of Propeller-Shaped  
Triphenylamine Derivatives**

(プロペラ構造を有する

トリフェニルアミンの自己組織化)

金 泰 勳



## **Table of Contents**



## **Chapter 1**

<b>General introduction .....</b>	<b>5</b>
<b>1.1 Molecular structure and associated property in self-assembly .....</b>	<b>7</b>
<b>1.2 Triphenylamine and its self-assembly .....</b>	<b>13</b>
<b>1.3 Objective .....</b>	<b>17</b>
<b>1.4 References .....</b>	<b>19</b>

## **Chapter 2**

### **Design and synthesis of propeller-shaped triphenylamine (TPA)**

<b>derivatives .....</b>	<b>25</b>
<b>2.1 Design and synthesis of propeller-shaped TPA derivatives .....</b>	<b>27</b>
<b>2.2 Experimental Section .....</b>	<b>30</b>
2.2.1 Materials .....	30
2.2.2 Methods .....	30
2.2.3 Synthesis .....	31
<b>2.3 References .....</b>	<b>61</b>

## **Chapter 3**

### **Amplification of supramolecular chirality in a self-assembly of**

<b>propeller-shaped TPA derivatives .....</b>	<b>63</b>
<b>3.1 Introduction .....</b>	<b>65</b>
<b>3.2 Propeller conformation of TPA in supramolecular helices .....</b>	<b>68</b>
<b>3.3 High amplification of supramolecular chirality .....</b>	<b>73</b>
<b>3.4 Effect of the position of side chain in chiral amplification .....</b>	<b>78</b>
<b>3.5 Hierarchy of propeller-shaped chiral sergeants .....</b>	<b>80</b>
<b>3.6 Conclusion .....</b>	<b>82</b>
<b>3.7 Experimental Section .....</b>	<b>83</b>
3.7.1 Quantification of sergeants and soldiers data .....	83
3.7.2 Supplementary figures for chiral amplification .....	84
<b>3.8 References .....</b>	<b>88</b>

## **Chapter 4**

<b>Self-assembly behavior of propeller-shaped TPA derivatives in diluted solution .....</b>	<b>91</b>
<b>4.1 Introduction .....</b>	<b>93</b>
<b>4.2 Effect of the length of alkyl chains.....</b>	<b>94</b>
<b>4.3 Effect of the position of long alkyl chains .....</b>	<b>99</b>
<b>4.4 Effect of the position of chiral chains .....</b>	<b>102</b>
<b>4.5 Conclusion.....</b>	<b>104</b>
<b>4.6 Experimental section.....</b>	<b>105</b>
<b>4.7 References .....</b>	<b>107</b>

## **Chapter 5**

<b>LC assembly of propeller-shaped TPA derivatives .....</b>	<b>109</b>
<b>5.1 Introduction .....</b>	<b>111</b>
<b>5.2 Hexagonal columnar assembly in LC mesophase .....</b>	<b>114</b>
<b>5.3 Thermal behavior in LC mesophase.....</b>	<b>118</b>
<b>5.4 Homeotropic alignment of TPA derivatives in LC mesophase .....</b>	<b>121</b>
<b>5.5 Conclusion.....</b>	<b>123</b>
<b>5.6 Experimental section.....</b>	<b>124</b>
5.6.1 Differential scanning calorimetry (DSC) Analysis .....	124
5.6.2 X-ray diffraction (XRD) analysis.....	128
5.6.3 Polarized optical microscopy (POM) analysis .....	130
<b>5.7 References .....</b>	<b>131</b>

## **Chapter 6**

<b>Summary and perspective .....</b>	<b>135</b>
<b>6.1 Summary and perspective .....</b>	<b>137</b>
<b>6.2 References .....</b>	<b>141</b>
<b>Curriculum Vitae .....</b>	<b>145</b>
<b>Acknowledgements .....</b>	<b>147</b>

# **Chapter 1**

## **General Introduction**





## 1.1 Molecular structure and associated property in self-assembly

Over the past few decades, the development of supramolecular self-assembly has played a role in creating new organic materials and devices with enhanced properties.<sup>1-7</sup> First, we could construct various kinds of supramolecular nanostructures such as capsules,<sup>8-12</sup> tubules<sup>13-23</sup> and porous networks<sup>24-31</sup> with well-defined shape and size. Because molecular self-assembly emerges as a result of the connection of small building blocks through non-covalent linkages such as hydrogen bonding, electrostatic interaction, or  $\pi$ - $\pi$  interaction, it is allowed that these self-assembled object formed ordered structures upon a spontaneous organization between monomers and aggregates by designing appropriate organic building blocks.<sup>32-34</sup> It means that the assembled structures reflect the feature of small building blocks such as molecular geometry, dipole moment, charge and so on. Therefore it is required to explore the fundamental and deep understanding about the molecular structure and their correlated feature at the molecular level. On the other hand, by the dynamic nature of non-covalent interaction, the reversible transition of monomer-to-polymer provides great capacity for adaptability, processability, self-healing and responsiveness toward chemical or physical stimuli.<sup>1-5, 35-37</sup> This spatial and temporal controllability has attracted from material scientists in order to create novel organic materials and devices, which have more sophisticated orientations and properties.

To utilize their electronic property with strong molecular stacking, many supramolecular nanostructures have been developed on the basis of various planar  $\pi$ -conjugated aromatics such as hexabenzocoronene (HBC), perylene bisimide (PBI) and oligothiophene. By appending suitable peripheral units for solubilizing, those aromatic

molecules form one-dimensional (1D) and two-dimensional (2D) nanostructures with improved properties for optoelectronics. For example, an amphiphilic HBC, substituted by phenyl oligoether and linear alkyl chains, uniformly formed graphite-like supramolecular nanotubes in tens to hundreds of micrometers scale and displays an electrical conductivity across a 180 nm-gap electrode after oxidization (Figure 1.1a).<sup>17</sup> In addition, the oligoether termini of an amphiphilic HBC can be substituted with functional groups such as chemically reactive groups, metal-binding functions, and chromophores.<sup>38-43</sup> This could be allowed to give a variation in the surface of graphite-like nanotube and to open another optoelectronic functionality. On the other hand, a rectangular shaped-PBI self-assembled into nanofiber in solution and exhibited outstanding fluorescence and charge transport properties.<sup>44-48</sup> Interestingly, the molecular stacking of PBI could be manipulated from H type to J type  $\pi$ - $\pi$  stacking by steric hindrances in the peripheral side chains (Figure 1.1b).<sup>49</sup> And a linear oligothiophene has a rod-like shape and easily produces 2D assembly that can be utilized for p-type semiconductor (Figure 1.1c).<sup>50-51</sup> Also, their photovoltaic properties can be tuned by changing the length of the oligothiophene segment.<sup>52-53</sup> Those examples above reveal that the investigation of relationship between molecular structure and associated properties is crucial for the development of organic nanomaterials.

However, the development of supramolecular self-assembly has been mostly focused on the assembly of planar and disk-shaped  $\pi$ -conjugated aromatic segments. On the other hand, non-planar  $\pi$ -conjugated aromatics were rarely utilized in supramolecular polymers, while they displayed unique properties and functions derived from their characteristic structures. For example, low symmetric order of non-planar

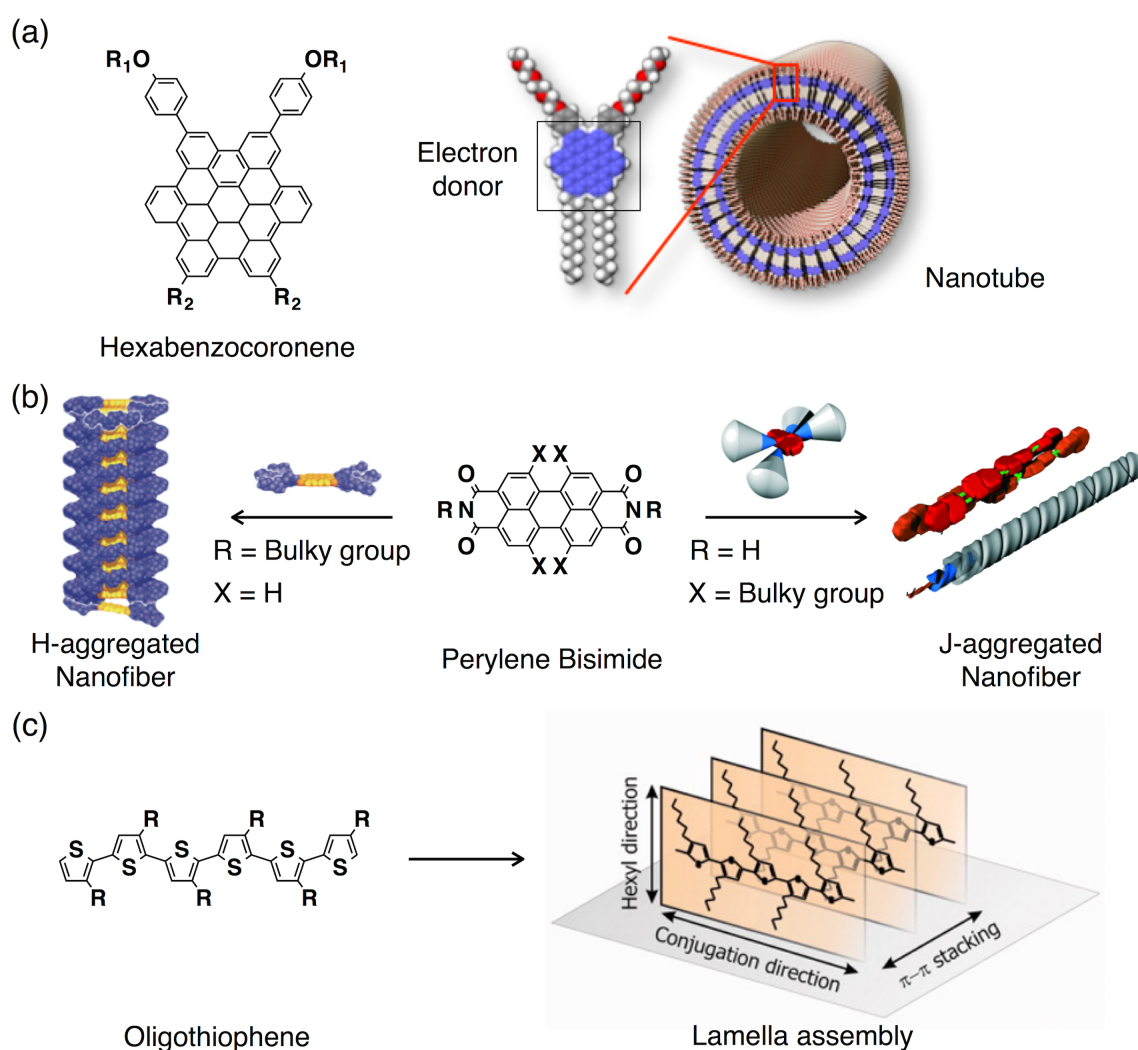


**Figure 1.1.** Schematic representation of three monomers and the corresponding supramolecular polymers. (a) An amphiphilic hexabenzocoronene substituted by phenyl triethylene glycol monomethyl ether and dodecyl chains formed a nanotube with a wall thickness defined by the dimension of monomeric units. (b) A rectangular shaped-peryene disimide assembled into H-type or J-type aggregates derived from molecular structure modification. (c) A rod-like oligothiophene constructed 2D lamella sheet that can be utilized for organic semiconductor.

molecules endows their assemblies with unique features such as macroscopic polarization and supramolecular chirality. Miyajima and Aida et al. reported the supramolecular assemblies of ball-shaped corannulene, which displayed hexagonal columnar alignment in response to an applied electric field in liquid crystal state while those of planar  $\pi$ -conjugated analogues were hardly responsive (Figure 1.2a).<sup>54</sup> More particularly, they found the metastable monomers of concave corannulene anchoring amide-appended thioalkyl side chains, which allowed the implementation of chain-growth supramolecular polymerization in diluted solution (Figure 1.2b).<sup>55,56</sup>

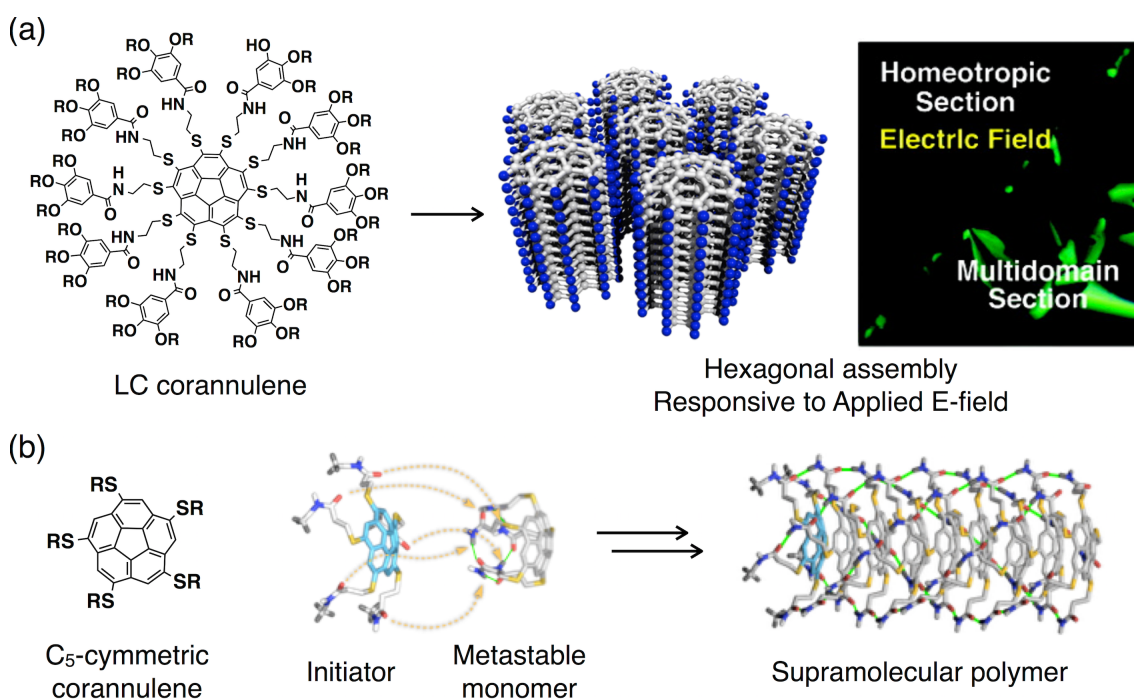


**Figure 1.2.** Schematic representation of self-assemblies of ball-shaped corannulene. (a) A liquid crystal corannulene formed hexagonal columnar assembly, which responded to applied electric field. (b) Schematic representation of the chain-growth supramolecular polymerization of  $C_5$ -symmetric corannulene. The growing polymer carries an initiator at one end (the initiating end), whereas the other end [the growing (active) end] adopts an analogous structure as initiator with free amide C=O groups.

Propeller-shaped molecules also have unique properties such as aggregation induced emission (AIE) and intrinsically helical conformation.<sup>57-59</sup> In general, the planar-shaped fluorophores such as pyrene possibly stack up as sandwich due to strong  $\pi$ - $\pi$  stacking interactions, which commonly induced fluorescent quenching with the increment of concentration in solution.<sup>60-61</sup> This phenomenon has been realized for many aromatic compounds and caused poor sensitivity in fluorescence sensory systems.<sup>62-64</sup> In contrast, non-planar and propeller-shaped dyes such as hexaphenylsilole (HPS) emit their fluorescent emissions with aggregate formation, due to the restricted intramolecular rotation (Figure 1.3a).<sup>65-66</sup> On the other hand, propeller-shaped molecules have also attracted attention as the origin of helicity in supramolecular system. For example, hexaphenylbenzene can adopt propeller conformation in a crystal phase and exhibit a chirality sensing through supramolecular chirality transfer (Figure 1.3b).<sup>67</sup> More particularly, Meijer and coworker found firstly the amplification of supramolecular chirality with  $C_3$ -symmetrical molecules (Figure 1.3c).<sup>68,69</sup> In assembled state, the molecules expect to adopt a propeller-like conformation with intermolecular hydrogen bonding among amide groups. However, the molecules can adopt a variety of conformations other than a propeller structure, which is hard to be convinced in diluted solution. Hence, it is still unclear the effect of propeller conformation in the assembly and is desirable to explore the self-assembly of propeller-shaped molecules.

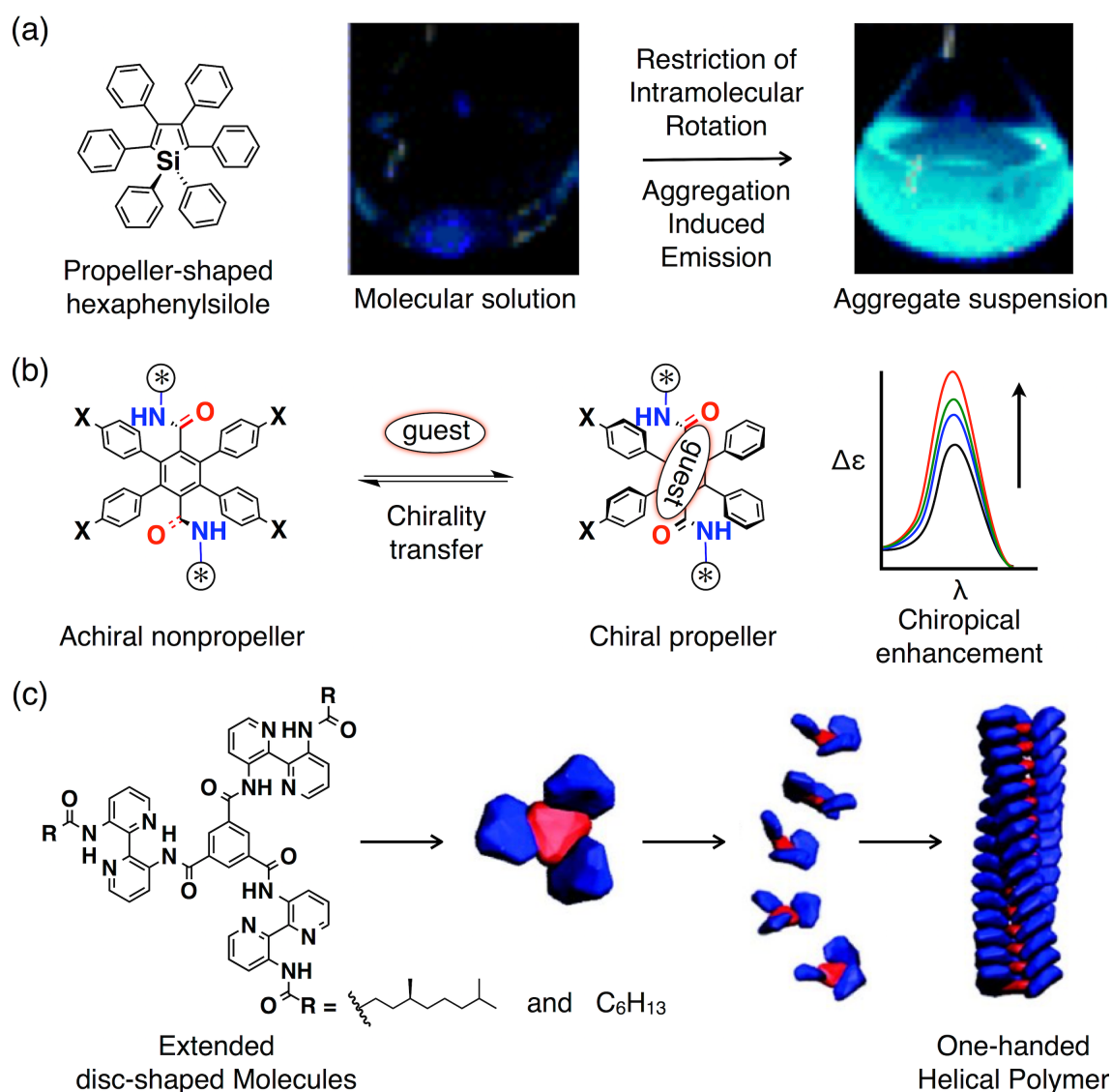


**Figure 1.3.** Schematic representations of the self-assemblies of propeller-shaped molecules. (a) Nonplanar propeller-shaped hexaphenylsilole emit their light emissions due to the restricted intramolecular rotation in the aggregates. (b) An terephthalamide host induces strong CD signaling upon complexation with chiral ditopic guests, which derived from conformational change from a nonpropeller structure to a propeller conformation of hexaphenylbenzene. (c) An extended disc-shaped molecule formed 1D helical supramolecular polymer and exhibits amplification of supramolecular chirality with 10 mol% of chiral analogues.

## 1.2 Triphenylamine and its self-assembly

Triphenylamine (TPA) is one of a well known non-planar  $\pi$ -conjugated aromatic molecules that has three-bladed propeller structure and the benzene blades make conrotatory angles of  $\sim 44^\circ$  with respect to the plane of central NCCC atoms in a crystal phase.<sup>70-73</sup> Based on the propeller structure, TPA is expected to give an intrigued motif for the control of molecular orientation and supramolecular chirality. In contrast to other propeller molecules such as hexaphenylbenzene, TPA have intrinsically propeller conformation even in monomer state (Figure 1.4a).<sup>88</sup> It indicates that TPA can contribute to the origin of chirality in molecular and supramolecular system.

TPA is also famous for a hole transporting ability with its easy oxidizability. TPA cation radical was formed by simple anodic oxidation of TPA and stabilized with para-substitution to electron donating group (figure 1.4b). Because TPA shows good glass-forming property, low ionization energy and reversible redox potential,<sup>74-78</sup> TPA-based organic materials have been studied for various kinds of electronic devices

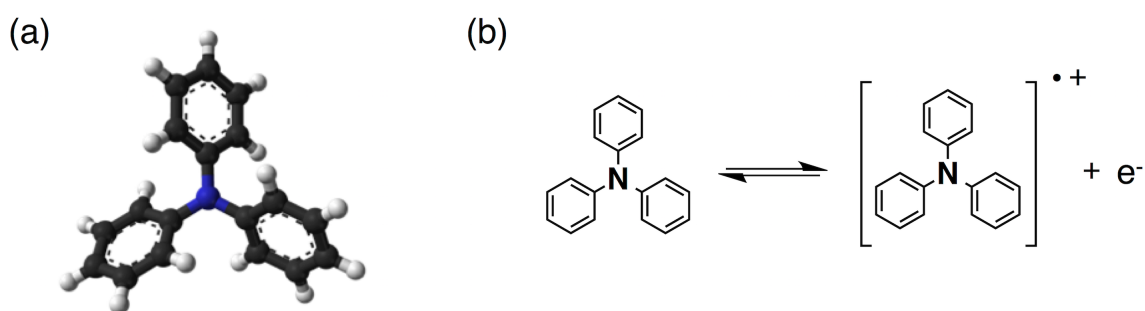


**Figure 1.4.** (a) Ball-and-stick model of the triphenylamine molecule,  $\text{NPh}_3$ . Single crystal X-ray diffraction data from Ref. 70. (b) Formation of a radical cation of triphenylamine.

including organic light-emitting diodes (OLEDs),<sup>77</sup> organic photovoltaic cells (OPVs)<sup>78,79</sup> and organic field-effect transistors (OFETs)<sup>80</sup> at small molecular and macromolecular levels. And it is well known that the addition of TPA into photoconductive materials improve imaging properties of the Xerox laser printers.<sup>81</sup> Although TPA has considered one of most promising material in the field of organic electronics, its derivatives and their correlated properties have been mainly studied in solid state. To achieve high processability and device performance, it is indispensable to investigate the properties of TPA either in liquid crystalline (LC) state or in solution. However, the self-assemblies of TPA and their correlated properties have been rarely studied.

After the development of first TPA-based liquid crystal, their thermodynamic behavior and optoelectronic properties was investigated in LC mesophase (Figure 1.5a).<sup>82-85</sup> However, it is hard to find a potential for good hole transporting materials, because the imine linkage in the mesogenic TPA derivatives can be susceptible to acid during the cyclic voltammetry and hence the poor chemical stability of the radical ions in dichloromethane solution.<sup>83</sup>

Recently, Giuseppone and coworker reported the self-assembly of TPA derivatives triggered by catalytic amounts of triarylammonium radicals, which stack with their neutral analogues (Figure 1.5b).<sup>86,87</sup> As a result, the supramolecular nanowire formed in chlorinated solvent under the simultaneous action of light. Surprisingly, the resultant organic nanowire exhibits a large conductivity value ( $\sim 5 \times 10^3 \text{ S m}^{-1}$ ) and a low interface resistance ( $\sim 2 \times 10^{-4} \text{ } \Omega \text{ m}$ ) between two metallic electrodes. Although the nanowire was too short to use a practical application, it is noteworthy that the easy solution process are shown to enable the molecular organization in pre-determined



positions by means of a bottom-up approach, making possible the addressed control of nanoscale organic devices.

As described above, TPA has good properties for organic electronics as well as unique structural feature for chirality generation. Although the self-assembly of TPA have already studied for molecular organization with structural analysis and optoelectronic properties, the effect of propeller conformation was rarely discussed what should be noticed and how to utilize it. Hence, it is desirable to explore the propeller conformation of TPA in supramolecular assembly and its associated properties.

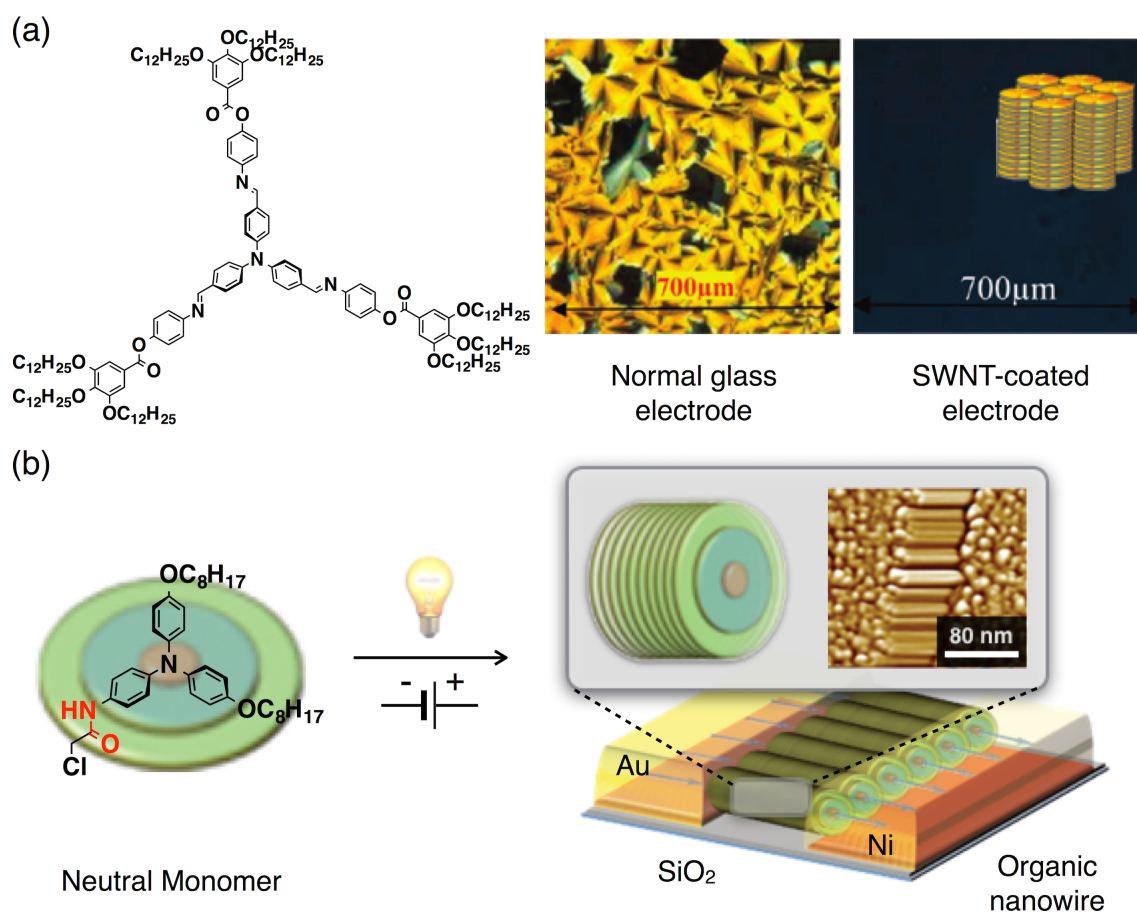


**Figure 1.5.** (a) A homeotropic alignment of TPA-based discotic liquid crystal based on nanostructured substrates of single-walled carbon nanotubes (SWNTs). (b) The self-assembly of supramolecular organic nanowires between two metallic electrodes, from a solution of triarylamine derivative.

### 1.3 Objective

By the mean of theoretical and experimental studies, TPA was found to exhibit a propeller structure with nearly planar central NCCC segments in solid state<sup>70-73</sup> as well as in the gas phase.<sup>88</sup> The propeller conformation of TPA is intrinsically chiral and is able to show either left- or right-handedness with their conformational flexibility. Both of left- and right-handed propeller chirality has thermodynamically same stability and an interconversion between both of two chirality can occurs in monomeric state.<sup>89</sup> If TPA formed one-dimensional helical assembly supramolecularly, however, the propeller conformation can be fixed and exhibit one of two propeller chirality, which is determined by the handedness of the resulting helices. Furthermore, it is well known that one-handed supramolecular helices could be selectively isolated by the employment of chiral auxiliaries at molecular and supramolecular levels. It indicates that the propeller conformation of TPA also selectively adopted one-handed chirality in one-handed supramolecular helix. Hence, the dynamic propeller chirality of TPA can be considered to be another intrigued motif for generating supramolecular chirality. More particularly, the fixed propeller chirality of TPA in a supramolecular helix can direct a propeller chirality of TPA monomers during elongation process in supramolecular polymerization, which is expected to result in high amplification of supramolecular chirality. Although various supramolecular helices has used for chiral amplification, it is desirable to find a new molecular motif and challenge the limit. In the current thesis, I demonstrate that the unprecedentedly high amplification of supramolecular chirality was realized by using propeller-shaped TPA derivatives. To further elucidate the effect of propeller conformation on the process of self-assembly and chiral amplification, their self-assembly behavior was systemically investigated by tuning peripheral side

group, which varied the critical temperature for supramolecular self-assembly in diluted solution and in LC mesophase. The key for these achievements is the dynamic propeller chirality of TPA, providing fresh insights on supramolecular assemblies together with chiral amplification of supramolecular helices.

## 1.4 References

- (1) Palmer, L.C.; Stupp, S.I. *Acc. Chem. Res.* **2008**, *41*, 1674–1684.
- (2) Aida, T.; Meijer, E. W.; Stupp, S. I. *Science* **2012**, *335*, 813–817.
- (3) Maggini, L.; Bonifazi, D. *Chem. Soc. Rev.* **2012**, *41*, 211–241.
- (4) Sengupta, S.; Würthner, F. *Acc. Chem. Res.* **2013**, *46*, 2498–2512.
- (5) Busseron, E.; Ruff, Y.; Moulin, E.; Giuseppone, N. *Nanoscale* **2013**, *5*, 7098–7140.
- (6) Tayi, A. S.; Kaeser, A.; Matsumoto, M.; Aida, T.; Stupp, S. I. *Nat. Chem.* **2015**, *7*, 281–294.
- (7) Krieg, E.; Bastings, M. M. C.; Besenius, P.; Rybtchinski, B. *Chem. Rev.* **2016**, *acs.chemrev.5b00369*.
- (8) Shklyarevskiy, I. O.; Jonkheijm, P.; Christianen, P. C. M.; Schenning, A. P. H. J.; Meijer, E. W.; Henze, O.; Kilbinger, A. F. M.; Feast, W. J.; Del Guerzo, A.; Desvergne, J.; Maan, J. C. *J. Am. Chem. Soc.* **2005**, *127*, 1112–1113.
- (9) Kim, J.-K.; Lee, E.; Lim, Y.-b.; Lee, M. *Angew. Chem. Int. Ed.* **2008**, *47*, 4662–4666.
- (10) van Dongen, S. F. M.; de Hoog, H.-P. M.; Peters, R. J. R. W.; Nallani, M.; Nolte, R. J. M.; van Hest, J. C. M. *Chem. Rev.* **2009**, *109*, 6212–6274.
- (11) Peterca, M.; Percec, V.; Leowanawat, P.; Bertin, A. *J. Am. Chem. Soc.* **2011**, *133*, 20507–20520.
- (12) Gaitzsch, J.; Huang, X.; Voit, B. *Chem. Rev.* **2015**, 150831110135007.
- (13) Schnur, J. M. *Science* **1993**, *262*, 1669–1676.
- (14) Bong, D. T.; Clark, T. D.; Granja, J. R.; Ghadiri, M. R. *Angew. Chem. Int. Ed.* **2001**, *40*, 988–1011.
- (15) Yan, D.; Zhou, Y.; Hou, J. *Science* **2004**, *303*, 65–67.
- (16) Shimizu, T.; Masuda, M.; Minamikawa, H. *Chem. Rev.* **2005**, *105*, 1401–1443.
- (17) Hill, J. P.; Jin, W.; Kosaka, A.; Fukushima, T.; Ichihara, H.; Shimomura, T.; Ito, K.; Hashizume, T.; Ishii, N.; Aida, T. *Science* **2004**, *304*, 1481–1483.
- (18) Chen, Y.; Zhu, B.; Zhang, F.; Han, Y.; and Bo, Z. *Angew. Chem. Int. Ed.* **2008**, *47*, 6015–6018.
- (19) Eisele, D. M.; Knoester, J.; Kirstein, S.; Rabe, J. P.; Bout, D. A. V. *Nat.*

- Nanotechnol.* **4**, 2009, 658 – 663.
- (20) Shao, H.; Seifert, J.; Romano, N. C.; Gao, M.; Helmus, J. J.; Jaroniec, C. P.; Modarelli, D. A.; Parquette, J. R. *Angew. Chem. Int. Ed.* **2010**, *49*, 7688–7691.
- (21) Iyoda, M.; Yamakawa, J.; Rahman, M. J. *Angew. Chem. Int. Ed.* **2011**, *50*, 10522–10553.
- (22) Kim, Y.; Kim, T.; Lee, M. *Polym. Chem.* **2013**, *4*, 1300–1308.
- (23) De Santis, E.; Ryadnov, M. G. *Chem. Soc. Rev.* **2015**, *44*, 8288–8300.
- (24) Beginn, U. *Adv. Mater.* **1998**, *10*, 1391–1394.
- (25) Sleytr, U. B.; Messner, P.; Pum, D.; Sára, M. *Angew. Chem., Int. Ed.* **1999**, *38*, 1034–1054.
- (26) Kim, J.-K.; Lee, E.; Jeong, Y.-H.; Lee, J.-K.; Zin, W.-C.; Lee, M. *J. Am. Chem. Soc.* **2007**, *129*, 6082–6083.
- (27) Jeon, S.-J.; Yi, G.-R.; Yang, S.-M. *Adv. Mater.*, **2008**, *20*, 4103–4108.
- (28) Kim, J.-K.; Lee, E.; Lim, Y.-B.; Lee, M. *Angew. Chem. Int. Ed.* **2008**, *47*, 4662–4666.
- (29) Christian, D. A.; Tian, A.; Ellenbroek, W. G.; Levental, I.; Rajagopal, K.; Janmey, P. A.; Liu, A. J.; Baumgart, T.; Discher, D. E. *Nat. Mater.* **2009**, *8*, 843–849.
- (30) Krieg, E.; Weissman, H.; Shirman, E.; Shimoni, E.; Rybtchinski, B. *Nat. Nanotechnol.* **2011**, *6*, 141–146.
- (31) Yu, H.; Qiu, X.; Nunes, S. P.; Peinemann, K.-V. *Nat. Commun.* **2014**, *5*, 4110–4120.
- (32) Lehn, J.-M. *Makromol. Chem., Macromol. Symp.* **1993**, *69*, 1–17.
- (33) Brunsveld, L.; Folmer, B. J. B.; Meijer, E. W.; Sijbesma, R. P. *Chem. Rev.* **2001**, *101*, 4071–4098.
- (34) De Greef, T. F. A.; Smulders, M. M. J.; Wolfs, M.; Schenning, A. P. H. J.; Sijbesma, R. P.; Meijer, E. W. *Chem. Rev.* **2009**, *109*, 5687–5754.
- (35) Stoddart, J. F. *Nat. Chem.* **2009**, *1*, 14–15.
- (36) Kim, H.-J.; Kim, T.; Lee, M. *Acc. Chem. Res.* **2011**, *44*, 72–82.
- (37) Rybtchinski, B. *ACS Nano* **2011**, *5*, 6791–6818.
- (38) Yamamoto, Y.; Fukushima, T.; Jin, W.; Kosaka, A.; Hara, T.; Nakamura, T.;

- Saeki, A.; Seki, S.; Tagawa, S.; Aida, T. *Adv. Mater.* **2006**, *18*, 1297–1300.
- (39) Yamamoto, Y.; Fukushima, T.; Saeki, A.; Seki, S.; Tagawa, S.; Ishii, N.; Aida, T. *J. Am. Chem. Soc.* **2007**, *129*, 9276–9277.
- (40) Zhang, W.; Jin, W.; Fukushima, T.; Ishii, N.; Aida, T. *Angew. Chem. Int. Ed.* **2009**, *48*, 4747–4750.
- (41) He, Y.; Yamamoto, Y.; Jin, W.; Fukushima, T.; Saeki, A.; Seki, S.; Ishii, N.; Aida, T. *Adv. Mater.* **2010**, *22*, 829–832.
- (42) Zhang, W.; Jin, W.; Fukushima, T.; Saeki, A.; Seki, S.; Aida, T. *Science* **2011**, *334*, 340–343.
- (43) Zhang, W.; Jin, W.; Fukushima, T.; Ishii, N.; Aida, T. *J. Am. Chem. Soc.* **2013**, *135*, 114–117.
- (44) Würthner, F. *Chem. Commun.* **2004**, 1564–1579.
- (45) Chen, Z.; Stepanenko, V.; Dehm, V.; Prins, P.; Siebbeles, L. D. A.; Seibt, J.; Marquetand, P.; Engel, V.; Würthner, F. *Chem. Eur. J.* **2007**, *13*, 436–449.
- (46) Kaiser, T. E.; Wang, H.; Stepanenko, V.; Würthner, F. *Angew. Chem. Int. Ed.* **2007**, *46*, 5541–5544.
- (47) Görl, D.; Zhang, X.; Würthner, F. *Angew. Chem. Int. Ed.* **2012**, *51*, 6328–6348.
- (48) Chen, S.; Slattum, P.; Wang, C.; Zang, L. *Chem. Rev.* **2015**, *115*, 11967–11998.
- (49) Ghosh, S.; Li, X.-Q.; Stepanenko, V.; Würthner, F. *Chem. Eur. J.* **2008**, *14*, 11343–11357.
- (50) Leclère, P.; Surin, M.; Viville, P.; Lazzaroni, R.; Kilbinger, A. F. M.; Henze, O.; Feast, W. J.; Cavallini, M.; Biscarini, F.; Schenning, A. P. H. J.; Meijer, E. W. *Chem. Mater.* **2004**, *16*, 4452–4466.
- (51) Mishra, A.; Ma, C.-Q.; Bäuerle, P. *Chem. Rev.* **2009**, *109*, 1141–1276.
- (52) Capozzi, B.; Dell, E. J.; Berkelbach, T. C.; Reichman, D. R.; Venkataraman, L.; Campos, L. M. *J. Am. Chem. Soc.* **2014**, *136*, 10486–10492.
- (53) Ma, Z.; Sun, W.; Himmelberger, S.; Vandewal, K.; Tang, Z.; Bergqvist, J.; Salleo, A.; Andreasen, J. W.; Inganäs, O.; Andersson, M. R.; Müller, C.; Zhang, F.; Wang, E. *Energy Environ. Sci.* **2014**, *7*, 361–369.
- (54) Miyajima, D.; Araoka, F.; Takezoe, H.; Kim, J.; Kato, K.; Takata, M.; Aida, T. *J. Am. Chem. Soc.* **2010**, *132*, 8530–8531.

- (55) Kang, J.; Miyajima, D.; Itoh, Y.; Mori, T.; Tanaka, H.; Yamauchi, M.; Inoue, Y.; Harada, S.; Aida, T. *J. Am. Chem. Soc.* **2014**, *136*, 10640–10644.
- (56) Kang, J.; Miyajima, D.; Mori, T.; Inoue, Y.; Itoh, Y.; Aida, T. *Science* **2015**, *347*, 646–651.
- (57) Zeng, Q.; Li, Z.; Dong, Y.; Di, C.; Qin, A.; Hong, Y.; Ji, L.; Zhu, Z.; Jim, C. K. W.; Yu, G.; Li, Q.; Li, Z.; Liu, Y.; Qin, J.; Tang, B. Z. *Chem. Commun.* **2007**, 70–72.
- (58) Ning, Z.; Chen, Z.; Zhang, Q.; Yan, Y.; Qian, S.; Cao, Y.; Tian, H. *Adv. Funct. Mater.* **2007**, *17*, 3799–3807.
- (59) Hong, Y.; Lam, J. W. Y.; Tang, B. Z. *Chem. Commun.* **2009**, 4332–4353.
- (60) Birks, J. B. *Photophysics of Aromatic Molecules*, Wiley, London, **1970**.
- (61) Malkin, J. *Photophysical and Photochemical Properties of Aromatic Compounds*, CRC, Boca Raton, **1992**.
- (62) Valeur, B. *Molecular Fluorescence: Principle and Applications*, Wiley-VCH, Weinheim, **2002**.
- (63) Sapsford, K. E.; Berti, L.; Medintz, I. L. *Angew. Chem. Int. Ed.*, **2006**, *45*, 4562–4588.
- (64) Borisov, S. M.; Wolfbeis, O. S. *Chem. Rev.*, **2008**, *108*, 423–461.
- (65) Luo, J.; Xie, Z.; Lam, J. W. Y.; Cheng, L.; Tang, B. Z.; Chen, H.; Qiu, C.; Kwok, H. S.; Zhan, X.; Liu, Y. *Chem. Commun.* **2001**, 1740–1741.
- (66) Tang, B. Z.; Zhan, X.; Yu, G.; Sze Lee, P. P.; Liu, Y.; Zhu, D. *J. Mater. Chem.* **2001**, *11*, 2974–2978.
- (67) Katoono, R.; Kawai, H.; Fujiwara, K.; Suzuki, T. *J. Am. Chem. Soc.* **2009**, *131*, 16896–16904.
- (68) Palmans, A. R. A.; Vekemans, J. A. J. M.; Havinga, E. E.; Meijer, E. W. *Angew. Chem. Int. Ed.* **1997**, *36*, 2648–2651.
- (69) van Gestel, J.; Palmans, A. R. A.; Titulaer, B.; Vekemans, J. A. J. M. *J. Am. Chem. Soc.* **2005**, *127* (15), 5490–5494.
- (70) Knobloch, P.; Stockhausen, M. *Angew. Chem. Int. Ed.* **1964**, *3*, 230–231.
- (71) Rodionov, A. N.; Ruch'eva, N. I.; Rogozhin, K. L.; Shigorin, D. N. *Zh. Prikl. Spektrosk.* **1974**, *20*, 409–410.



- (72) Sobolev, A. N.; Belsky, V. K.; Romm, I. P.; Chernikova, N. Y.; Guryanova, E. N. *Acta Crystallogr. Sect. C*, **1985**, *41*, 967–971.
- (73) Meijer, G.; Berden, G.; Meerts, W. L.; Hunziker, H. E.; de Vries, M. S.; Wendt, H. R. *Chem. Phys.* **1992**, *163* (2), 209–222.
- (74) Yuan Chiu, K.; Xiang Su, T.; Hong Li, J.; Lin, T.-H.; Liou, G.-S.; Cheng, S.-H. *J. Electroanalytical Chem.* **2005**, *575*, 95–101.
- (75) Son, J.-M.; Mori, T.; Ogino, K.; Sato, H.; Ito, Y. *Macromolecules* **1999**, *32*, 4849–4854.
- (76) Leung, M.-K.; Chou, M.-Y.; Su, Y.O.; Chiang, C.L.; Chen, H.-L.; Yang, C.F.; Yang, C.-C.; Lin, C.-C.; Chen, H.-T. *Org. Lett.* **2003**, *5*, 839–842.
- (77) Ning, Z.; Tian, H. *Chem. Commun.* **2009**, 5483–5495.
- (78) Liang, M.; Chen, J. *Chem. Soc. Rev.* **2013**, *42*, 3453–3488.
- (79) Huang, F.; Cheng, Y.-J.; Zhang, Y.; Liu, M. S.; Jen, A. K.-Y.; *J. Mater. Chem.* **2008**, *18*, 4495–4509.
- (80) Song, Y.; Di, C. A.; Xi, W.; Liu, Y.; Zhang, D.; Zhu, D.; *J. Mater. Chem.* **2007**, *17*, 4483–4491.
- (81) Thelakkat, M.; *Macromol. Mater. Eng.* **2002**, *287*, 442–461.
- (82) Wang, Y.-J.; Sheu, H.-S.; Lai, C. K. *Tetrahedron* **2007**, *63*, 1695–1705.
- (83) Majumdar, K. C.; Pal, N.; Debnath, P.; Rao, N. V. S. *Tetrahedron Lett.* **2007**, *48*, 6330–6333.
- (84) Majumdar, K. C.; Chattopadhyay, B.; Shyam, P. K.; Pal, N. *Tetrahedron Lett.* **2009**, *50*, 6901–6905.
- (85) Choudhury, T. D.; Rao, N. V. S.; Tenent, R.; Blackburn, J.; Gregg, B.; Smalyukh, I. I. *J. Phys. Chem. B* **2011**, *115*, 609–617.
- (86) Moulin, E.; Niess, F.; Maaloum, M.; Buhler, E.; Nyrkova, I.; Giuseppone, N. *Angew. Chem. Int. Ed.* **2010**, *49*, 6974–6978.
- (87) Faramarzi, V.; Niess, F.; Moulin, E.; Maaloum, M.; Dayen, J.-F.; Beaufrand, J.-B.; Zanettini, S.; Doudin, B.; Giuseppone, N. *Nat. Chem.* **2012**, *4*, 485–490.
- (88) Meijer, G.; Berden, G.; Meerts, W. L.; Hunziker, H. E.; de Vries, M. S.; Wendt, H. R.; *Chem. Phys.*, **1992**, *163*, 209–222.
- (89) Reva, I.; Lapinski, L.; Chattopadhyay, N.; Fausto, R. *Phys. Chem. Chem. Phys.*

**2003**, 5, 3844–3850.

## **Chapter 2**

### **Design and Synthesis of Propeller-Shaped Triphenylamine (TPA) Derivatives**



## **2.1 Design and synthesis of propeller-shaped TPA derivatives**

My molecular design was based on the propeller-shaped TPA core and the three peripheral paraffinic wedges at para-position via amide linkages, which expected to form hydrogen bondings in the LC state and in the nonpolar solvents (Figure 2.1). As described in the chapter 1.2, the propeller-shaped TPA core could contribute to the origin of propeller chirality in supramolecular system. It means that the propeller conformation of TPA is identical with each other in same supramolecular helices. It could be allowed to exhibit unexpected phenomena in supramolecular chirality.

It is well known that the amide group triggers strong hydrogen bonding for supramolecular polymerization. This 3-folded amide groups would induce the formation of 1D supramolecular helical polymer with their helical array. In addition, this aromatic amide unit can act as E-field-responsive handle that enables large-area unidirectional columnar orientation of columnarly assembled LC mesophase. Miyajima et al. reported that discotic LC compounds with aromatic amides responded to the applied E-field regardless of the structures of aromatic core and branched paraffinic tails. Furthermore, the columnar orientation developed by the E-field is maintained long time after the E-field is off. Hence, the TPA compounds are also expected to show E-field responsiveness, if they exhibit LC mesophase in certain temperature range.

Finally, the paraffinic wedges support the formation of 1D supramolecular polymer in diluted solution as well as columnar assembly in LC mesophase. There are many examples of discotic molecules with appropriate paraffinic wedges, which stabilized LC mesophase over wide temperature range. Also, this branched paraffinic tails expected to help the implementation of the amide handle for large-area columnar orientation in LC mesophase.

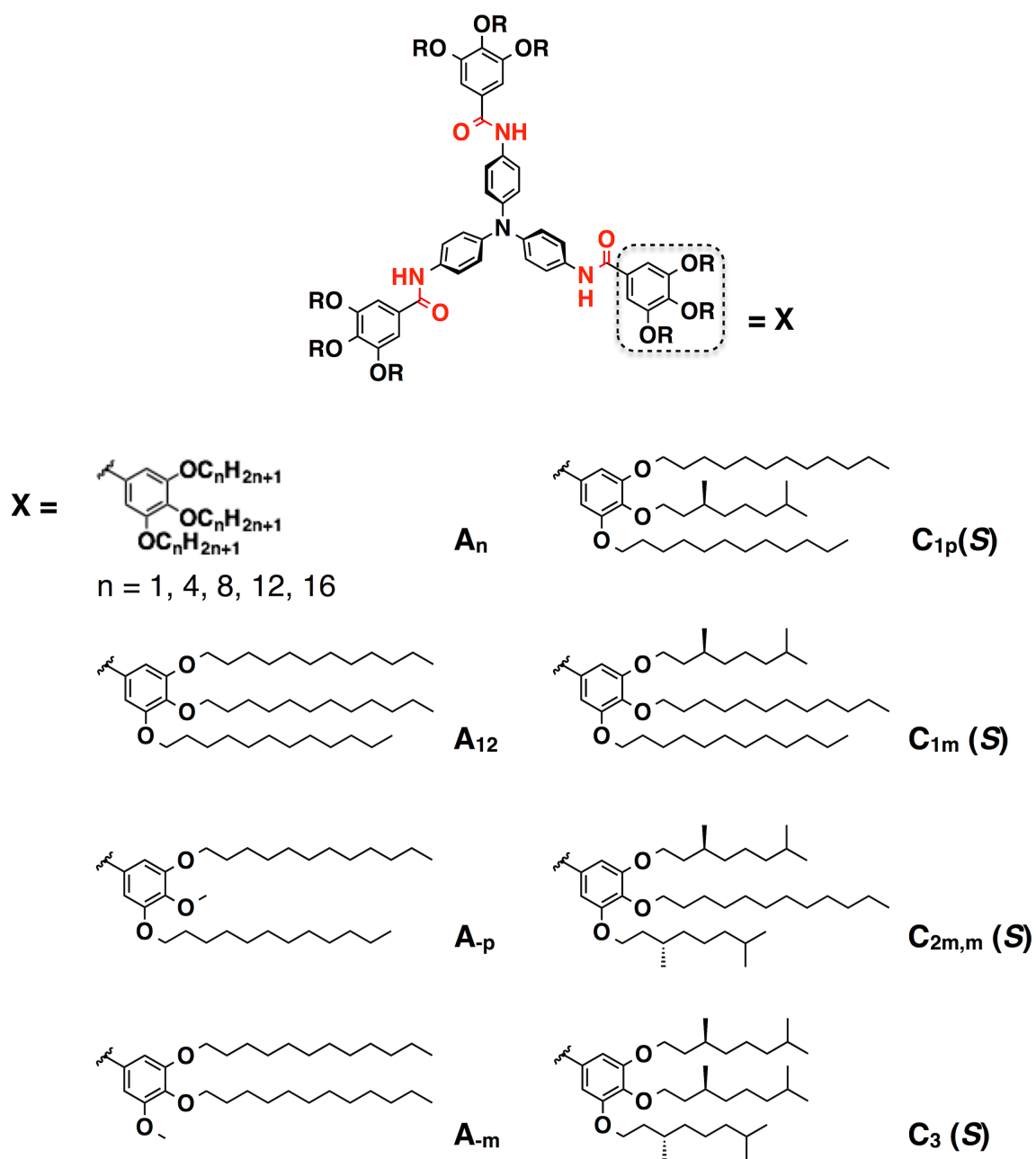


**Figure 2.1** Chemical structures of propeller-shaped TPA derivatives.

To elucidate the spatial effect of side chains, the alkoxy groups in outer phenyls were substituted on the basis of three structural variation; 1) the different length of alkyl chains ( $\mathbf{A}_4$ ,  $\mathbf{A}_8$ ,  $\mathbf{A}_{12}$  and  $\mathbf{A}_{16}$ ), 2) the lack of long linear alkyls ( $\mathbf{A}_{-p}$  and  $\mathbf{A}_{-m}$ ), 3) the existence of branched chiral chains [ $\mathbf{C}_{1m}(S)$ ,  $\mathbf{C}_{1p}(S)$ ,  $\mathbf{C}_{2m,m}(S)$ ,  $\mathbf{C}_3(S)$ ]. By probing individually the role of these three structural variations on self-assembly of propeller-shaped TPA, it could provide us with a valuable insight for precise control of molecular organization toward functional materials.

These TPA derivatives were synthesized by amide coupling with tris-(4-aminophenyl)amine and appropriate 3,4,5-substituted benzoic acid chloride in dichloromethane. Each paraffinic side chain was produced by an etherification of commercially available methyl 3,4,5-trihydroxybenzoate with appropriate alkyl halides according to methods reported by Würthner and co-workers with minor modifications.<sup>2</sup> All compounds were unambiguously characterized by  $^1\text{H}$  and  $^{13}\text{C}$  NMR spectroscopy along with mass spectrometry.

## 2.2 Experimental Section

### 2.2.1. Materials

Tris(4-aminophenyl)amine, 1-bromododecane, iodomethane and (-)- $\beta$ -citronellol from TCI and Tokyo Kasei were used as received. Palladium, 10 wt. % (dry basis), on activate carbon, wet, Degussa type E101 NE/W and (*R*)-citronellyl bromide from Aldrich were used as received. 3,4,5-Trihydroxymethyl benzoate, *N*-bromosuccinimide, thionyl chloride, triethylamine, potassium carbonate and potassium hydroxide were used as received. Unless otherwise indicated, all starting materials were obtained from commercial suppliers (Wako Pure Chemical, Kanto, and TCI, etc.) and were used without purification. Methylene chloride, hexane, DMF, and Ethanol were distilled before use. Visualization was accomplished with UV light, iodine vapor or by staining using base solution of cerium ammonium molybdate. Flash chromatography was carried out with Silica Gel 60 (230-400 mesh) from Wako Pure Chemical Industries, Ltd.

### 2.2.2. Method

$^1\text{H-NMR}$  and  $^{13}\text{C-NMR}$  was recorded from  $\text{CDCl}_3$  solutions at 25 °C on a JEOL JNM-ECA500 spectrometer, operating at 500 and 125 MHz, respectively, where chemical shifts ( $\delta$  in ppm) were determined using tetramethylsilane as an internal reference. Matrix-assisted laser desorption ionization time-of-flight (MALDI-TOF) mass spectrometry was performed in the reflector mode on a Bruker model autoflex TM speed spectrometer using  $\alpha$ -cyano-4-hydroxy cinnamic acid (CHCA) as matrix. The purity of the products was checked by thin layer chromatography (TLC; Merck, silica gel 60). Compounds were synthesized according to the procedure described

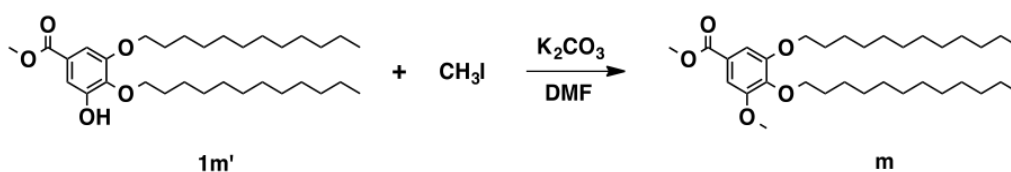


below and then purified by silica gel column chromatography, flash chromatography system (Yamazen Smart Flash EPCLC AI-580S) and prep. recycling HPLC (YMC LC-Forte/R).

### 2.2.3. Synthesis

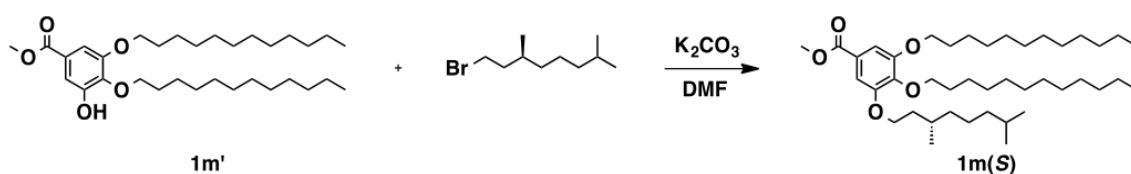
Synthesis of methyl 3,4-bis(dodecyloxy)-5-hydroxybenzoate, **1m'**,<sup>[S1]</sup> methyl 4-[(*S*)-3,7-dimethyloctyloxy]-3,5-dihydroxybenzoate, **1p'(S)**,<sup>[S2]</sup> methyl 4-[(*R*)-3,7-dimethyloctyloxy]-3,5-dihydroxybenzoate, **1p'(R)**,<sup>[S2]</sup> methyl 4-dodecyloxy-3,5-dihydroxybenzoate, **2m,m'**,<sup>[S1]</sup> 3,5-bis(dodecyloxy)-4-methoxybenzoic acid, **pA**,<sup>[S3]</sup> 3,4,5-tris(dodecyloxy)benzoic acid, **A'**,<sup>[S2]</sup> 3,4,5-[tris-(*S*)-3,7-dimethyloctyloxy]benzoic acid, **3A(S)**<sup>[S4]</sup> and 3,4,5-[tris-(*R*)-3,7-dimethyloctyloxy]benzoic acid, **3A(R)**,<sup>[S4]</sup> were described previously. The other substituted 3,4,5-trisalkoxybenzoic acid were synthesized by means of similar procedures. (*R*)-3,7-dimethyloctyl bromide<sup>[S5]</sup> and (*S*)-3,7-dimethyloctyl bromide<sup>[S6]</sup> was synthesized from (*R*)-citronellyl bromide and (*S*)-citronellol, respectively, as previous report.

#### 2.2.3.1 Synthesis of m, 1m(S), 1p(S), 1p(R), and 2m,m(S)



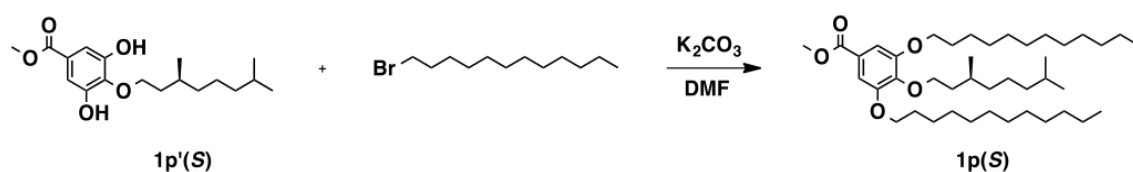
**Methyl 3,4-bis(dodecyloxy)-5-methoxybenzoate (m):** To a DMF solution (20 mL) of a mixture of **1m'** (150 mg, 0.29 mmol) and excess K<sub>2</sub>CO<sub>3</sub> was added iodomethane (46 mg, 0.33 mmol), and the mixture was stirred for 12 h at 80 °C under a positive pressure of argon. The reaction mixture was washed twice with water (50 mL), dried over Na<sub>2</sub>SO<sub>4</sub>, and evaporated to dryness under reduced pressure. The residue was

chromatographed on silica gel with hexane/AcOEt (9/1 = v/v) as an eluent, where the first fraction was collected and evaporated under reduced pressure to give **m** as colorless liquid (140 mg, 0.25 mmol, 86%). <sup>1</sup>H NMR (500 MHz, CDCl<sub>3</sub>, 25 °C, TMS) δ (ppm) = 7.27 (s, 2H), 4.02 (q, *J* = 6.3 Hz, 4H), 3.89 (s, 3H), 3.88 (s, 3H), 1.82 (quint, *J* = 6.9 Hz, 2H), 1.75 (quint, *J* = 6.9 Hz, 2H), 1.53-1.09 (overlapped m, 36H), 0.88 (t, *J* = 6.9 Hz, 6H); <sup>13</sup>C NMR (125 MHz, CDCl<sub>3</sub>, 25 °C, TMS) δ (ppm) = 166.8, 152.9, 141.8, 124.7, 107.9, 106.5, 73.5, 69.0, 56.2, 52.2, 31.9, 30.3-25.9, 22.6, 14.1.



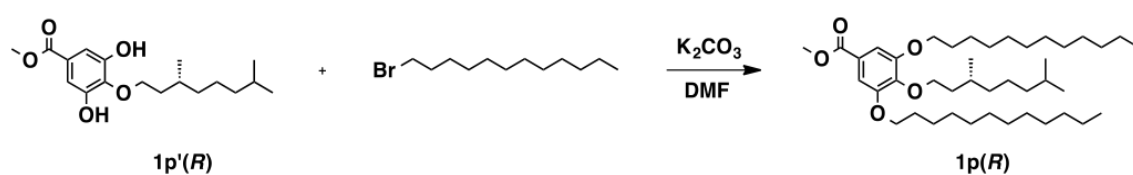
**Methyl 3-[[*(S)*-3,7-dimethyloctyl]oxy]-4,5-bis(dodecyloxy)benzoate**

**[1m(S)]:** To a DMF solution (20 mL) of a mixture of **1m'** (100 mg, 0.19 mmol) and excess K<sub>2</sub>CO<sub>3</sub> was added (*S*)-3,7-dimethyloctyl bromide (46 mg, 0.21 mmol), and the mixture was stirred for 12 h at 80 °C under a positive pressure of argon. The reaction mixture was washed twice with water (50 mL), dried over Na<sub>2</sub>SO<sub>4</sub>, and evaporated to dryness under reduced pressure. The residue was chromatographed on silica gel with hexane/AcOEt (9/1 = v/v) as an eluent, where the first fraction was collected and evaporated under reduced pressure to give **1m(S)** as colorless liquid (110 mg, 0.17 mmol, 89%). <sup>1</sup>H NMR (500 MHz, CDCl<sub>3</sub>, 25 °C, TMS) δ (ppm) = 7.25 (overlapped s, *J* = 2.3 Hz, 2H), 4.06-3.9 (m, 6H), 3.89 (s, 3H), 1.82-1.66 (m, 6H), 1.51-1.12 (overlapped m, 44H), 0.94 (d, *J* = 6.9 Hz, 3H), 0.88 (m, 12H); <sup>13</sup>C NMR (125 MHz, CDCl<sub>3</sub>, 25 °C, TMS) δ (ppm) = 166.9, 152.8, 142.3, 124.6, 107.9, 73.5, 69.1, 67.4, 52.1, 39.2, 37.3, 36.3, 31.9, 30.3, 29.8-26.0, 24.7, 22.6, 19.6, 14.1.



**Methyl 4-[(S)-3,7-dimethyloctyl]oxy}-3,5-bis(dodecyloxy)benzoate**

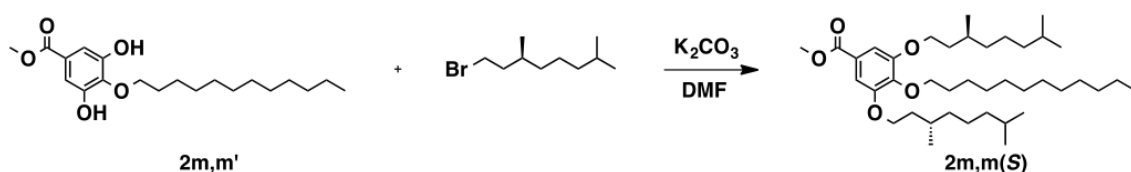
**[1p(S)]:** To a DMF solution (50 mL) of a mixture of **1p'(S)** (300 mg, 0.92 mmol) and excess  $\text{K}_2\text{CO}_3$  was added 1-bromododecane (691 mg, 2.78 mmol), and the mixture was stirred for 12 h at 80 °C under a positive pressure of argon. The reaction mixture was washed twice with water (100 mL), dried over  $\text{Na}_2\text{SO}_4$ , and evaporated to dryness under reduced pressure. The residue was chromatographed on silica gel with hexane/AcOEt (9/1 = v/v) as an eluent, where the first fraction was collected and evaporated under reduced pressure to give **1p(S)** as colorless liquid (525 mg, 0.78 mmol, 85%).  $^1\text{H}$  NMR (500 MHz,  $\text{CDCl}_3$ , 25 °C, TMS)  $\delta$  (ppm) = 7.25 (s, 2H), 4.18-3.90 (m, 6H), 3.89 (s, 3H), 1.86-1.68 (m, 6H), 1.57-1.44 (m, 6H), 1.40-1.09 (overlapped m, 42H), 0.92 (d,  $J$  = 6.9 Hz, 3H), 0.87 (m, 12H);  $^{13}\text{C}$  NMR (125 MHz,  $\text{CDCl}_3$ , 25 °C, TMS)  $\delta$  (ppm) = 166.9, 152.8, 142.4, 124.6, 107.9, 71.7, 69.1, 39.3, 37.5, 31.9, 29.7-26.1, 24.7, 22.6, 19.5, 14.1.



**Methyl 4-[(R)-3,7-dimethyloctyl]oxy}-3,5-bis(dodecyloxy)benzoate**

**[1p(R)]:** To a DMF solution (30 mL) of a mixture of **1p'(R)** (200 mg, 0.62 mmol) and excess  $\text{K}_2\text{CO}_3$  was added 1-bromododecane (338 mg, 1.36 mmol), and the mixture was stirred for 12 h at 80 °C under a positive pressure of argon. The reaction mixture was washed twice with water (60 mL), dried over  $\text{Na}_2\text{SO}_4$ , and evaporated to dryness under reduced pressure. The residue was chromatographed on silica gel with hexane/AcOEt

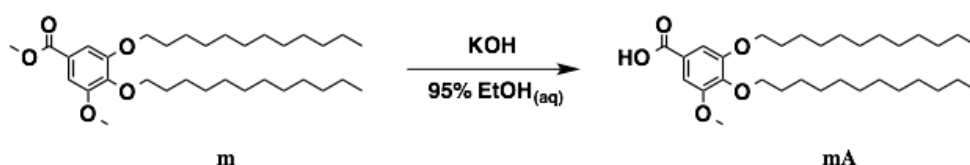
(9/1 = v/v) as an eluent, where the first fraction was collected and evaporated under reduced pressure to give **1p(R)** as colorless liquid (330 mg, 0.50 mmol, 81%).  $^1\text{H}$  NMR (500 MHz,  $\text{CDCl}_3$ , 25 °C, TMS)  $\delta$  (ppm) = 7.25 (s, 2H), 4.18-3.90 (m, 6H), 3.89 (s, 3H), 1.86-1.68 (m, 6H), 1.57-1.44 (m, 6H), 1.40-1.09 (overlapped m, 42H), 0.92 (d,  $J$  = 6.9 Hz, 3H), 0.87 (m, 12H);  $^{13}\text{C}$  NMR (125 MHz,  $\text{CDCl}_3$ , 25 °C, TMS)  $\delta$  (ppm) = 166.9, 152.8, 142.4, 124.6, 107.9, 71.7, 69.1, 39.3, 37.5, 31.9, 29.7-26.1, 24.7, 22.6, 19.5, 14.1.



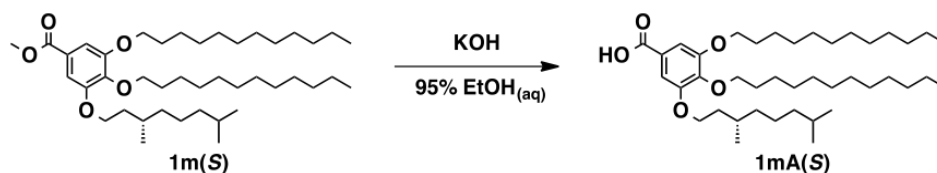
### Methyl 3,5-bis{[(S)-3,7-dimethyloctyl]oxy}-4-(dodecyloxy)benzoate

**[2m,m(S)]**: To a DMF solution (50 mL) of a mixture of **2m,m'** (300 mg, 0.92 mmol) and excess  $\text{K}_2\text{CO}_3$  was added (S)-3,7-dimethyloctyl bromide (472 mg, 2.78 mmol), and the mixture was stirred for 12 h at 80 °C under a positive pressure of argon. The reaction mixture was washed twice with water (100 mL), dried over  $\text{Na}_2\text{SO}_4$ , and evaporated to dryness under reduced pressure. The residue was chromatographed on silica gel with hexane/AcOEt (9/1 = v/v) as an eluent, where the first fraction was collected and evaporated under reduced pressure to give **2m,m(S)** as colorless liquid (475 mg, 0.80 mmol, 87%).  $^1\text{H}$  NMR (500 MHz,  $\text{CDCl}_3$ , 25 °C, TMS)  $\delta$  (ppm) = 7.26 (s, 2H), 4.08-3.98 (m, 6H), 3.89 (s, 3H), 1.86 (m, 2H), 1.77-1.42 (m, 10H), 1.39-1.20 (overlapped m, 28H), 0.94 (d,  $J$  = 6.9 Hz, 6H), 0.88 (m, 15H);  $^{13}\text{C}$  NMR (125 MHz,  $\text{CDCl}_3$ , 25 °C, TMS)  $\delta$  (ppm) = 166.9, 152.8, 142.3, 124.6, 107.9, 73.4, 67.4, 60.4, 52.1, 39.2, 37.3, 36.3, 31.9, 30.3, 29.8-26.0, 24.7, 22.6, 19.6, 14.1

### 2.2.3.2 Synthesis of mA, 1mA(S), 1pA(S), 1pA(R) and 2m,mA(S)

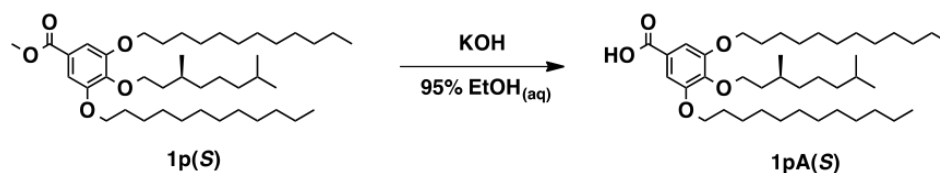


**3,4-Bis(dodecyloxy)-5-methoxybenzoic acid (mA):** To a 95% ethanol solution (20 mL) of a mixture of **m** (140 mg, 0.26 mmol) and KOH (100 mg, 1.79 mmol) was stirred for 2 h at 100 °C under a positive pressure of argon. The emulsion became a clear solution, indicating the progress of the reaction. The reaction mixture was cooled to RT and the solution was acidified with dilute HCl to pH 1. The solution was poured into water (100 mL) to precipitate of a white solid. The residue was chromatographed on silica gel with hexane/AcOEt (3/1 = v/v) as an eluent, where the last fraction was collected and evaporated under reduced pressure to give **mA** as white solid (100 mg, 0.19 mmol, 74%). <sup>1</sup>H NMR (500 MHz, CDCl<sub>3</sub>, 25 °C, TMS) δ (ppm) = 7.35 (overlapped s, *J* = 2.9 Hz, 2H), 4.04 (m, 4H), 3.89 (s, 3H), 1.88-1.73 (m, 4H), 1.53-1.21 (overlapped m, 36H), 0.88 (t, *J* = 6.9 and 7.4 Hz, 6H); <sup>13</sup>C NMR (125 MHz, CDCl<sub>3</sub>, 25 °C, TMS) δ (ppm) = 171.3, 153.0, 142.8, 123.6, 107.8, 73.6, 69.2, 56.2, 31.9, 30.2-26.1, 22.7, 14.1.



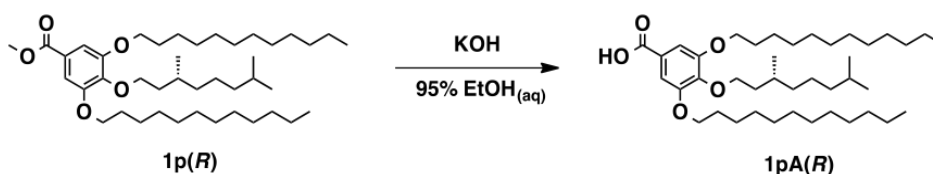
**3-[(S)-3,7-dimethyloctyl]oxy-4,5-bis(dodecyloxy)benzoic acid [1mA(S)]:** To a 95% ethanol solution (20 mL) of a mixture of **1m(S)** (110 mg, 0.17 mmol) and KOH (65 mg, 1.16 mmol) was stirred for 2 h at 100 °C under a positive pressure of argon. The emulsion became a clear solution, indicating the progress of the reaction. The reaction mixture was cooled to RT and the solution was acidified with dilute HCl to

pH 1. The solution was poured into water (100 mL) to precipitate of a white solid. The residue was chromatographed on silica gel with hexane/AcOEt (3/1 = v/v) as an eluent, where the last fraction was collected and evaporated under reduced pressure to give **1mA(S)** as white solid (100 mg, 0.15 mmol, 88%). <sup>1</sup>H NMR (500 MHz, CDCl<sub>3</sub>, 25 °C, TMS) δ (ppm) = 7.34 (overlapped s, *J* = 2.9 Hz, 2H), 4.11-3.99 (m, 6H), 1.82-1.66 (m, 6H), 1.51-1.12 (overlapped m, 44H), 0.95 (d, *J* = 6.3 Hz, 3H), 0.88 (m, 12H); <sup>13</sup>C NMR (125 MHz, CDCl<sub>3</sub>, 25 °C, TMS) δ (ppm) = 172.1, 152.8, 143.1, 123.6, 108.5, 73.5, 69.1, 67.5, 52.1, 39.2, 37.3, 36.2, 31.9, 30.3, 29.8-26.0, 24.7, 22.6, 19.6, 14.1.



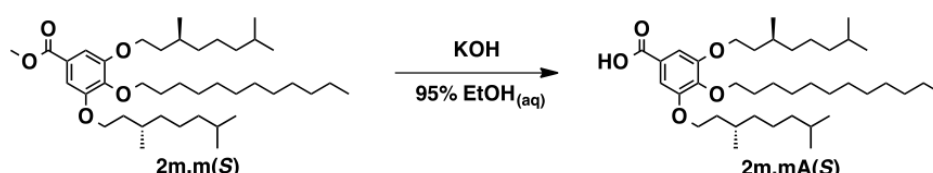
**4-[[*S*]-3,7-dimethyloctyl]oxy]-3,5-bis(dodecyloxy)benzoic acid [1pA(S)]:**

To a 95% ethanol solution (50 mL) of a mixture of **1p(S)** (525 mg, 0.79 mmol) and KOH (312 mg, 5.56 mmol) was stirred for 2 h at 100 °C under a positive pressure of argon. The emulsion became a clear solution, indicating the progress of the reaction. The reaction mixture was cooled to RT and the solution was acidified with dilute HCl to pH 1. The solution was poured into water (200 mL) to precipitate of a white solid. The residue was chromatographed on silica gel with hexane/AcOEt (3/1 = v/v) as an eluent, where the last fraction was collected and evaporated under reduced pressure to give **1pA(S)** as white solid (450 mg, 0.69 mmol, 87%). <sup>1</sup>H NMR (500 MHz, CDCl<sub>3</sub>, 25 °C, TMS) δ (ppm) = 7.32 (s, 2H), 4.18-3.98 (m, 6H), 1.87-1.67 (m, 6H), 1.57-1.44 (m, 6H), 1.40-1.09 (overlapped m, 42H), 0.93 (d, *J* = 6.3 Hz, 3H), 0.87 (m, 12H); <sup>13</sup>C NMR (125 MHz, CDCl<sub>3</sub>, 25 °C, TMS) δ (ppm) = 172.2, 152.9, 143.0, 123.6, 108.5, 71.8, 69.4, 52.1, 39.3, 37.4, 31.9, 29.3-26.1, 24.7, 22.6, 19.5, 14.1.



**4-[[*(R)*-3,7-dimethyloctyl]oxy]-3,5-bis(dodecyloxy)benzoic acid [1pA(*R*):**

To a 95% ethanol solution (30 mL) of a mixture of **1p(R)** (330 mg, 0.50 mmol) and KOH (196 mg, 3.50 mmol) was stirred for 2 h at 100 °C under a positive pressure of argon. The emulsion became a clear solution, indicating the progress of the reaction. The reaction mixture was cooled to RT and the solution was acidified with dilute HCl to pH 1. The solution was poured into water (150 mL) to precipitate of a white solid. The residue was chromatographed on silica gel with hexane/AcOEt (3/1 = v/v) as an eluent, where the last fraction was collected and evaporated under reduced pressure to give **1pA(R)** as white solid (324 mg, 0.49 mmol, 99%). <sup>1</sup>H NMR (500 MHz, CDCl<sub>3</sub>, 25 °C, TMS) δ (ppm) = 7.32 (s, 2H), 4.18-3.98 (m, 6H), 1.87-1.67 (m, 6H), 1.57-1.44 (m, 6H), 1.40-1.09 (overlapped m, 42H), 0.93 (d, *J* = 6.3 Hz, 3H), 0.87 (m, 12H); <sup>13</sup>C NMR (125 MHz, CDCl<sub>3</sub>, 25 °C, TMS) δ (ppm) = 172.2, 152.9, 143.0, 123.6, 108.5, 71.8, 69.4, 52.1, 39.3, 37.4, 31.9, 29.3-26.1, 24.7, 22.6, 19.5, 14.1.

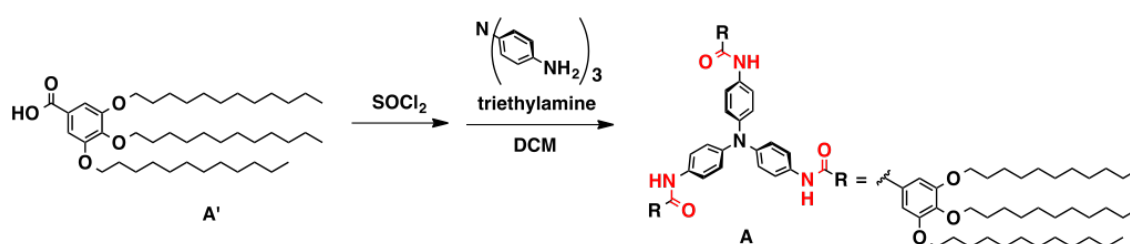


**3,5-Bis[[*(S)*-3,7-dimethyloctyl]oxy]-4-(dodecyloxy)benzoic acid [2m,mA**

**(S)]:** To a 95% ethanol solution (50 mL) of a mixture of **2m,m(S)** (475 mg, 0.75 mmol) and KOH (295 mg, 5.26 mmol) was stirred for 2 h at 100 °C under a positive pressure of argon. The emulsion became a clear solution, indicating the progress of the reaction. The reaction mixture was cooled to RT and the solution was acidified with dilute HCl to

pH 1. The solution was poured into water (200 mL) to precipitate of a white solid. The residue was chromatographed on silica gel with hexane/AcOEt (3/1 = v/v) as an eluent, where the last fraction was collected and evaporated under reduced pressure to give **2m,mA(S)** as white solid (420 mg, 0.67 mmol, 90%).  $^1\text{H}$  NMR (500 MHz,  $\text{CDCl}_3$ , 25 °C, TMS)  $\delta$  (ppm) = 7.33 (s, 2H), 4.11-4.01 (m, 6H), 1.87 (m, 2H), 1.78-1.43 (m, 10H), 1.39-1.20 (overlapped m, 28H), 0.95 (d,  $J$  = 6.9 Hz, 6H), 0.88 (m, 15H);  $^{13}\text{C}$  NMR (125 MHz,  $\text{CDCl}_3$ , 25 °C, TMS)  $\delta$  (ppm) = 171.5, 152.8, 143.1, 123.6, 108.5, 73.5, 67.5, 65.0, 58.5, 39.2, 37.3, 36.2, 31.9, 30.3, 29.8-26.0, 24.7, 22.6, 19.6, 14.1.

### 2.3.3.3. Synthesis of **A**, **A<sub>p</sub>**, **A<sub>m</sub>**, **C<sub>1m</sub>(S)**, **C<sub>1p</sub>(S)**, **C<sub>1p</sub>(R)**, **C<sub>2m,m</sub>(S)**, **C<sub>3</sub>(S)** and **C<sub>3</sub>(R)**

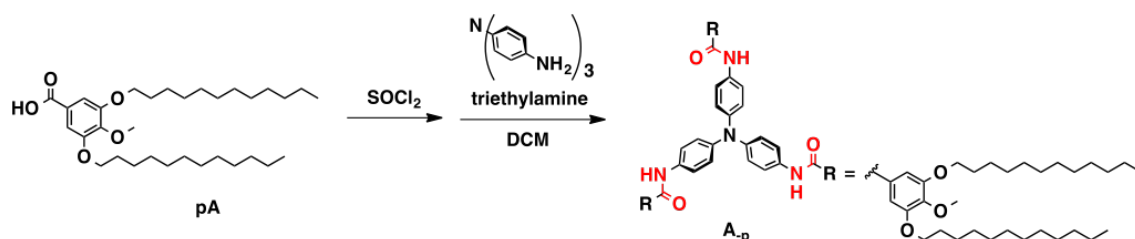


#### Tris-{4-[3,4,5-tris(dodecyloxy)benzoylamino]phenyl}amine (**A**):

**A** thionyl chloride (50 mL) solution of **A'** (1.02 g, 1.48 mmol) was refluxed for 6 h, and the reaction mixture was evaporated to dryness. To a N-Methyl-2-pyrrolidone (NMP) solution (50 mL) of the residue were successively added a mixture of tris(4-aminophenyl)amine (100 mg, 0.37 mmol), pyridine (5 mL) and excess LiCl was stirred for 2 h at 80 °C under a positive pressure of argon. The solution was poured into ethanol (200 mL) to precipitate of a white solid. The residue was chromatographed on silica gel with  $\text{CHCl}_3/\text{EtOH}$  (99/1 = v/v) as an eluent, where the second fraction was collected and evaporated to dryness. The residue was subjected to recycling preparative HPLC (YMC LC-forte/R) with  $\text{CHCl}_3$  as an eluent at a flow rate of  $10 \text{ mL min}^{-1}$ , where



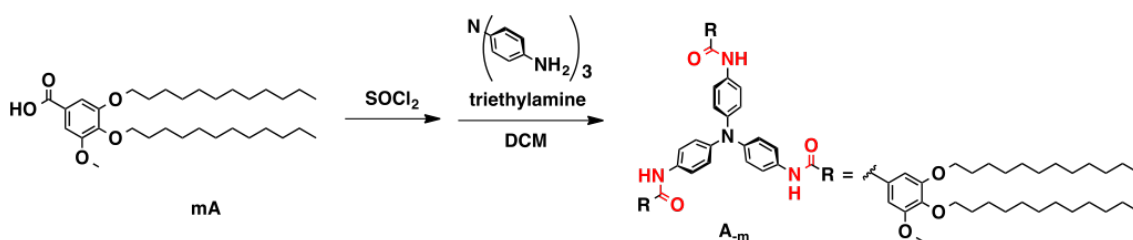
the first fraction was collected and evaporated to dryness under reduced pressure to give **A** as white solid (2.24 g, 0.25 mmol, 68%).  $^1\text{H}$  NMR (500 MHz,  $\text{CDCl}_3$ , 25 °C, TMS)  $\delta$  (ppm) = 7.83 (s, 3H), 7.50 (d,  $J$  = 9.2 Hz, 6H), 7.06 (m, 12H), 4.00 (m, 12H), 1.83-1.72 (m, 18H), 1.52-1.15 (overlapped m, 168H), 0.88 (m, 27H);  $^{13}\text{C}$  NMR (125 MHz,  $\text{CDCl}_3$ , 25 °C, TMS)  $\delta$  (ppm) = 165.6, 153.2, 144.2, 141.5, 132.9, 129.8, 124.4, 121.6, 105.8, 73.6, 69.4, 31.9, 30.3-29.3, 26.1, 22.7, 14.1. MALDI-TOF mass:  $m/z$  calculated, for compound **A**  $[\text{M} + \text{H}]^+$ , 2259.88; Found:  $[\text{M} + \text{H}]^+$ , 2260.16.



**Tris-{4-[3,5-bis(dodecyloxy)-4-methoxybenzoylamino]phenyl}amine (**A<sub>p</sub>**)**

**A<sub>p</sub>**: A thionyl chloride (10 mL) solution of **pA** (223 mg, 0.43 mmol) was refluxed for 6 h, and the reaction mixture was evaporated to dryness. To a NMP solution (20 mL) of the residue were successively added a mixture of tris(4-aminophenyl)amine (31 mg, 0.11 mmol), pyridine (2 mL) and excess LiCl was stirred for 2 h at 80 °C under a positive pressure of argon. The solution was poured into ethanol (100 mL) to precipitate of a white solid. The residue was chromatographed on silica gel with  $\text{CHCl}_3/\text{EtOH}$  (99/1 = v/v) as an eluent, where the second fraction was collected and evaporated to dryness. The residue was subjected to recycling preparative HPLC (YMC LC-forte/R) with  $\text{CHCl}_3$  as an eluent at a flow rate of  $10 \text{ mL min}^{-1}$ , where the first fraction was collected and evaporated to dryness under reduced pressure to give **A<sub>p</sub>** as white solid (122 mg, 0.27 mmol, 63%).  $^1\text{H}$  NMR (500 MHz,  $\text{CDCl}_3$ , 25 °C, TMS)  $\delta$  (ppm) = 7.74 (s, 3H), 7.51 (d,  $J$  = 9.2 Hz, 6H), 7.08 (d,  $J$  = 9.2 Hz, 6H), 7.05 (s, 6H),

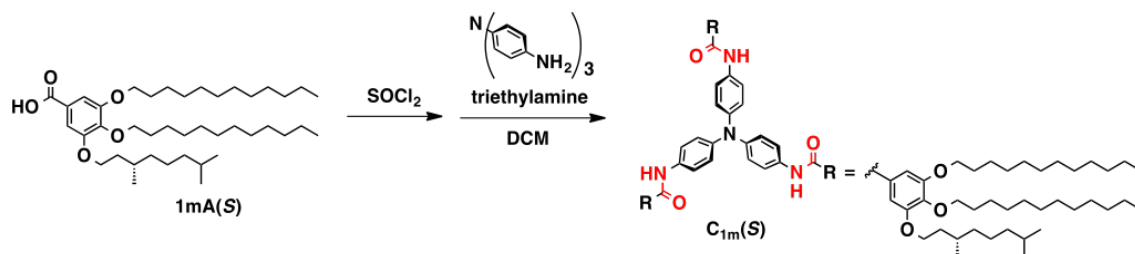
4.04 (t,  $J = 6.3$  Hz, 12H), 3.89 (s, 9H), 1.82 (quint,  $J = 6.9$  Hz, 12H), 1.51-1.21 (overlapped m, 108H), 0.88 (t,  $J = 6.9$  Hz, 18H);  $^{13}\text{C}$  NMR (125 MHz,  $\text{CDCl}_3$ , 25 °C, TMS)  $\delta$  (ppm) = 165.5, 153.0, 144.2, 142.1, 132.9, 130.0, 124.4, 121.5, 105.8, 69.5, 60.8, 31.9, 29.7-29.3, 26.0, 22.7, 14.1. MALDI-TOF mass:  $m/z$  calculated, for compound **A<sub>p</sub>**  $[\text{M} + \text{H}]^+$ , 1797.36; Found:  $[\text{M} + \text{H}]^+$ , 1797.60.



**Tris-{4-[3,4-bis(dodecyloxy)-5-methoxybenzoylamino]phenyl}amine (A<sub>m</sub>)**

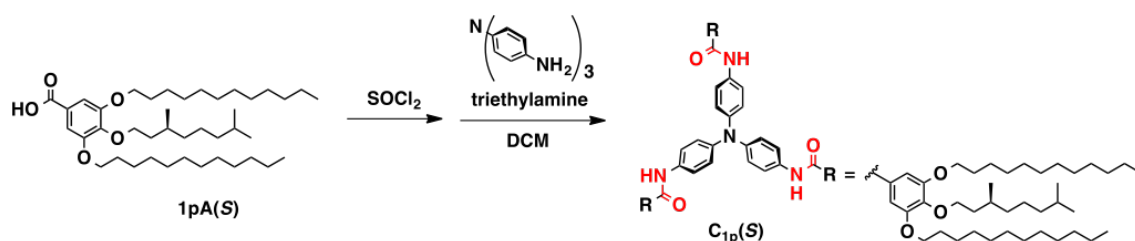
**A<sub>m</sub>**: A thionyl chloride (5 mL) solution of **mA** (100 mg, 0.19 mmol) was refluxed for 6 h, and the reaction mixture was evaporated to dryness. To a NMP solution (10 mL) of the residue were successively added a mixture of tris(4-aminophenyl)amine (16 mg, 0.054 mmol), pyridine (1 mL) and excess LiCl was stirred for 2 h at 80 °C under a positive pressure of argon. The solution was poured into ethanol (50 mL) to precipitate of a white solid. The residue was chromatographed on silica gel with  $\text{CHCl}_3/\text{EtOH}$  (99/1 = v/v) as an eluent, where the second fraction was collected and evaporated to dryness. The residue was subjected to recycling preparative HPLC (YMC LC-forte/R) with  $\text{CHCl}_3$  as an eluent at a flow rate of 10 mL  $\text{min}^{-1}$ , where the first fraction was collected and evaporated to dryness under reduced pressure to give **A<sub>m</sub>** as white solid (67 mg, 0.037 mmol, 69%).  $^1\text{H}$  NMR (500 MHz,  $\text{CDCl}_3$ , 25 °C, TMS)  $\delta$  (ppm) = 7.86 (s, 3H), 7.45 (d,  $J = 9.2$  Hz, 6H), 7.06 (m, 12H), 4.01 (m, 12H), 3.87 (s, 9H), 1.86-1.71 (m, 12H), 1.51-1.21 (overlapped m, 108H), 0.88 (m, 18H);  $^{13}\text{C}$  NMR (125 MHz,  $\text{CDCl}_3$ , 25 °C, TMS)  $\delta$  (ppm) = 165.5, 153.3, 144.2, 141.0, 132.8, 129.8, 124.3, 121.6, 105.7,

104.4, 73.6, 69.3, 56.4, 31.9, 30.2-29.4, 26.0, 22.7, 14.1. MALDI-TOF mass:  $m/z$  calculated, for compound  $A_m$   $[M + H]^+$ , 1797.36; Found:  $[M + H]^+$ , 1797.58.

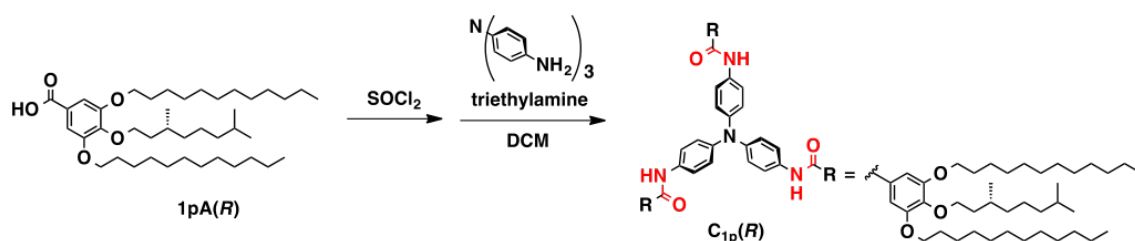


**Tris-[4-(3-[(*S*)-3,7-dimethyloctyl]oxy)-4,5-bis(dodecyloxy)benzoylamino**

**)phenyl]amine [ $C_{1m}(S)$ ]:** A thionyl chloride (5 mL) solution of **1mA(S)** (100 mg, 0.15 mmol) was refluxed for 6 h, and the reaction mixture was evaporated to dryness. To a NMP solution (10 mL) of the residue were successively added a mixture of tris(4-aminophenyl)amine (11 mg, 0.039 mmol), pyridine (1 mL) and excess LiCl was stirred for 2 h at 80 °C under a positive pressure of argon. The solution was poured into ethanol (50 mL) to precipitate of a white solid. The residue was chromatographed on silica gel with  $CHCl_3/EtOH$  (99/1 = v/v) as an eluent, where the second fraction was collected and evaporated to dryness. The residue was subjected to recycling preparative HPLC (YMC LC-forte/R) with  $CHCl_3$  as an eluent at a flow rate of 10 mL  $min^{-1}$ , where the first fraction was collected and evaporated to dryness under reduced pressure to give  $C_{1m}(S)$  as white solid (57 mg, 0.026 mmol, 67%).  $^1H$  NMR (500 MHz,  $CDCl_3$ , 25 °C, TMS)  $\delta$  (ppm) = 7.67 (s, 3H), 7.51 (d,  $J$  = 8.6 Hz, 6H), 7.09 (d,  $J$  = 8.6 Hz, 6H), 7.04 (ss, 6H), 4.03 (m, 18H), 1.92-1.10 (overlapped m, 150H), 0.95 (d,  $J$  = 6.9 Hz, 9H), 0.88 (m, 36H);  $^{13}C$  NMR (125 MHz,  $CDCl_3$ , 25 °C, TMS)  $\delta$  (ppm) = 165.5, 153.3, 141.5, 132.9, 129.9, 124.4, 121.4, 105.7, 73.5, 67.8, 39.2, 37.3, 36.4, 31.9, 30.3-29.4, 28.0, 26.1, 24.7, 22.6, 19.6, 14.1. MALDI-TOF mass:  $m/z$  calculated, for compound  $C_{1m}(S)$   $[M + H]^+$ , 2175.78; Found:  $[M + H]^+$ , 2176.12.

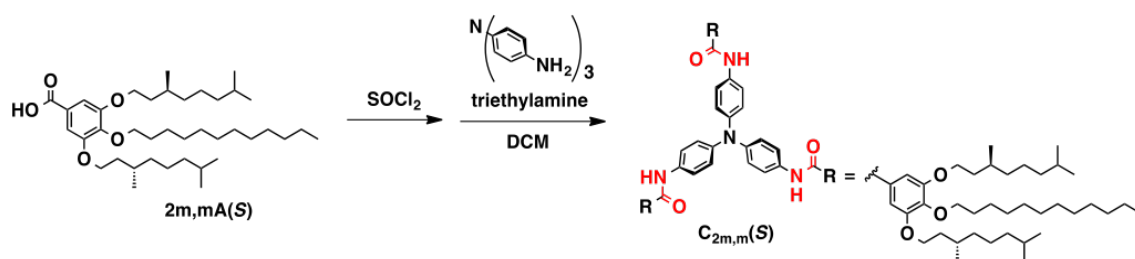


**Tris-[4-(4-[(*S*)-3,7-dimethyloctyl]oxy)-3,5-bis(dodecyloxy)benzoylamino]phenylamine [C<sub>1p(S)</sub>]:** A thionyl chloride (10 mL) solution of **1pA(S)** (220 mg, 0.34 mmol) was refluxed for 6 h, and the reaction mixture was evaporated to dryness. To a NMP solution (20 mL) of the residue were successively added a mixture of tris(4-aminophenyl)amine (25 mg, 0.085 mmol), pyridine (2 mL) and excess LiCl was stirred for 2 h at 80 °C under a positive pressure of argon. The solution was poured into ethanol (100 mL) to precipitate of a white solid. The residue was chromatographed on silica gel with  $\text{CHCl}_3/\text{EtOH}$  (99/1 = v/v) as an eluent, where the second fraction was collected and evaporated to dryness. The residue was subjected to recycling preparative HPLC (YMC LC-forte/R) with  $\text{CHCl}_3$  as an eluent at a flow rate of  $10 \text{ mL min}^{-1}$ , where the first fraction was collected and evaporated to dryness under reduced pressure to give **C<sub>1p(S)</sub>** as white solid (67 mg, 0.031 mmol, 36%).  $^1\text{H NMR}$  (500 MHz,  $\text{CDCl}_3$ , 25 °C, TMS)  $\delta$  (ppm) = 7.81 (s, 3H), 7.50 (d,  $J = 8.6 \text{ Hz}$ , 26H), 7.06 (m, 12H), 4.04 (m, 18H), 1.92-1.67 (m, 18H), 1.58-1.42 (m, 18H), 1.40-1.12 (overlapped m, 114H), 0.93 (d,  $J = 6.3 \text{ Hz}$ , 9H), 0.88 (m, 36H);  $^{13}\text{C NMR}$  (125 MHz,  $\text{CDCl}_3$ , 25 °C, TMS)  $\delta$  (ppm) = 165.5, 153.2, 144.1, 141.4, 132.9, 129.8, 124.3, 121.5, 105.7, 71.8, 69.4, 39.3, 37.4, 31.9, 29.7-29.4, 28.0, 26.1, 24.7, 22.6, 19.5, 14.1. MALDI-TOF mass:  $m/z$  calculated, for compound **C<sub>1p(S)</sub>**  $[\text{M} + \text{H}]^+$ , 2175.78; Found:  $[\text{M} + \text{H}]^+$ , 2176.01.



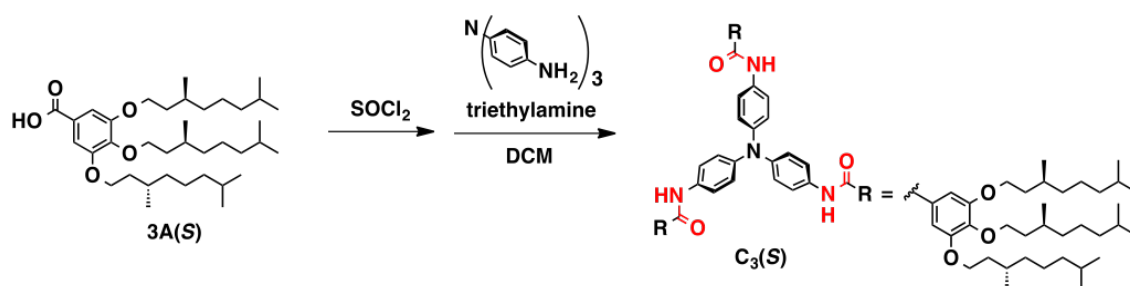
**Tris-[4-(4-[(*R*)-3,7-dimethyloctyl]oxy)-3,5-bis(dodecyloxy)benzoylamino**

**)phenyl]amine [C<sub>1p</sub>(*R*)]:** A thionyl chloride (10 mL) solution of **1pA(R)** (332 mg, 0.50 mmol) was refluxed for 6 h, and the reaction mixture was evaporated to dryness. To a NMP solution (20 mL) of the residue were successively added a mixture of tris(4-aminophenyl)amine (36 mg, 0.13 mmol), pyridine (2 mL) and excess LiCl was stirred for 2 h at 80 °C under a positive pressure of argon. The solution was poured into ethanol (100 mL) to precipitate of a white solid. The residue was chromatographed on silica gel with CHCl<sub>3</sub>/EtOH (99/1 = v/v) as an eluent, where the second fraction was collected and evaporated to dryness. The residue was subjected to recycling preparative HPLC (YMC LC-forte/R) with CHCl<sub>3</sub> as an eluent at a flow rate of 10 mL min<sup>-1</sup>, where the first fraction was collected and evaporated to dryness under reduced pressure to give **C<sub>1p</sub>(R)** as white solid (95 mg, 0.044 mmol, 34%). <sup>1</sup>H NMR (500 MHz, CDCl<sub>3</sub>, 25 °C, TMS) δ (ppm) = 7.69 (s, 3H), 7.50 (d, *J* = 8.6 Hz, 26H), 7.07 (m, 12H), 4.05 (m, 18H), 1.90-1.67 (m, 18H), 1.58-1.43 (m, 18H), 1.41-1.12 (overlapped m, 114H), 0.93 (d, *J* = 6.3 Hz, 9H), 0.88 (m, 36H); <sup>13</sup>C NMR (125 MHz, CDCl<sub>3</sub>, 25 °C, TMS) δ (ppm) = 165.5, 153.3, 144.2, 141.5, 133.0, 129.9, 124.4, 121.5, 105.8, 71.8, 69.5, 39.4, 37.5, 32.0, 29.7-29.4, 28.0, 26.1, 24.7, 22.7, 19.6, 14.1. MALDI-TOF mass: *m/z* calculated, for compound **C<sub>1p</sub>(R)** [M + H]<sup>+</sup>, 2175.78; Found: [M + H]<sup>+</sup>, 2175.79.



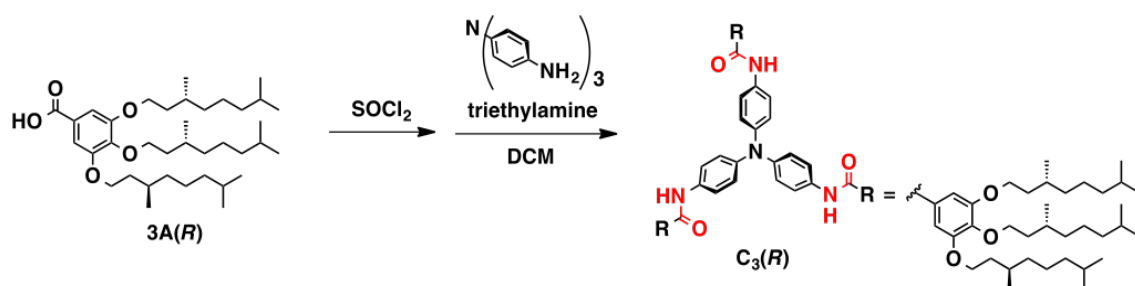
**Tris-[4-(3,5-Bis{[(S)-3,7-dimethyloctyl]oxy}-4-(dodecyloxy)benzoylamino**

**)phenyl]amine [C<sub>2m,m(S)</sub>]:** A thionyl chloride (10 mL) solution of **2m,mA(S)** (210 mg, 0.34 mmol) was refluxed for 6 h, and the reaction mixture was evaporated to dryness. To a NMP solution (20 mL) of the residue were successively added a mixture of tris(4-aminophenyl)amine (25 mg, 0.085 mmol), pyridine (2 mL) and excess LiCl was stirred for 2 h at 80 °C under a positive pressure of argon. The solution was poured into ethanol (100 mL) to precipitate of a white solid. The residue was chromatographed on silica gel with  $\text{CHCl}_3/\text{EtOH}$  (99/1 = v/v) as an eluent, where the second fraction was collected and evaporated to dryness. The residue was subjected to recycling preparative HPLC (YMC LC-forte/R) with  $\text{CHCl}_3$  as an eluent at a flow rate of  $10 \text{ mL min}^{-1}$ , where the first fraction was collected and evaporated to dryness under reduced pressure to give **C<sub>2m,m(S)</sub>** as white solid (98 mg, 0.048 mmol, 56%).  $^1\text{H NMR}$  (500 MHz,  $\text{CDCl}_3$ , 25 °C, TMS)  $\delta$  (ppm) = 7.86 (s, 3H), 7.50 (d,  $J = 9.2 \text{ Hz}$ , 6H), 7.06 (m, 12H), 4.02 (m, 18H), 1.91-1.43 (m, 36H), 1.41-1.08 (overlapped m, 74H), 0.93 (d,  $J = 6.9 \text{ Hz}$ , 18H), 0.87 (m, 45H);  $^{13}\text{C NMR}$  (125 MHz,  $\text{CDCl}_3$ , 25 °C, TMS)  $\delta$  (ppm) = 165.6, 153.2, 144.1, 141.4, 132.9, 129.8, 124.3, 121.6, 105.7, 73.5, 67.7, 39.2, 37.3, 36.3, 31.9, 30.3-29.4, 28.0, 26.1, 24.7, 22.6, 19.6, 14.1. MALDI-TOF mass:  $m/z$  calculated, for compound **C<sub>2m,m(S)</sub>**  $[\text{M} + \text{H}]^+$ , 2091.69; Found:  $[\text{M} + \text{H}]^+$ , 2091.97.



**Tris-[4-Tris(-3,4,5-[(S)-3,7-dimethyloctyl]oxy}benzoylamino)phenyl]**

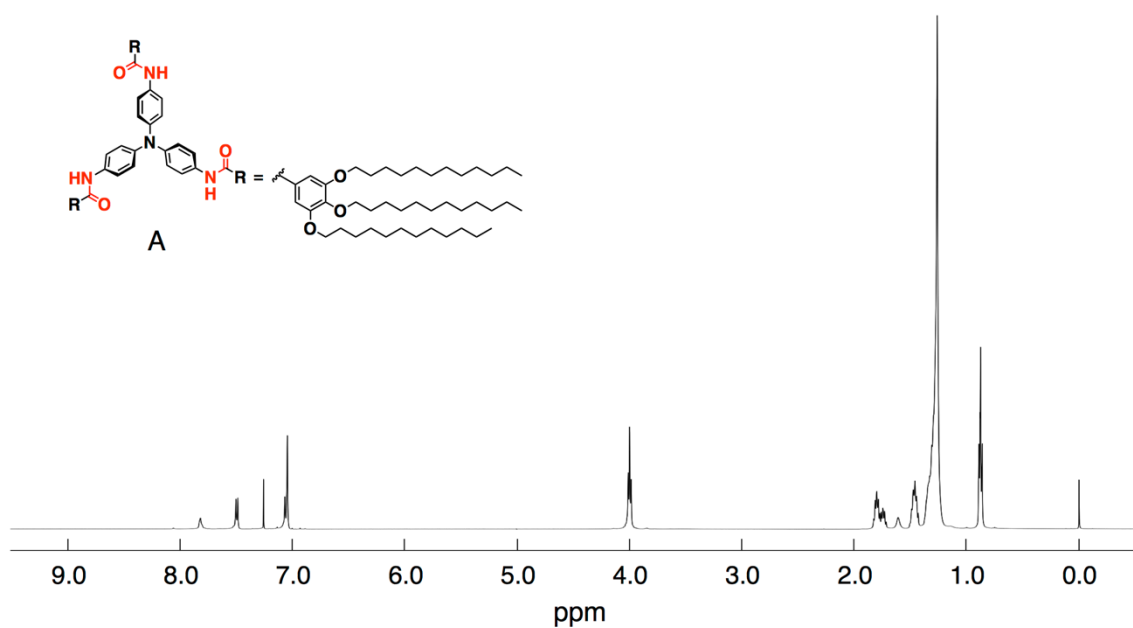
**amine [C<sub>3</sub>(S)]:** A thionyl chloride (30 mL) solution of 3A(S) (481 mg, 0.79 mmol) was refluxed for 6 h, and the reaction mixture was evaporated to dryness. To a NMP solution (30 mL) of the residue were successively added a mixture of tris(4-aminophenyl)amine (65 mg, 0.22 mmol), pyridine (3 mL) and excess LiCl was stirred for 2 h at 80 °C under a positive pressure of argon. The solution was poured into ethanol (150 mL) to precipitate of a white solid. The residue was chromatographed on silica gel with CHCl<sub>3</sub>/EtOH (99/1 = v/v) as an eluent, where the second fraction was collected and evaporated to dryness. The residue was subjected to recycling preparative HPLC (YMC LC-forte/R) with CHCl<sub>3</sub> as an eluent at a flow rate of 10 mL min<sup>-1</sup>, where the first fraction was collected and evaporated to dryness under reduced pressure to give C<sub>3</sub>(S) as white solid (212 mg, 0.11 mmol, 50%). <sup>1</sup>H NMR (500 MHz, CDCl<sub>3</sub>, 25 °C, TMS) δ (ppm) = 7.82 (s, 3H), 7.50 (d, *J* = 9.2 Hz, 6H), 7.07 (m, 12H), 4.05 (m, 18H), 1.92-1.46 (m, 36H), 1.41-1.08 (overlapped m, 54H), 0.93 (m, 27H), 0.87 (d, *J* = 6.3 Hz, 54H); <sup>13</sup>C NMR (125 MHz, CDCl<sub>3</sub>, 25 °C, TMS) δ (ppm) = 165.6, 153.2, 144.2, 141.4, 132.9, 129.8, 124.4, 121.6, 105.7, 71.8, 67.7, 39.3, 37.4, 36.3, 29.8, 29.6, 28.0, 24.7, 22.6, 19.6. MALDI-TOF mass: *m/z* calculated, for compound C<sub>3</sub>(S) [M + H]<sup>+</sup>, 2007.59; Found: [M + H]<sup>+</sup>, 2007.91.



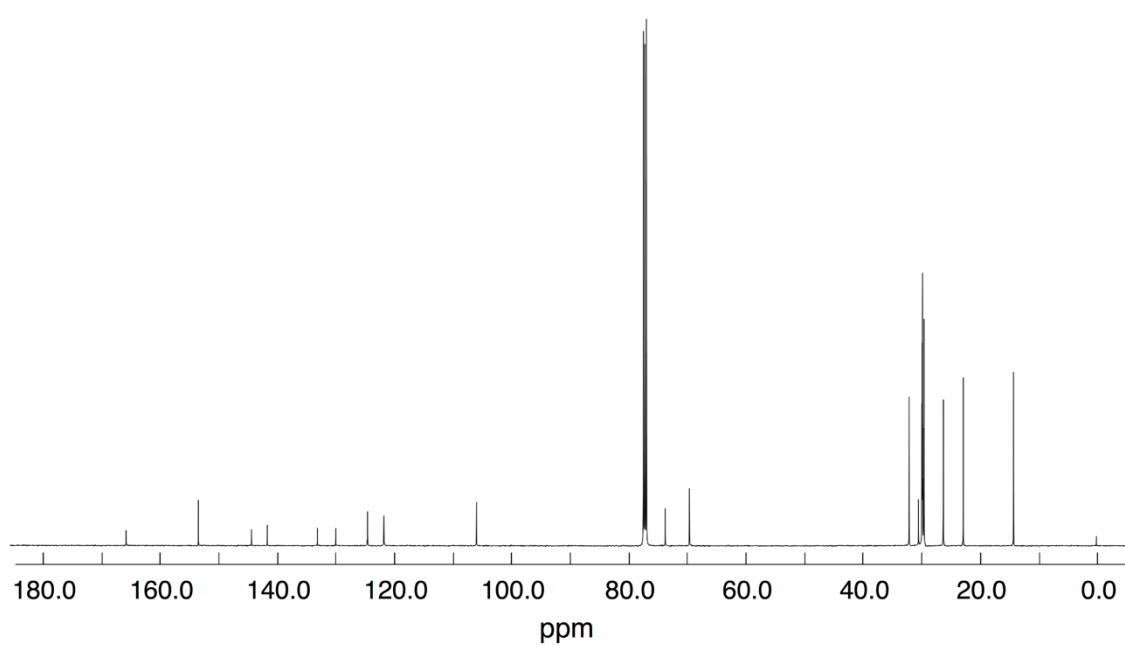
**Tris-[4-Tris(-3,4,5-[(*R*)-3,7-dimethyloctyl]oxy)benzoylamino)phenyl]**

**amine** [**C<sub>3</sub>(*R*)**]: A thionyl chloride (10 mL) solution of **3A(*R*)** (207 mg, 0.34 mmol) was refluxed for 6 h, and the reaction mixture was evaporated to dryness. To a NMP solution (20 mL) of the residue were successively added a mixture of tris(4-aminophenyl)amine (28 mg, 0.10 mmol), pyridine (2 mL) and excess LiCl was stirred for 2 h at 80 °C under a positive pressure of argon. The solution was poured into ethanol (100 mL) to precipitate of a white solid. The residue was chromatographed on silica gel with CHCl<sub>3</sub>/EtOH (99/1 = v/v) as an eluent, where the second fraction was collected and evaporated to dryness. The residue was subjected to recycling preparative HPLC (YMC LC-forte/R) with CHCl<sub>3</sub> as an eluent at a flow rate of 10 mL min<sup>-1</sup>, where the first fraction was collected and evaporated to dryness under reduced pressure to give **C<sub>3</sub>(*R*)** as white solid (109 mg, 0.054 mmol, 54%). <sup>1</sup>H NMR (500 MHz, CDCl<sub>3</sub>, 25 °C, TMS) δ (ppm) = 7.68 (s, 3H), 7.51 (d, *J* = 9.2 Hz, 6H), 7.08 (m, 12H), 4.05 (m, 18H), 1.87-1.47 (m, 36H), 1.42-1.09 (overlapped m, 54H), 0.94 (m, 27H), 0.86 (d, *J* = 6.3 Hz, 54H); <sup>13</sup>C NMR (125 MHz, CDCl<sub>3</sub>, 25 °C, TMS) δ (ppm) = 165.5, 153.3, 144.3, 141.5, 132.9, 129.8, 124.4, 121.5, 105.7, 71.8, 67.8, 39.3, 37.4, 36.4, 29.8, 29.6, 28.0, 24.7, 22.6, 19.6. MALDI-TOF mass: *m/z* calculated, for compound **C<sub>3</sub>(*R*)** [**M + H**]<sup>+</sup>, 2007.59; Found: [**M + H**]<sup>+</sup>, 2007.65.

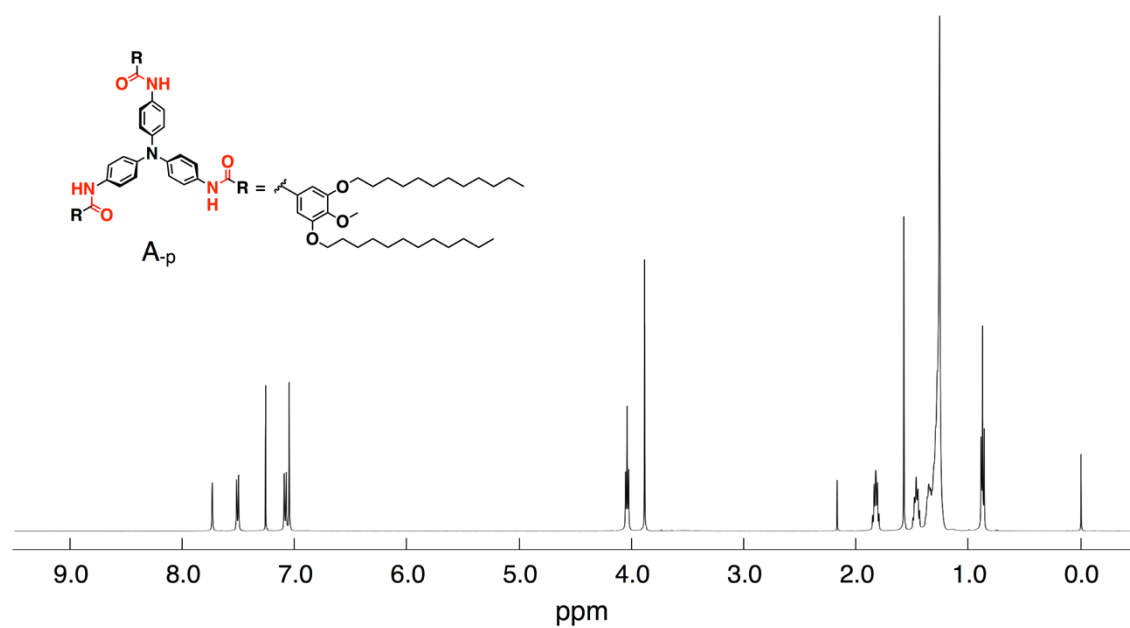




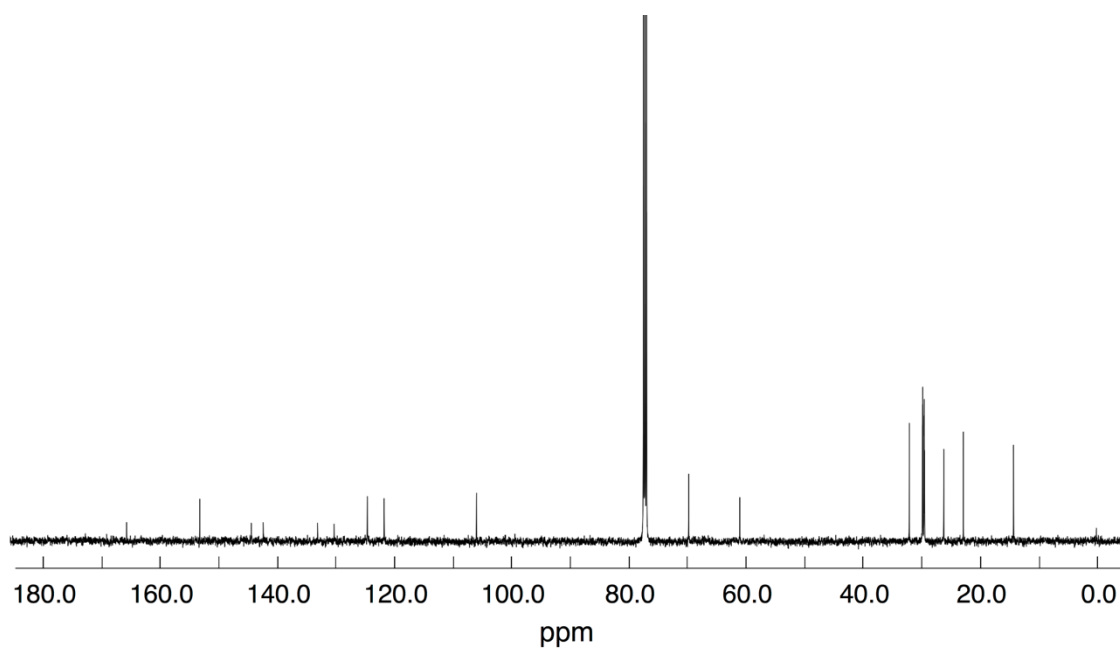
**Figure 2.1** (a)  $^1\text{H}$  NMR spectrum (500 MHz) of **A** in  $\text{CDCl}_3$  at 25 °C.



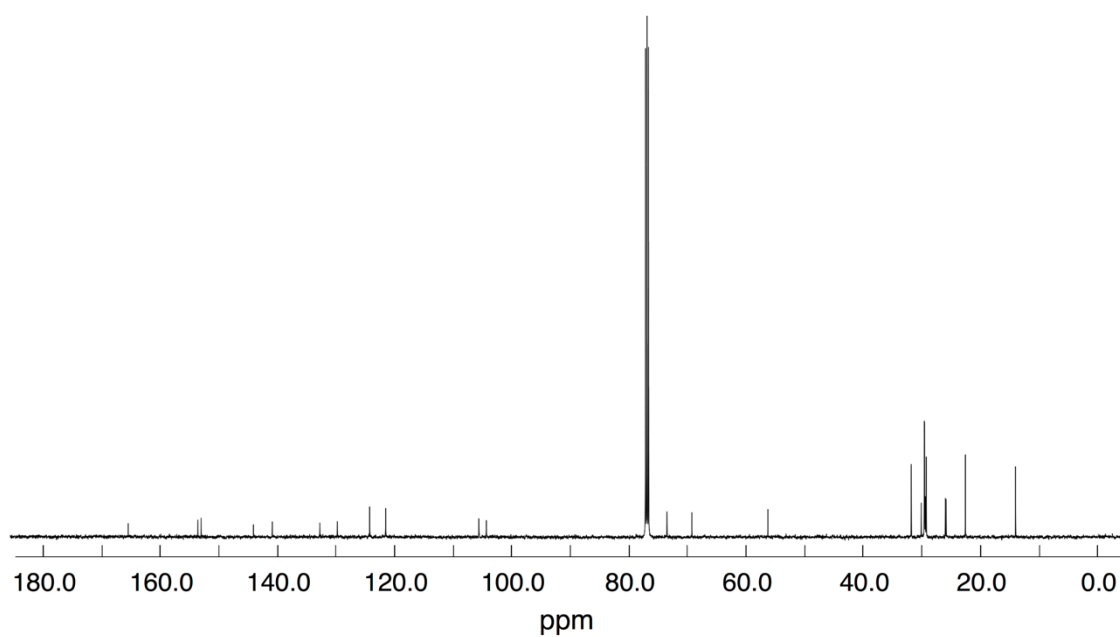
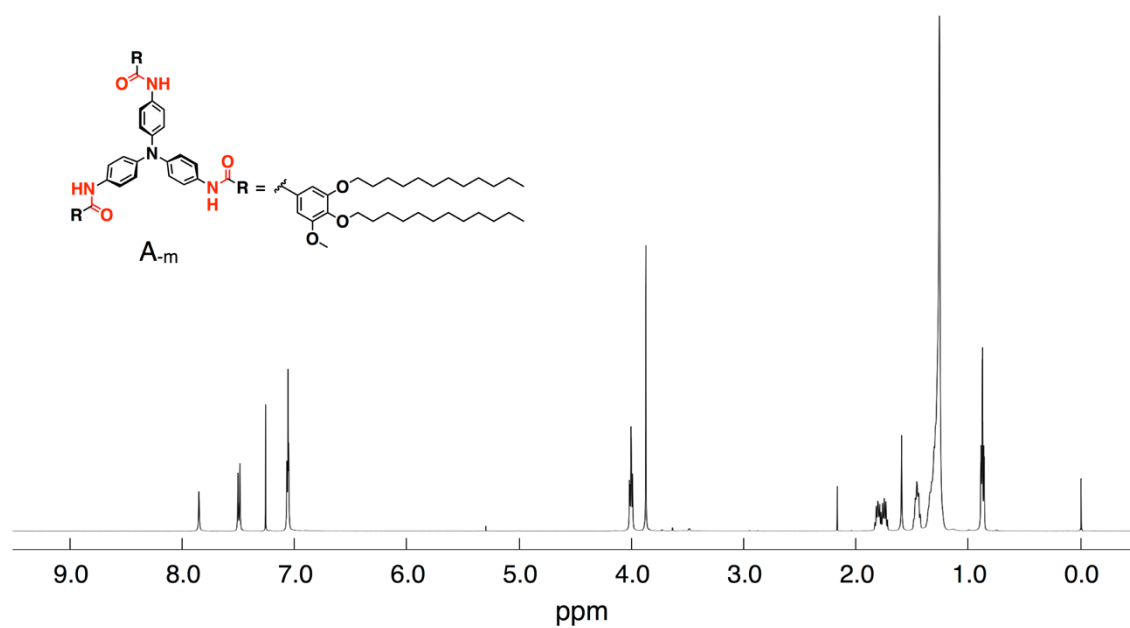
**Figure 2.1** (b)  $^{13}\text{C}$  NMR spectrum (125 MHz) of **A** in  $\text{CDCl}_3$  at 25 °C.



**Figure 2.2** (a) <sup>1</sup>H NMR spectrum (500 MHz) of **A<sub>p</sub>** in CDCl<sub>3</sub> at 25 °C.



**Figure 2.2** (b) <sup>13</sup>C NMR spectrum (125 MHz) of **A<sub>p</sub>** in CDCl<sub>3</sub> at 25 °C.



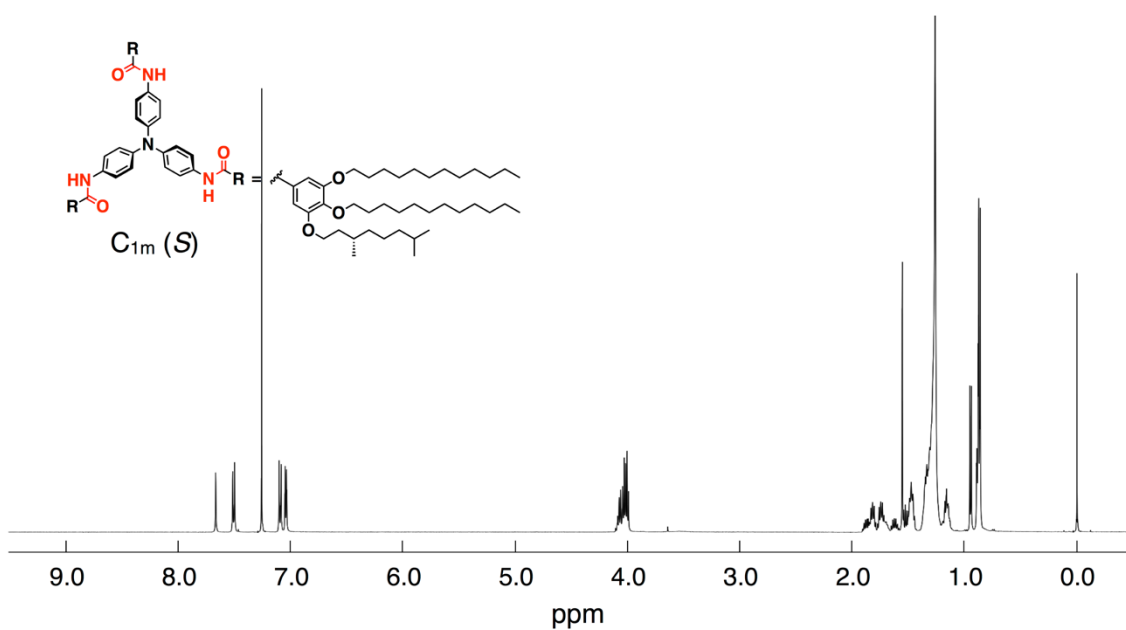


**Figure 2.4** (a)  $^1H$  NMR spectrum (500 MHz) of  $C_{1m}(S)$  in  $CDCl_3$  at 25 °C.

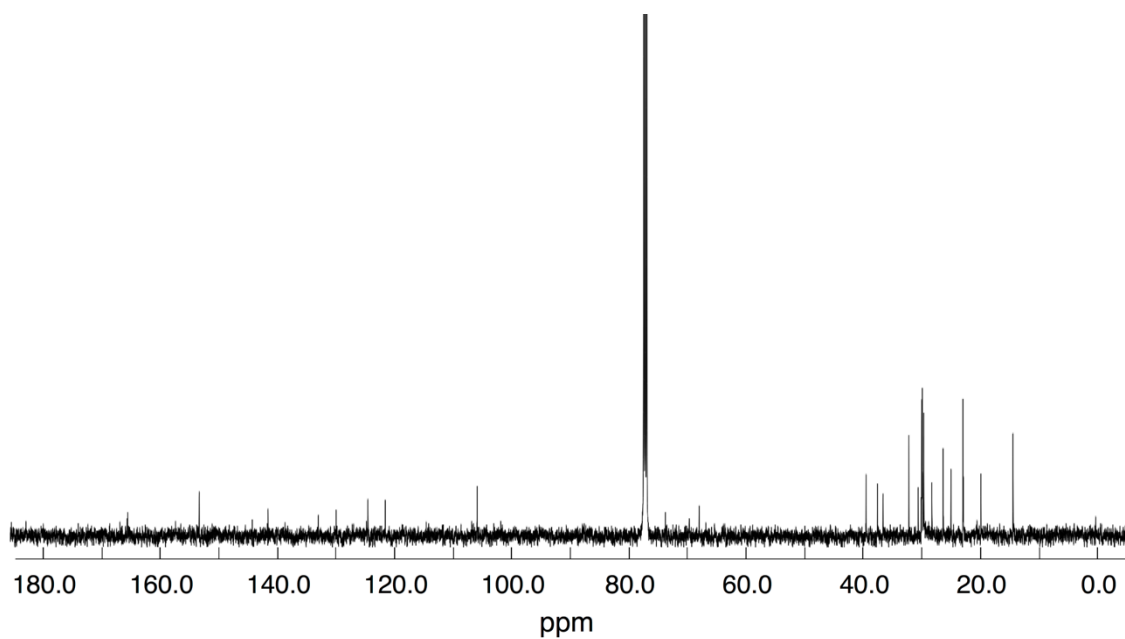


**Figure 2.4** (b)  $^{13}C$  NMR spectrum (125 MHz) of  $C_{1m}(S)$  in  $CDCl_3$  at 25 °C.

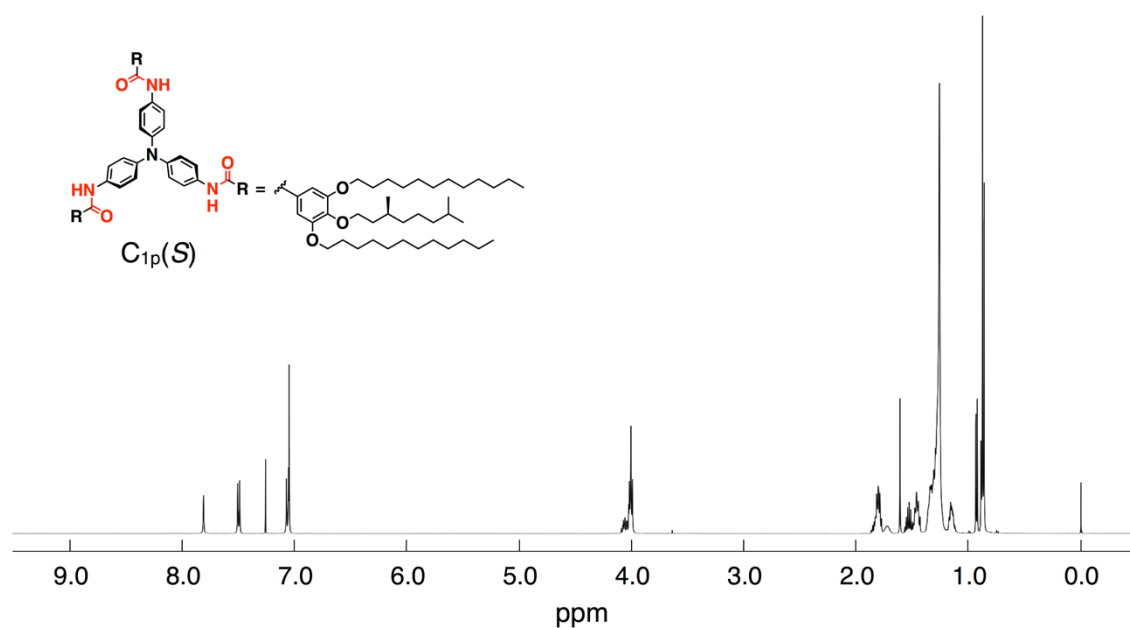


**Figure 2.5** (a)  $^1H$  NMR spectrum (500 MHz) of  $C_{1p}(S)$  in  $CDCl_3$  at 25 °C.

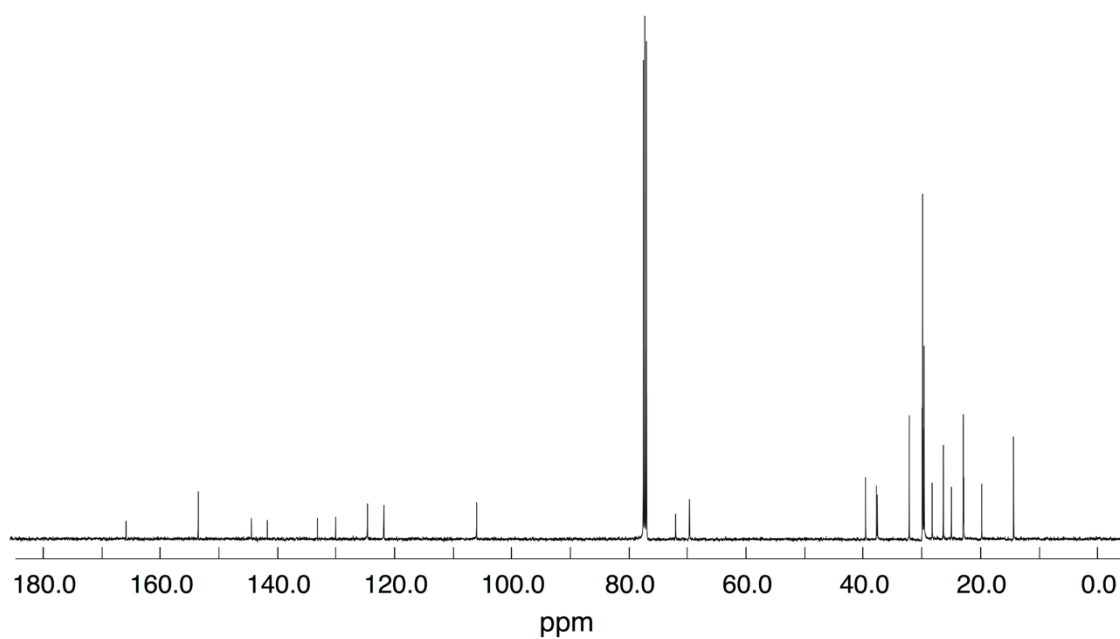


**Figure 2.5** (b)  $^{13}C$  NMR spectrum (125 MHz) of  $C_{1p}(S)$  in  $CDCl_3$  at 25 °C.

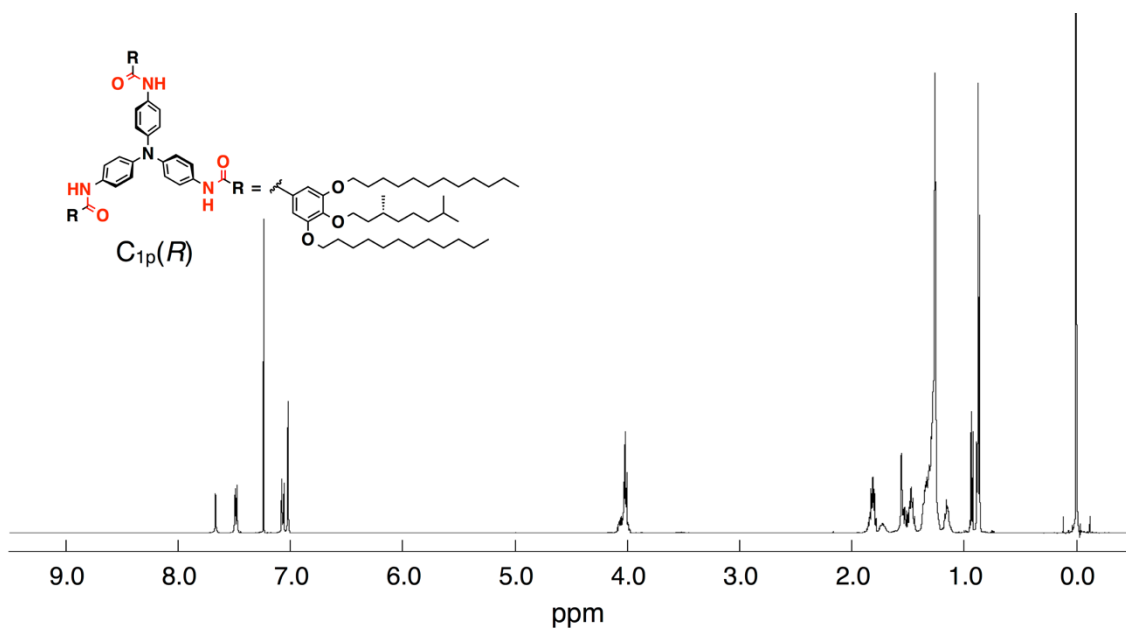


**Figure 2.6** (a)  $^1H$  NMR spectrum (500 MHz) of  $C_{1p}(R)$  in  $CDCl_3$  at 25 °C.

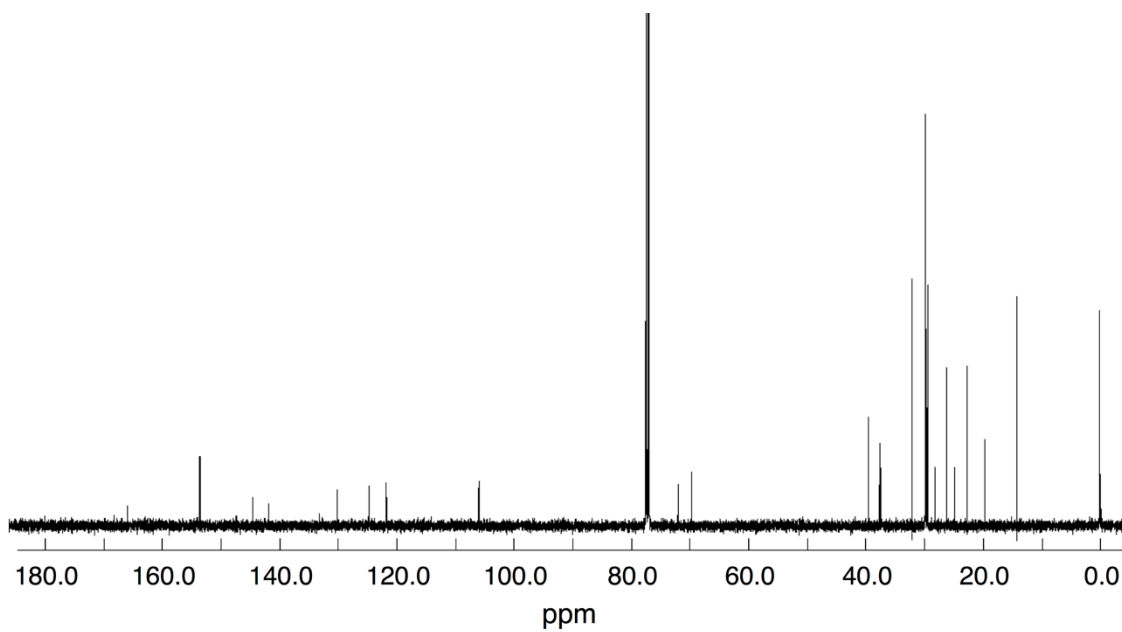


**Figure 2.6** (b)  $^{13}C$  NMR spectrum (125 MHz) of  $C_{1p}(R)$  in  $CDCl_3$  at 25 °C.

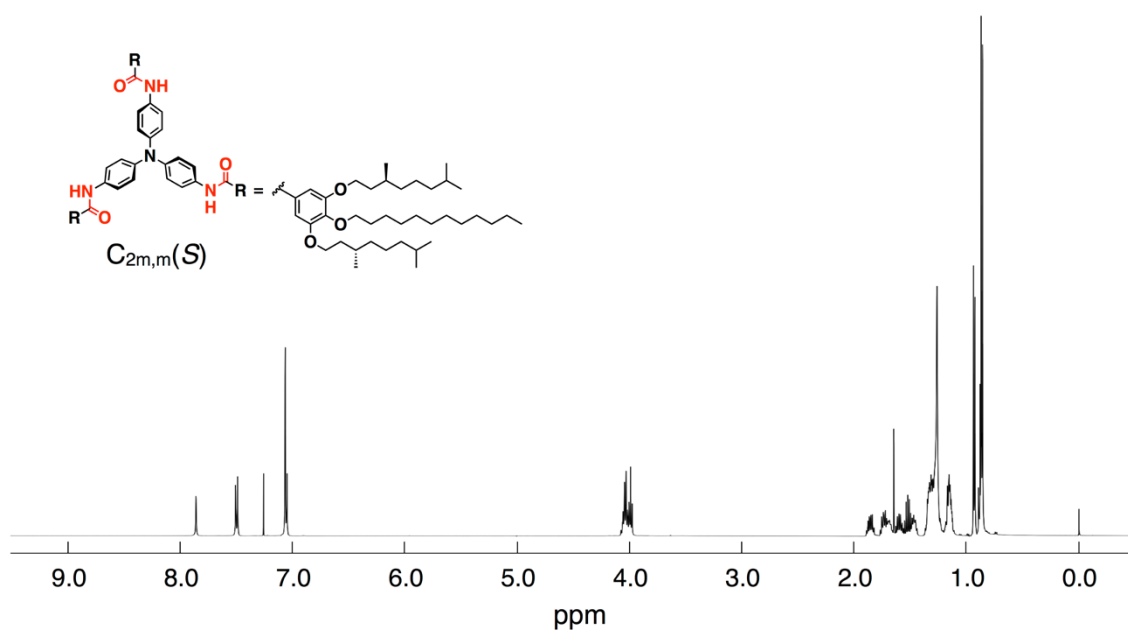


**Figure 2.7** (a)  $^1H$  NMR spectrum (500 MHz) of  $C_{2m,m}(S)$  in  $CDCl_3$  at 25 °C.

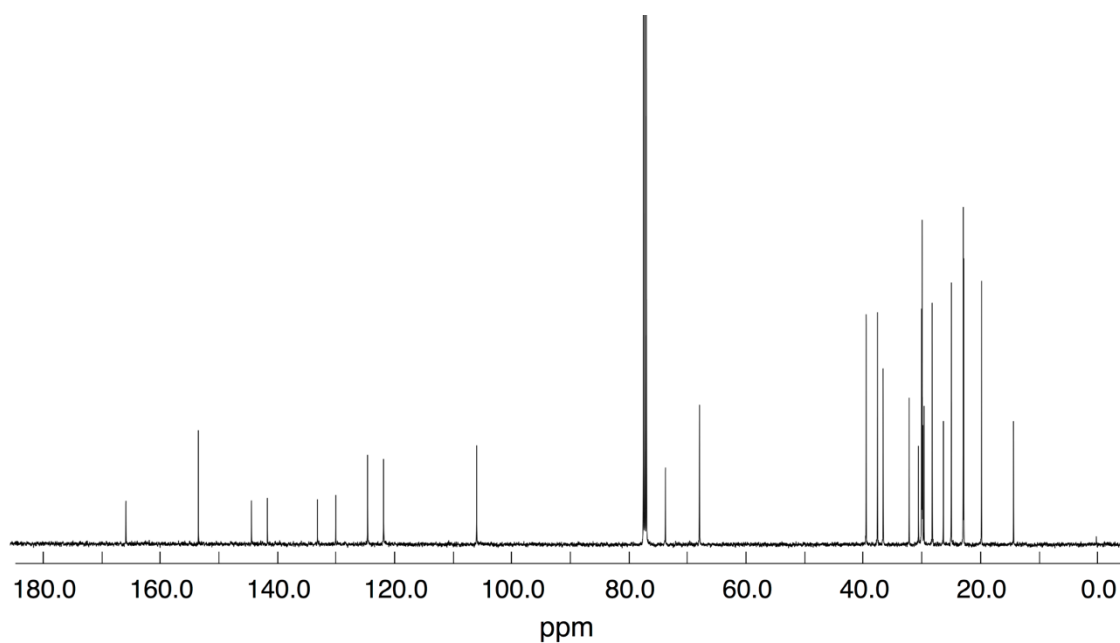


**Figure 2.7** (b)  $^{13}C$  NMR spectrum (125 MHz) of  $C_{2m,m}(S)$  in  $CDCl_3$  at 25 °C.

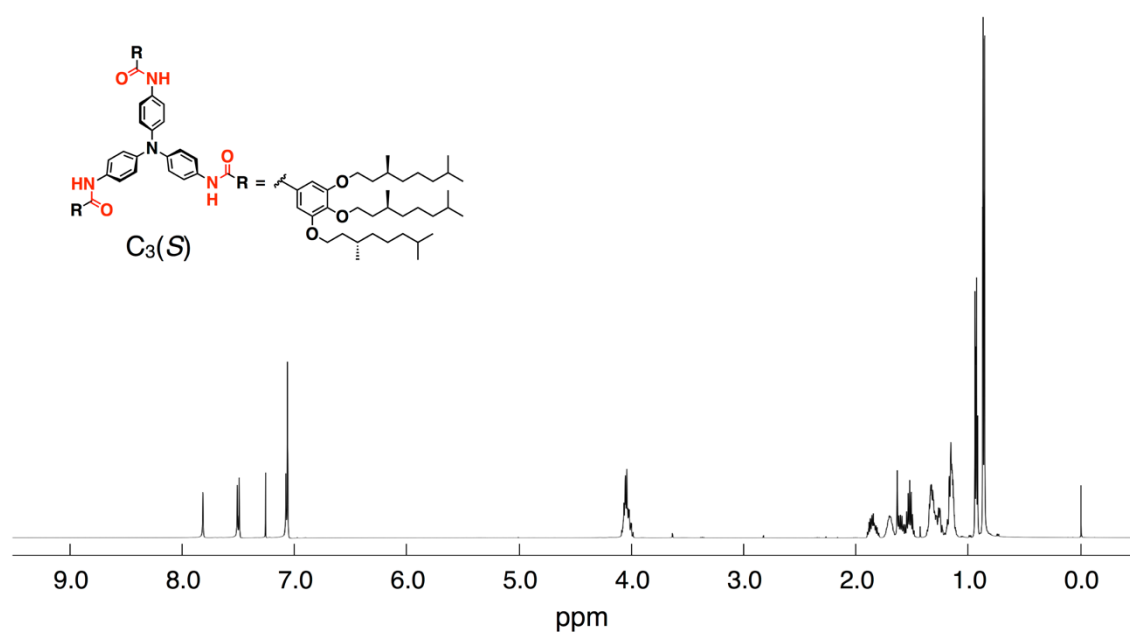


**Figure 2.8** (a)  $^1H$  NMR spectrum (500 MHz) of  $C_3(S)$  in  $CDCl_3$  at 25 °C.

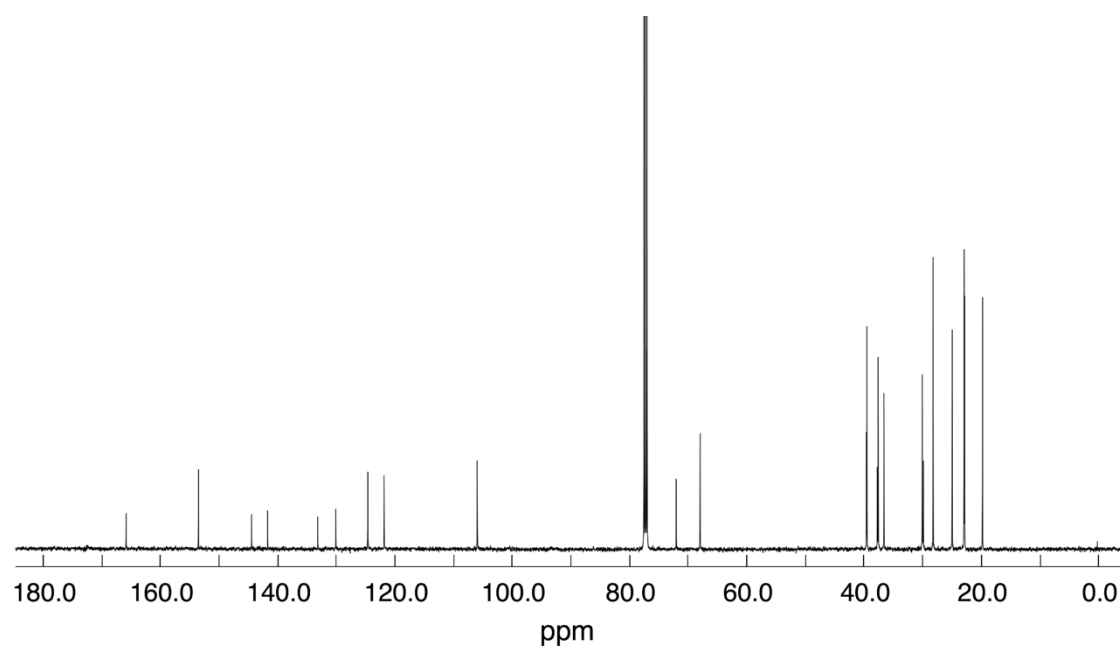


**Figure 2.8** (b)  $^{13}C$  NMR spectrum (125 MHz) of  $C_3(S)$  in  $CDCl_3$  at 25 °C.



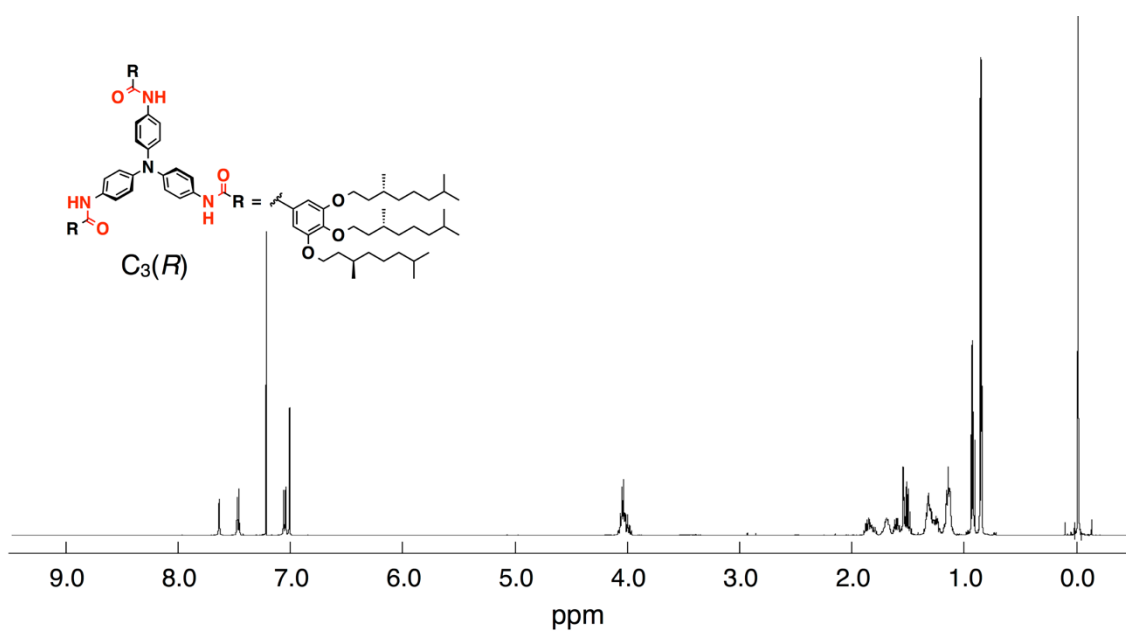


**Figure 2.9** (a)  $^1H$  NMR spectrum (500 MHz) of  $C_3(R)$  in  $CDCl_3$  at 25 °C.

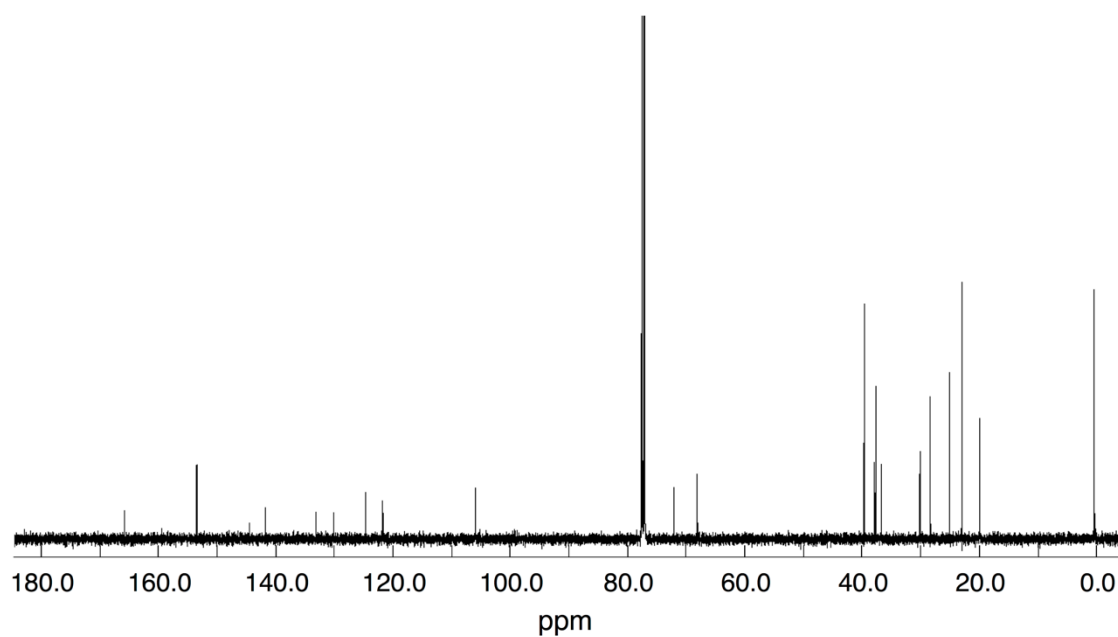


**Figure 2.9** (b)  $^{13}C$  NMR spectrum (125 MHz) of  $C_3(R)$  in  $CDCl_3$  at 25 °C.

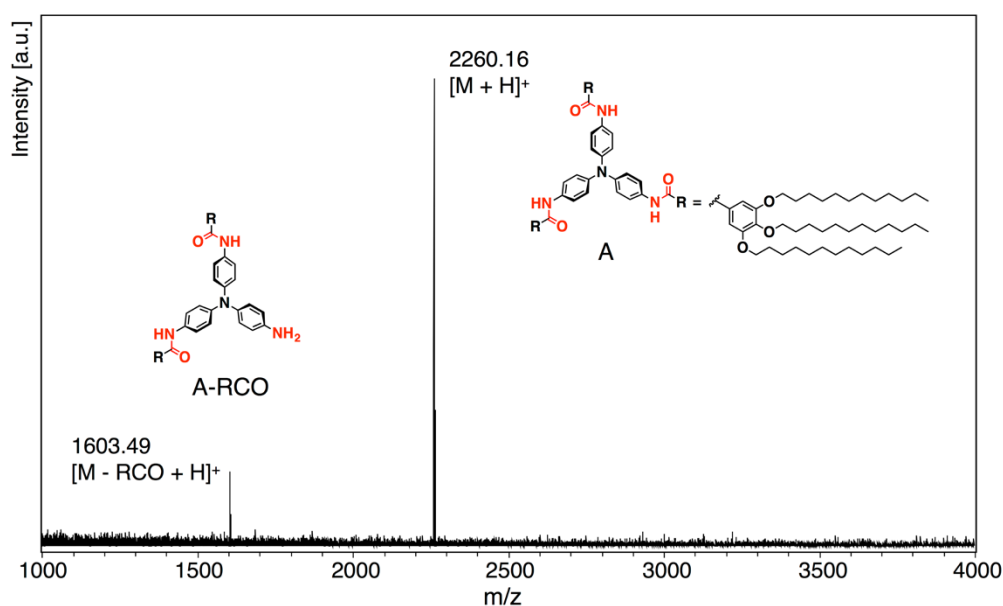


**Figure 2.10** MALDI-TOF-MS spectrum of **A** using CHCA as a matrix. The peak due to  $[M - RCO + H]^+$  became more intense when a larger laser power was applied. Therefore, the laser power was adjusted to be as small as possible in order to avoid fragmentation.

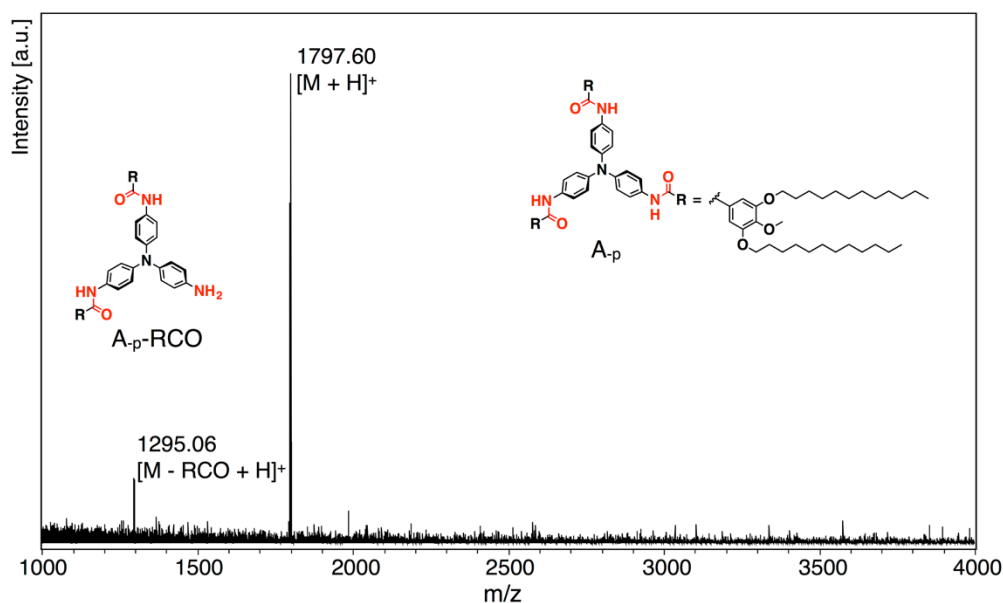


**Figure 2.11** MALDI-TOF-MS spectrum of **A<sub>p</sub>** using CHCA as a matrix. The peak due to  $[M - RCO + H]^+$  became more intense when a larger laser power was applied. Therefore, the laser power was adjusted to be as small as possible in order to avoid fragmentation.

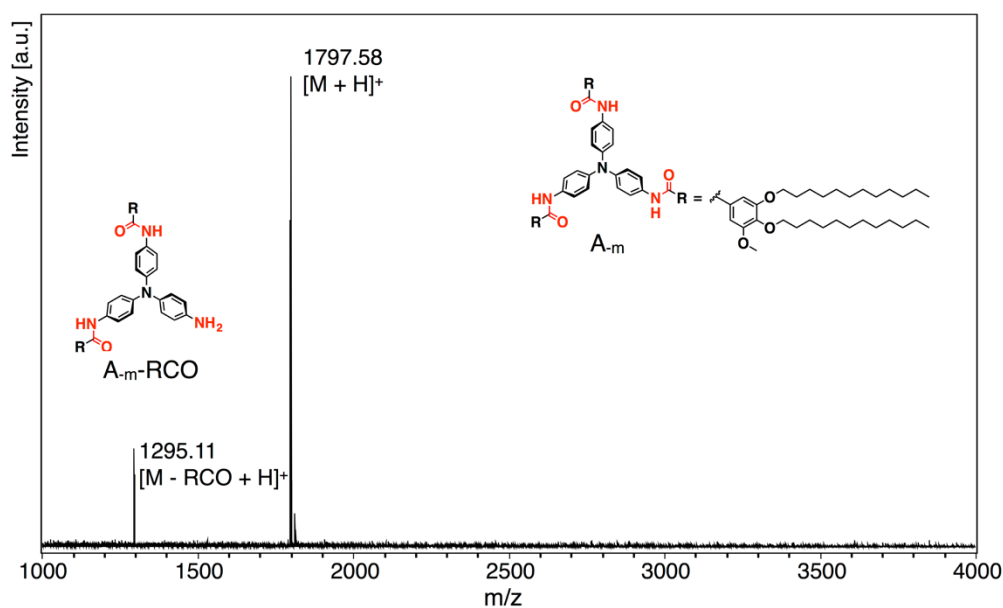


**Figure 2.12** MALDI-TOF-MS spectrum of  $A_m$  using CHCA as a matrix. The peak due to  $[M - RCO + H]^+$  became more intense when a larger laser power was applied. Therefore, the laser power was adjusted to be as small as possible in order to avoid fragmentation.

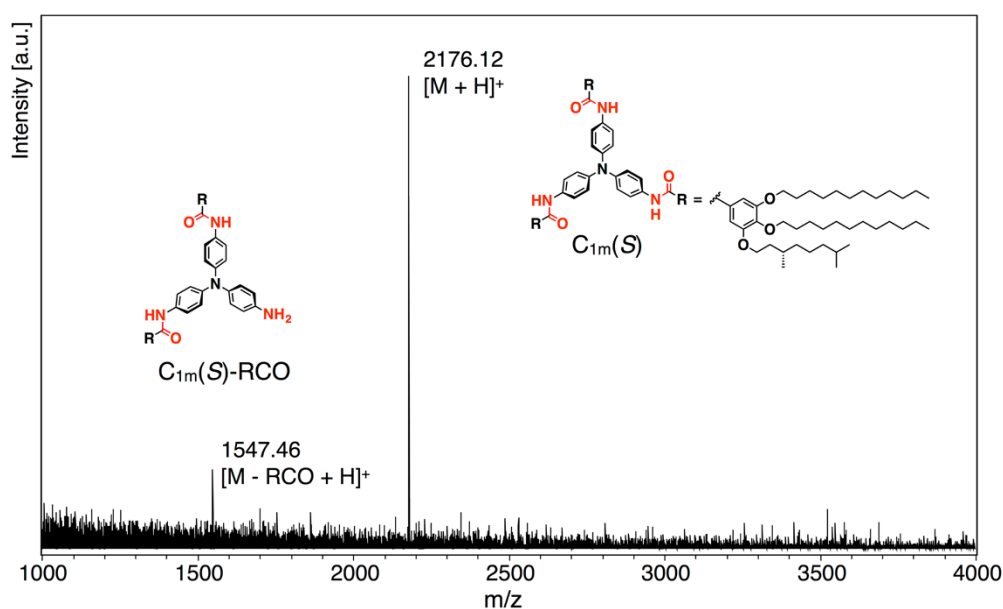


**Figure 2.13** MALDI-TOF-MS spectrum of  $C_{1m}(S)$  using CHCA as a matrix. The peak due to  $[M - RCO + H]^+$  became more intense when a larger laser power was applied. Therefore, the laser power was adjusted to be as small as possible in order to avoid fragmentation.

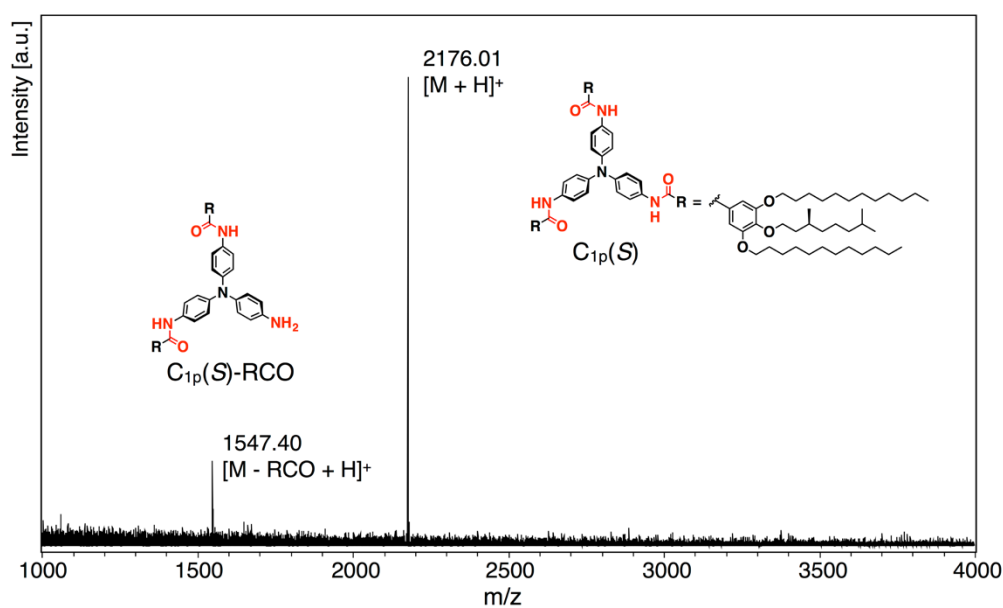


**Figure 2.14** MALDI-TOF-MS spectrum of  $C_{1p}(S)$  using CHCA as a matrix. The peak due to  $[M - RCO + H]^+$  became more intense when a larger laser power was applied. Therefore, the laser power was adjusted to be as small as possible in order to avoid fragmentation.

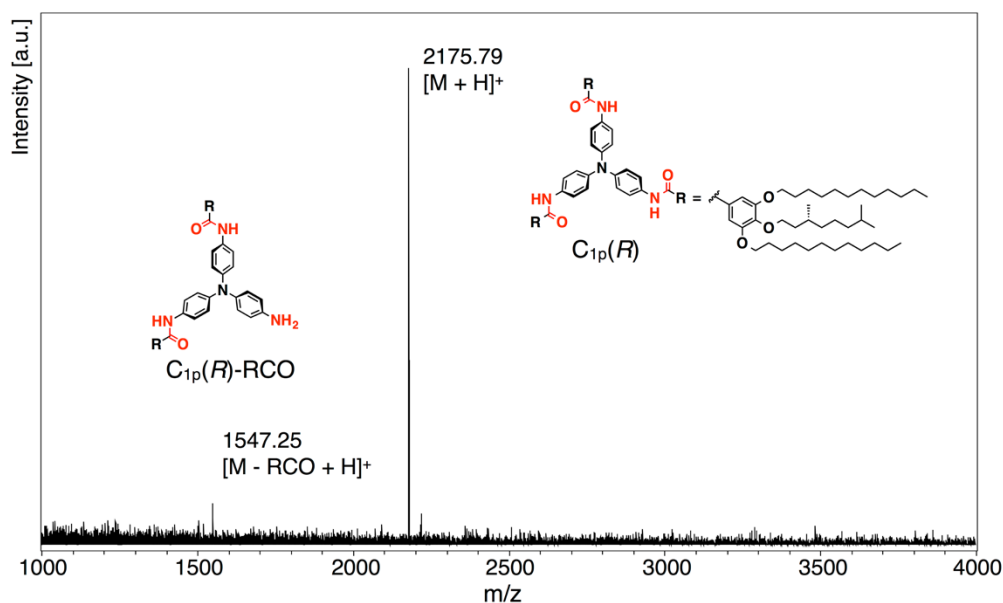


**Figure 2.15** MALDI-TOF-MS spectrum of  $C_{1p}(R)$  using CHCA as a matrix. The peak due to  $[M - RCO + H]^+$  became more intense when a larger laser power was applied. Therefore, the laser power was adjusted to be as small as possible in order to avoid fragmentation.

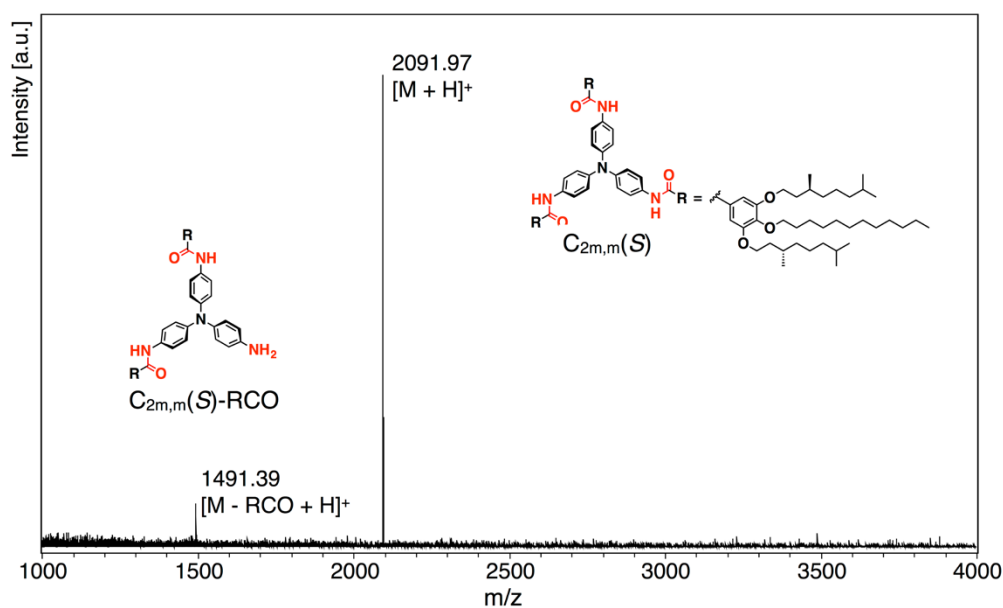


**Figure 2.16** MALDI-TOF-MS spectrum of  $C_{2m,m}(S)$  using CHCA as a matrix. The peak due to  $[M - RCO + H]^+$  became more intense when a larger laser power was applied. Therefore, the laser power was adjusted to be as small as possible in order to avoid fragmentation.

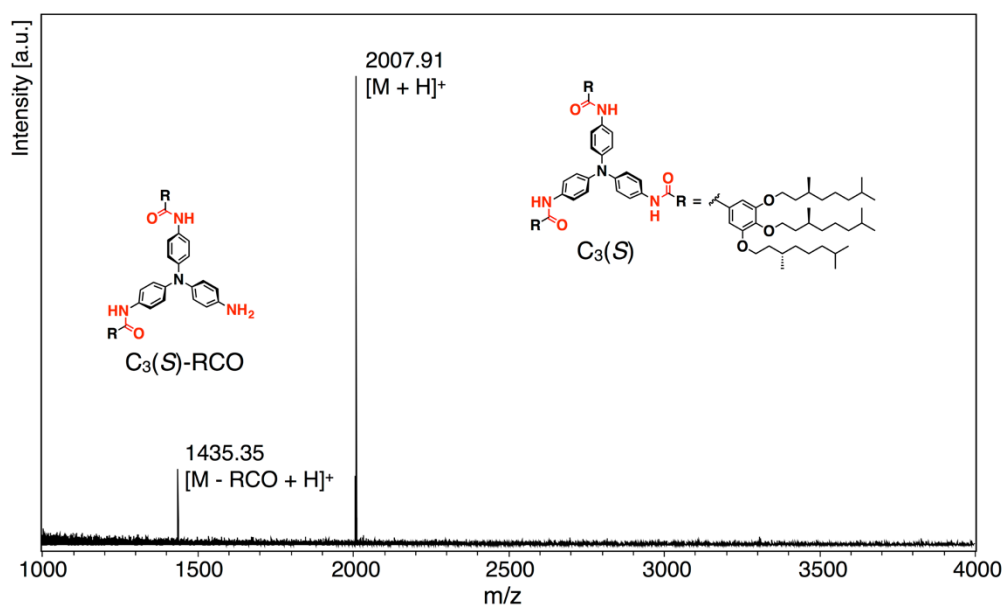


**Figure 2.17** MALDI-TOF-MS spectrum of  $C_3(S)$  using CHCA as a matrix. The peak due to  $[M - RCO + H]^+$  became more intense when a larger laser power was applied. Therefore, the laser power was adjusted to be as small as possible in order to avoid fragmentation.

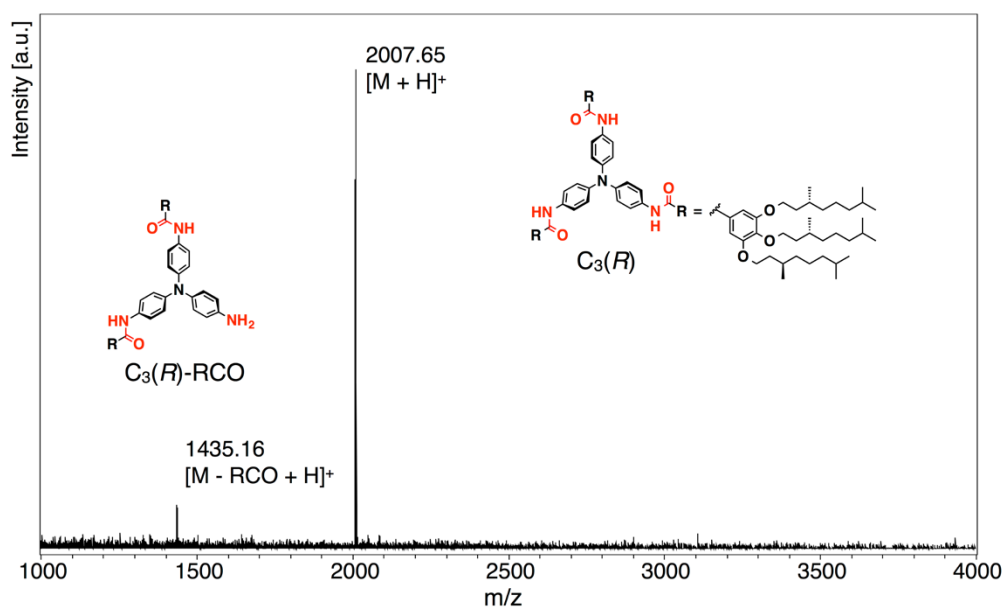


**Figure 2.18** MALDI-TOF-MS spectrum of  $C_3(R)$  using CHCA as a matrix. The peak due to  $[M - RCO + H]^+$  became more intense when a larger laser power was applied. Therefore, the laser power was adjusted to be as small as possible in order to avoid fragmentation.

## 2.3 References

- (1) P. Nguyen, L. Douce, R. Ziessel, *Tetrahedron Lett.*, **2002**, *43*, 5441-5444.
- (2) S. Ghosh, X.-Q. Li, V. Stepanenko, F. Würthner. *Chem. Eur. J.* **2008**, *14*, 11343-11357.
- (3) H. Tamiaki, K. Ogawa, K. Enomoto, K. Taki, A. Hotta, K. Toma, *Tetrahedron* **2010**, *66*, 1661–1666.
- (4) J. van Gestel, A. R. A. Palmans, B. Titulaer, J. A. J. M. Vekemans, E. W. Meijer, *J. Am. Chem. Soc.* **2005**, *127*, 5490–5494.
- (5) F. Vera, R. M. Tejedor, P. Romero, J. Barberá, M. B. Ros, J. L. Serrano, T. Sierra, *Angew. Chem. Int. Ed.* **2007**, *46*, 1873-1877.
- (6) R. Abbel, M. Wolffs, R. A. A. Bovee, J. L. J. Dongen, X.Lou, O. Henze, W. J. Feast, E. W. Meijer, A. P. H. J. Schenning, *Adv. Mater.* **2009**, *21*, 597-602





## **Chapter 3**

### **Amplification of supramolecular chirality in a self-assembly of propeller-shaped TPA derivatives**



### **3.1 Introduction**

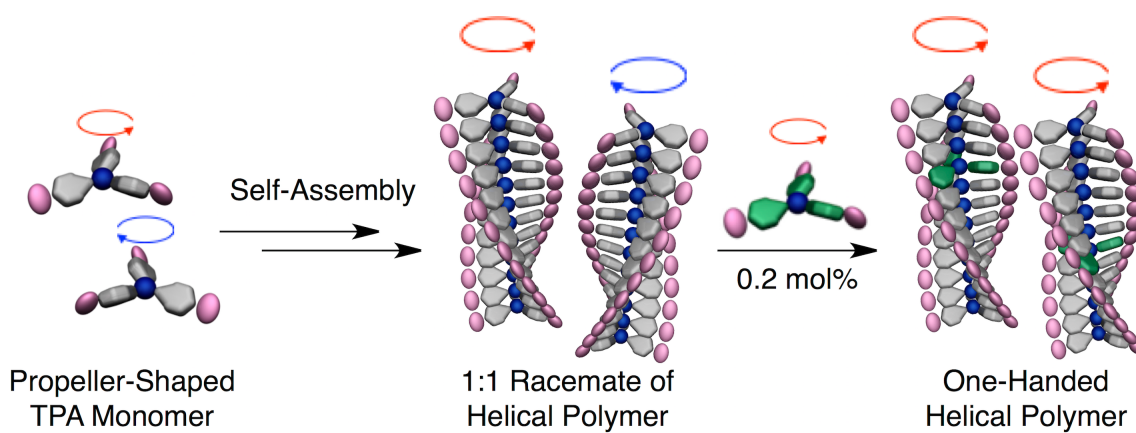
The helix has attracted wide attention of material scientists owing to its vital roles in biological systems and the potential for practical applications such as chiral separation or asymmetric catalysis as well as its structural beauty.<sup>1-11</sup> The helix is intrinsically chiral and can be either left- and right-handed. Hence, in order to take the best of their potential, it is important to selectively synthesize or isolate one-handed helices. For this purposes, it is the most simple and established method that to introduce chiral auxiliaries into helical racemate at molecular and supramolecular levels.<sup>5,12-15</sup> Due to the presence of an extra chiral source, left- and right-handed helices become a diastereomer of each other and, as a result, one of two helices is selectively obtainable. On the other hand, such introductions of chiral auxiliaries alter the conformation of helices and their physical properties as well. Therefore, it is desirable to control the handedness of helices with a less amount of chiral auxiliaries in terms of helicity control. For example, some achiral monomers, giving a racemic mixture of both right- and left-handed helices through their polymerization, can be biased to one-handed helices via copolymerization with a small amount of chiral monomers. Because a small fraction of chiral monomers governs the chiral conformations of a large amount of achiral monomers, it is known as sergeant (chiral monomer) and soldier (achiral monomers) principle.<sup>14,25,26</sup> There are two important parameters to describe this phenomenon, which results in one-handed helices with a less amount of sergeants. One is mismatch penalty (MMP), which is an energetic penalty paid by a system when sergeants are incorporated in unpreferred helices. The other one is helical reversal penalty (HRP), correspond to the energetic barrier to invert the helicity of supramolecular helices. As these two parameters increase, helicity of the corresponding

helices can be controlled with a less amount of sergeants. As the best example of sergeant and soldier principle, some helical polymers, consisting of achiral monomers, are known to perfectly control their helicity only with chiral initiators. By realizing high MMP, the initiator surely controls the helicity of the dimers obtained by the initiation reaction, while large HRP allows for stereoselective polymerization of achiral monomers according to the helicity of the dimer. Because one chiral molecule (initiator) controls the chiral conformation of a large amount of achiral monomers, indicating that the degree of chiral amplification reaches many thousands.

On the other hand, the degree of chiral amplification for the sergeant and soldier principle of the dynamic supramolecular helices is not so high. Even though MMP of sergeant can be simply increased by introducing a large number of chiral side chains per sergeant, which not necessarily give high chiral amplification, possibly because they are not efficiently incorporated into the corresponding supramolecular helices due to the steric hindrance of chiral side chains. Therefore, in order to realize high chiral amplification for dynamic supramolecular helices, it is important to increase MMP without decreasing the association constant for the resultant assembly.

Here we report the unprecedentedly high amplification of supramolecular chirality in sergeants and soldiers system using a propeller-shaped aromatic core in which only one sergeant controls the supramolecular helices with 500 soldiers on average (Scheme 3.1). Through the systematic studies, we elucidated how such propeller conformation realized the high MMP with the stereogenic centers in their side chains. Furthermore, we have substantiated the hierarchy of sergeant molecules depending on the MMP. The unique features of propeller-shaped compounds could give a fresh insight into supramolecular chirality beyond that of conventional molecular

assemblies.



**Scheme 3.1.** Schematic illustration of the self-assembly of propeller-shaped TPA molecules and amplification of their supramolecular chirality.

### 3.2 Propeller conformation of TPA in supramolecular helices

This study began with simple curiosity on whether TPA, a propeller-shaped molecule, selectively adopts left- or right-handed conformation according to the handedness of supramolecular helices. For this purpose, I first performed the density functional theory (DFT) computational study,<sup>16,17</sup> to predict the optimal conformation of trimeric **A**<sub>1</sub>, a simplified model compound consisting of a propeller-shaped TPA as a core and three methoxylated benzamide groups (Figure 3.1a). As expected, the obtained DFT calculation result model supported that **A**<sub>1</sub> formed a helical trimer through intermolecular hydrogen bonding of the amides and all of TPA cores selectively adopted the same propeller chirality. Inspired by this result, I have synthesized the similar TPA derivatives (Figure 2.1) and investigated their self-assembling behavior in cyclohexane. The dynamic light scattering (DLS) measurements suggested that **A**<sub>12</sub> was molecularly dispersed in cyclohexane at 75 °C and formed supramolecular aggregates at low temperature (25 °C, Figure 3.1b). Although the absorption spectra of **A**<sub>12</sub> at 75 °C and at 25 °C were very similar to one another (Figure 3.1c), a characteristic valley in the spectra around 315 nm appeared at 55 °C on cooling process, indicating that formation of the supramolecular aggregates. A tapping-mode atomic force microscopy (AFM) measurement of the air-dried sample on a silicon wafer reveals that **A**<sub>12</sub> forms one-dimensional supramolecular polymers in cyclohexane possibly by connecting one another through the intermolecular hydrogen bondings together with  $\pi$ - $\pi$  interactions (Figure 3.1d). On the other hand, **C**<sub>3</sub>(**R**) exhibits the characteristic CD spectrum in cyclohexane with clear exciton splitting at 312 nm and 328 nm (Figure 3.2a). Furthermore, **C**<sub>3</sub>(**S**) gives the mirror image CD spectrum of that with **C**<sub>3</sub>(**R**) under the same condition, indicating that they formed one-

handed helices (Figure 3.2a). Considering the result of DFT calculation together with the similarity in the absorption spectra between  $A_{12}$  and  $C_3(S)$  of their assembled states (Figure 3.2), we concluded that  $A_{12}$  also forms supramolecular helices though they are a racemic mixture of left- and right-handed helices.

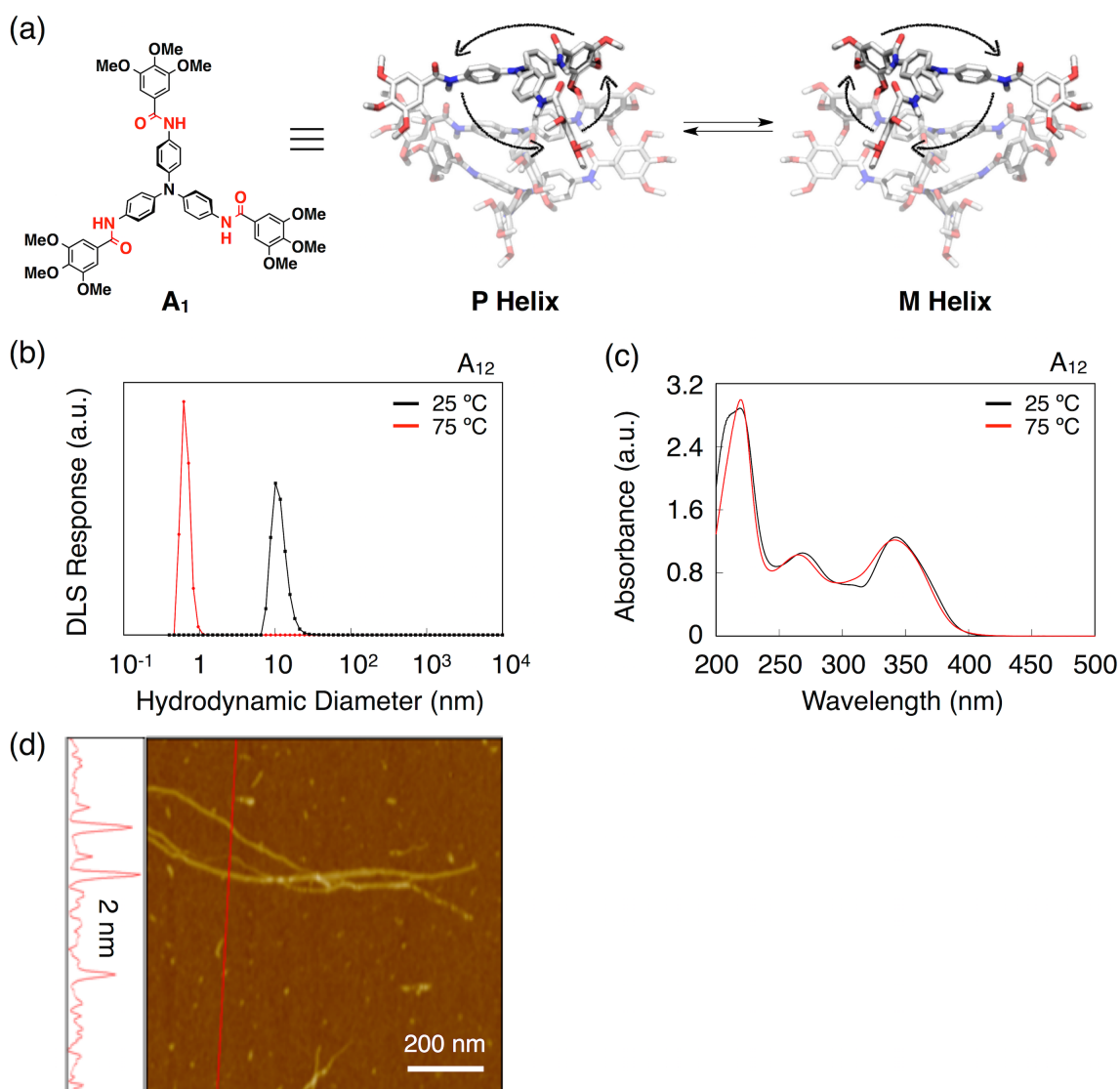


**Figure 3.1.** (a) Schematic representation of a possibly stacked structure in the supramolecular polymers. The molecular assembly model was optimized by DFT calculation. (b) UV/Vis absorption spectra for  $30 \mu\text{M}$  of  $A_{12}$  and, (c) Size distribution for  $100 \mu\text{M}$  of  $A_{12}$  in cyclohexane measured by dynamic light scattering (DLS) instrument at assembled state,  $25 \text{ }^\circ\text{C}$ , and at molecular dissolved state,  $75 \text{ }^\circ\text{C}$ , respectively.

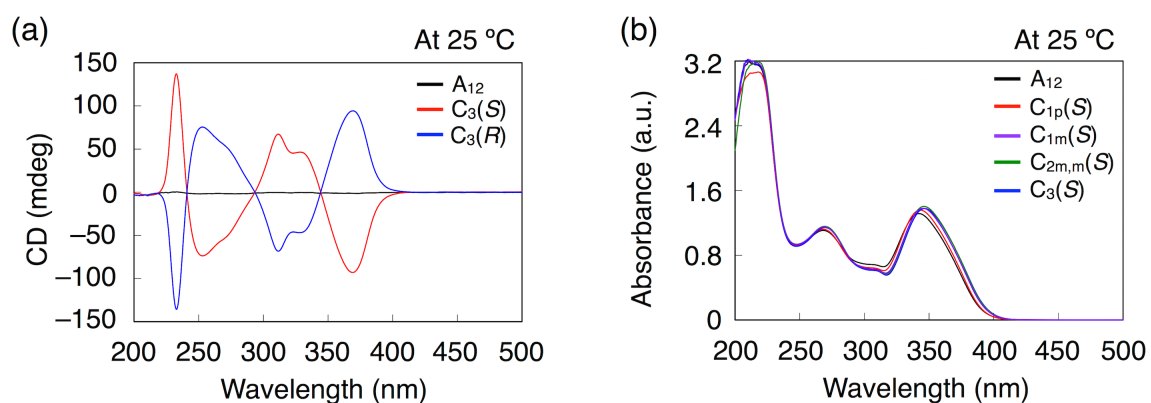


**Figure 3.2.** (a) Full CD absorption spectra for 30  $\mu$ M mixture of  $A_{12}$ ,  $C_3(R)$  and  $C_3(S)$  at 25 °C in cyclohexane. (a) Full UV/Vis absorption spectra for 30  $\mu$ M mixture of  $A_{12}$ ,  $C_{1p}(S)$ ,  $C_{1m}(S)$ ,  $C_{2m,m}(S)$  and  $C_3(S)$  at 25 °C in cyclohexane.



In order to scrutinize whether TPA core selectively adopts one of two propeller conformations according to the helicity of the supramolecular helices, we performed vibrational circular dichroism (VCD) measurements<sup>18-20</sup> of the methylcyclohexane solution of  $C_3(\mathbf{R})$  and  $C_3(\mathbf{S})$ , respectively. As shown in Figure 3.3a, they exhibited clear mirror images spectra of one another except for a few wavenumber ranges, highlighted in grey, due to the large absorption by solvents. The VCD peaks between  $1639\text{ cm}^{-1}$  and  $1584\text{ cm}^{-1}$  correspond with the stretching vibration of C=O bond and the bending vibration of N-H bond, respectively.<sup>18-22</sup> It suggests that the amide groups forms a helical array in the assembled state. Moreover, strong absorption bands with Cotton effect around  $1500\text{ cm}^{-1}$  correspond with the stretching vibration of the C=C double bonds of the aromatic groups of both TPA and the side chains.<sup>21,22</sup> Furthermore, the peaks at around  $1322\text{ cm}^{-1}$  and  $1242\text{ cm}^{-1}$  correspond to C-N stretching vibrational bands of the outer amine linked with TPA and the central amine presented in TPA, respectively. Those VCD data clearly suggests that the propeller chirality of TPA monomers are linked with the handedness of the supramolecular helices. However, only with these VCD spectra, it is difficult to exclude the possibility that the propeller chirality of TPA is decided by the side chain chirality. Hence, we performed VCD experiments of a mixed system with  $A_{12}/C_3(\mathbf{R})$  and  $A_{12}/C_3(\mathbf{S})$ , respectively, at the mole ratio of 9 to 1. As a result, we obtained almost identical VCD results to those with only  $C_3(\mathbf{R})$  and  $C_3(\mathbf{S})$ , indicating that TPA adopts a single propeller chirality according to the helicity of the supramolecular helices (Figure 3.3).

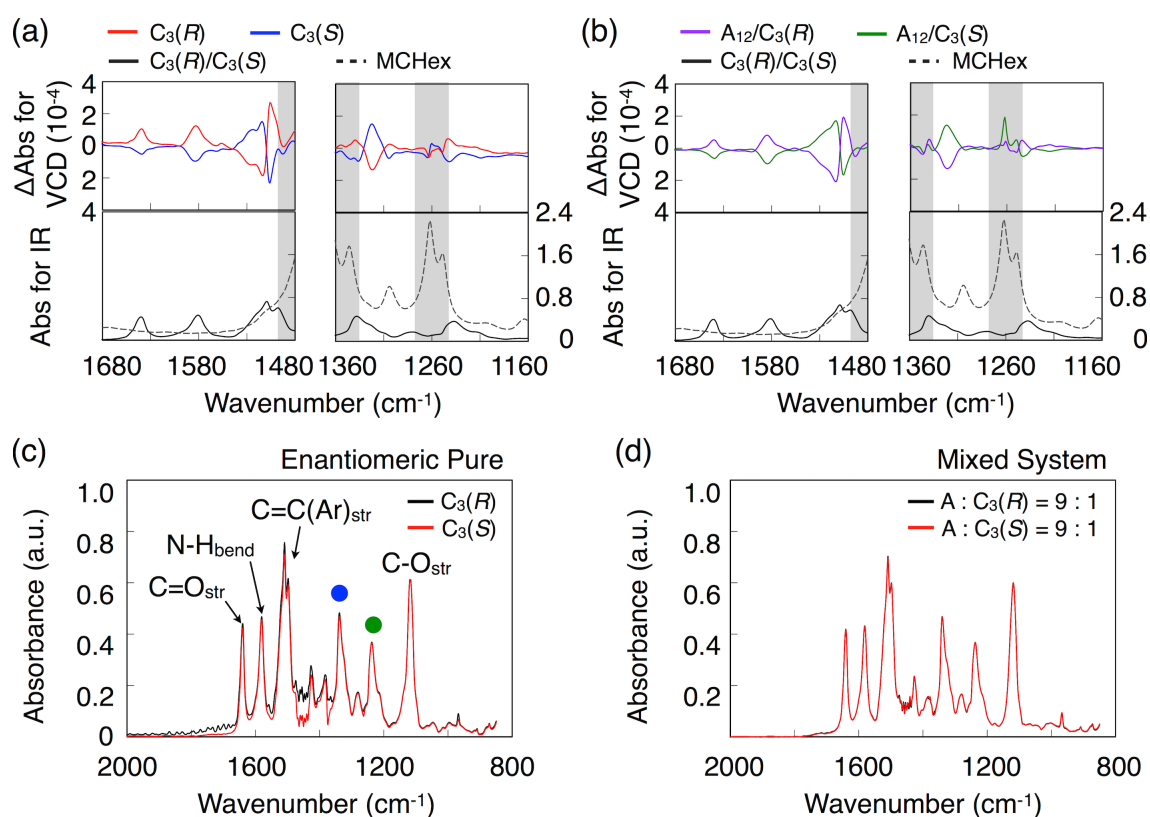


**Figure 3.3.** VCD (upper) and IR (lower) spectra at 20 °C for 5 mM of (a)  $C_3(R)$  and  $C_3(S)$ , and of (b)  $A_{12}$  with 10 mol%  $C_3(R)$  and  $A_{12}$  with 10 mol%  $C_3(S)$  in methylcyclohexane (MCHex), respectively. Dashed line displayed IR spectra of MCHex carrying interference because of high absorption. FT-IR spectra for 5 mM of (c) Enantiomeric Pure  $C_3(R)$  and  $C_3(S)$  and (d) 1:1 Mixture of  $A/C_3(R)$  and  $A/C_3(S)$  in methylcyclohexane at 25 °C. Stretching vibration bands at  $1322\text{ cm}^{-1}$  (blue) and  $1242\text{ cm}^{-1}$  (green) assigned C-N vibrational modes of the outer amine linked with TPA and the central amine presented in TPA, respectively. Each absorption band assigned according to previous report.

### 3.3 High amplification of supramolecular chirality

During a course of the above studies, we noticed that one-handed supramolecular helices of  $\mathbf{A}_{12}$  can be obtained with unusually a small fraction of  $\mathbf{C}_3(\mathbf{S})$ . In order to accurately estimate how small fraction of  $\mathbf{C}_3(\mathbf{S})$  can fully bias the helicity of the supramolecular helices of  $\mathbf{A}_{12}$ , I performed sergeants and soldiers experiment over various fraction of  $\mathbf{C}_3(\mathbf{S})$ . As shown in Figure 3.4a and 3.4b, the plots of CD intensities of the peak tops at 232, 253, 311, and 367 nm decreased as the fraction of  $\mathbf{C}_3(\mathbf{S})$  decreased with two characteristic features regardless of the peak top positions. The first feature is the minor change of the CD intensity around 40 mol% of fraction. The same feature was observed in the plots of electronic absorption at the same wavelengths (Figure 3.4d). Although the electronic absorption spectra of  $\mathbf{A}_{12}$  and  $\mathbf{C}_3(\mathbf{S})$  are almost identical to one another, the peak tops of  $\mathbf{C}_3(\mathbf{S})$  are red-shifted by 1 ~ 2 nm on average (Figure 3.4c), meaning that the helical conformation of the supramolecular helices of  $\mathbf{A}_{12}$  and  $\mathbf{C}_3(\mathbf{S})$  are slightly different. We assumed that a co-assembly of  $\mathbf{A}_{12}$  and  $\mathbf{C}_3(\mathbf{S})$  adopted a helical conformation similar to either homo-assembly of  $\mathbf{A}_{12}$  or that of  $\mathbf{C}_3(\mathbf{S})$ , and the transition of such helical conformation occurred around 40 mol% fraction of  $\mathbf{C}_3(\mathbf{S})$ , resulting in the observed discontinuous changes of  $g$ -values. The second feature is the drastic and discontinuous changes observed at very small fraction of  $\mathbf{C}_3(\mathbf{S})$  simply because the fraction of  $\mathbf{C}_3(\mathbf{S})$  was too small to fully bias the helicity of supramolecular helices of  $\mathbf{A}_{12}$ . Therefore, in the following studies, I used the plots of CD intensity at 252 nm normalized by the value at 20% fraction of  $\mathbf{C}_3(\mathbf{S})$ , because the absorption at 252 nm showed the minimum absorption change over the various fraction of  $\mathbf{C}_3(\mathbf{S})$ . To

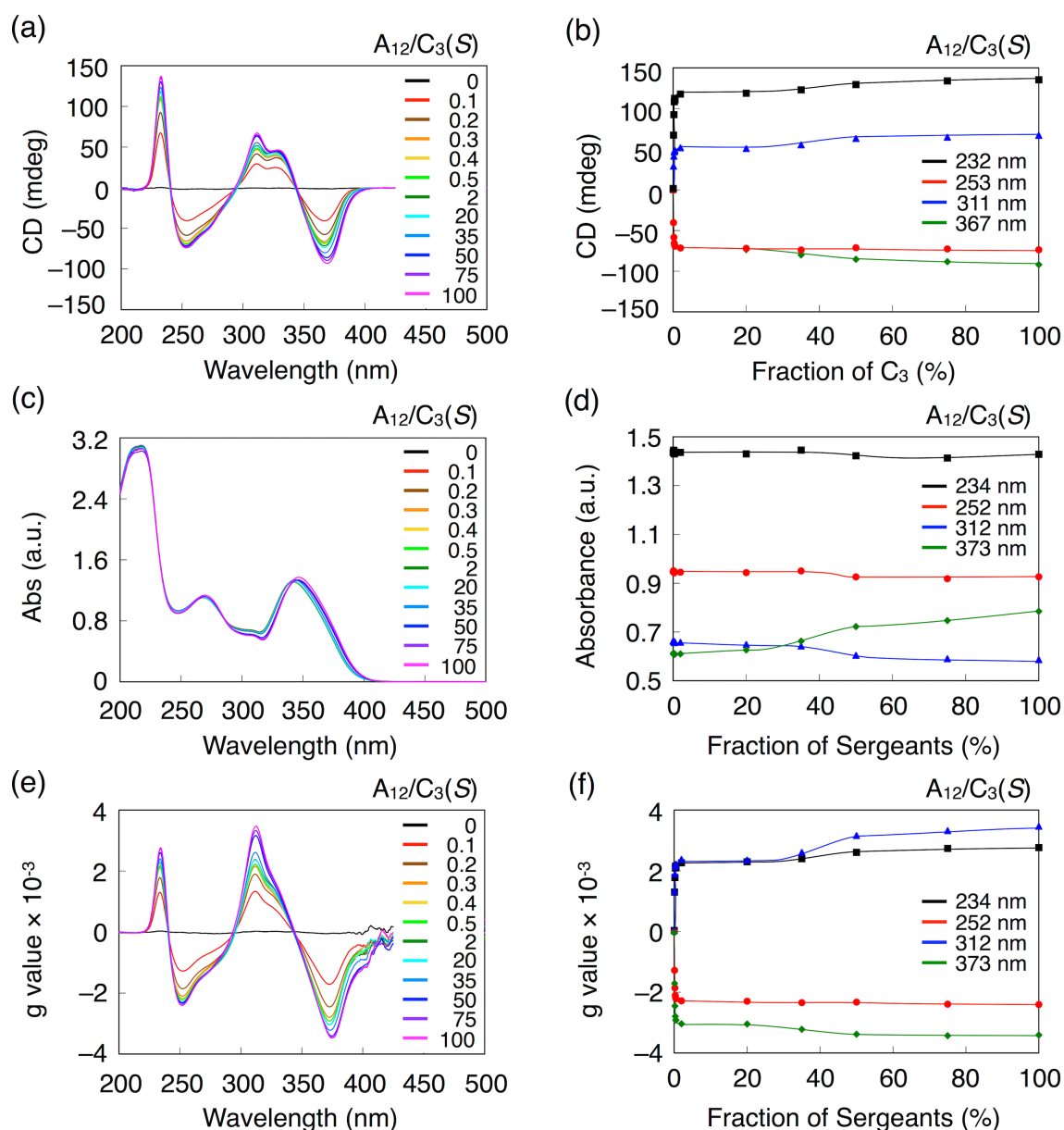


**Figure 3.4** (a) Full CD and (c) UV/Vis absorbance spectra, and (e)  $g$ -value for  $30 \mu\text{M}$  mixture of  $A_{12}$  and  $C_3(S)$  at various fraction of  $C_3(S)$  in cyclohexane, respectively. (b) CD effect versus fraction of sergeants for  $30 \mu\text{M}$  mixture of  $A/C_3(S)$  at several wavelength. (d) UV/Vis absorbance versus fraction of sergeants for  $30 \mu\text{M}$  mixture of  $A/C_3(S)$  at several wavelength. (f)  $g$ -value versus fraction of sergeants for  $30 \mu\text{M}$  mixture of  $A/C_3(S)$  at several wavelength.

quantify CD effect more correctly, the  $g$ -value was derived from measured CD and UV/Vis absorption spectra. It is noteworthy that  $g$ -value is independent of the concentration and of the pathlength, which is not necessarily to be known or measured. In order to clarify how much  $g$ -values decrease or increase as a function of fraction of sergeants, we used the net helicity as a probe for the degree of chiral amplification. Accordingly, the net helicity is obtained from dividing the  $g$ -value for a certain composition the  $g$ -value for 20 mol% fraction of sergeants at 252 nm. As shown in the inset of Figure 3.5a, we clearly concluded that the net helicity was saturated with an addition of 0.3 mol% fraction of sergeants. In other words, one molecule of  $C_3(S)$  control the helicity of supramolecular helices with 333 molecules of  $A_{12}$  on average. At such high level of chiral amplification, the average length of supramolecular helices might affect the result. However, the degree of chiral amplification of this system showed no change even at 10-fold diluted concentration (Figure 3.5b), suggesting that the average length of supramolecular helices is ineffective for the corresponding concentration ranges.<sup>24</sup> To the best of my knowledge, so far 1 mol% sergeant was the minimum fraction to fully bias the handedness of supramolecular helices of soldiers.<sup>23</sup> Hence, my TPA system unexpectedly exceeded the limit of the conventional sergeants and soldiers system.

In order to understand the origin of this high amplification of supramolecular chirality, we estimated mismatch penalty (MMP) and helical reversal penalty (HRP) according to the amplification model developed by Meijer and coworker.<sup>14,25,26</sup> Here MMP is an energetic penalty paid by a system when sergeants are incorporated in unpreferred helices. On the other hand, HRP corresponds to the energetic barrier to invert the helicity of supramolecular helices. In general (sergeants and soldiers system),

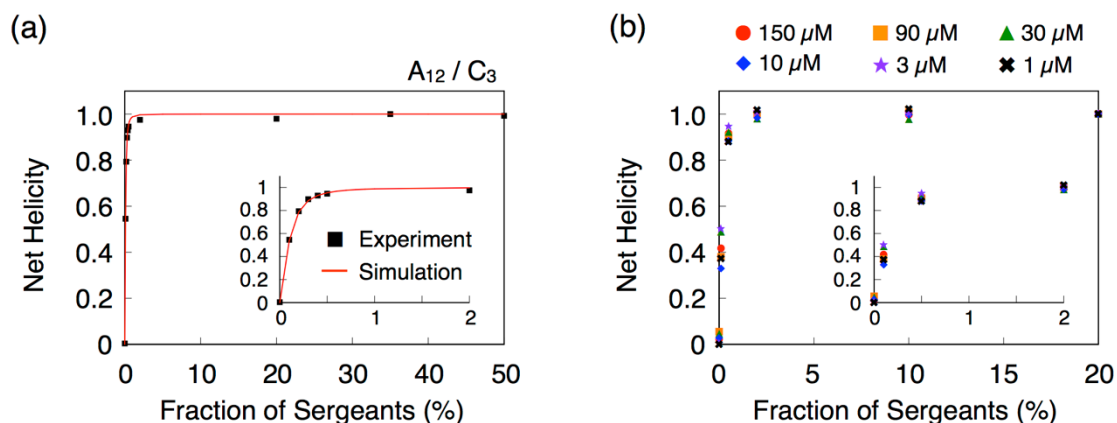


**Figure 3.5** (a) Net helicity versus fraction of sergeants for 30  $\mu\text{M}$  mixture of  $\text{A}_{12}/\text{C}_3(\text{S})$ . Contour plot of the sum of squared residuals obtained from fitting  $\text{A}_{12}/\text{C}_3(\text{S})$  Sergeant-and-Soldiers data with the minimum at which the dotted lines cross ( $\sigma = 6.3 \cdot 10^{-8}$  and  $\omega = 0.68$ , please see the experimental section). (b) Net helicity versus fraction of sergeants for mixture of  $\text{A}_{12}/\text{C}_3(\text{S})$  depends on concentration in the range of 1 ~ 150  $\mu\text{M}$ . The trace of net helicity is almost independent of the concentration of mixed system.

**Table 3.1** Energy Penalties Determined from Fitting the Sergeants-and-Soldiers Data

Molecular core	HRP ( $\text{kJ mol}^{-1}$ )	MMP ( $\text{kJ mol}^{-1}$ )
Triphenylamine	20.5	1.0
Benzene tricarboxamide <sup>25</sup>	12.6	> 0.5
Porphyrin <sup>26</sup>	16.6	0.2

degree of chiral amplification increases as those values increase. Interestingly, a mixed system of  $A_{12}$  and  $C_3(S)$  showed the highest MMP and HRP values in those ever reported (Table 3.1).<sup>14,25,26</sup> Compared to previous sergeants and soldiers system with conventional supramolecular helices, the propeller conformation of TPA is only a characteristic feature in molecular design. Hence, I assumed that this structural feature was key factor for such high amplification of supramolecular chirality. Because the propeller conformation of TPA is determined from the helicity of their supramolecular helices, an extra HRP is generated from the rotational barrier of TPA propeller to invert the supramolecular helices. As a result, high HRP is exhibited in the supramolecular helices of propeller-shaped TPA derivatives. On the other hand, it is more difficult to discuss the underlying mechanism to decide the degree of MMP than that of HRP. Particularly when the stereogenic centers are introduced in flexible side chains, it is difficult to predict what kinds of conformation they adopt and how they interact one another. However, in contrast to conventional supramolecular helices, there is an extra origin of MMP in our system (the assembly of TPA derivatives), which is the MMP between the side chain chirality and chiral propeller conformation of TPA. Therefore, we assume that the observed result is originated in the general feature of the propeller-shaped molecules.

### 3.4 Effect of the position of side chain in chiral amplification

To further elucidate the origin of MMP and improve the record of the chiral amplification, we prepared the various sergeant and soldiers (Figure 2.1). Fortunately, all the samples show almost identical absorption spectra to one another (Figure 3.2b and 3.6a,c). Hence, the following discussions are based on the assumption that those TPA derivatives form the supramolecular helices with the same conformations as  $\mathbf{A}_{12}$  and  $\mathbf{C}_3(\mathbf{S})$ . At first, we investigated the degree of chiral amplification in the mixed system with  $\mathbf{A}_{12}$  and chiral analogues  $\mathbf{C}_{1m}(\mathbf{S})$ ,  $\mathbf{C}_{1p}(\mathbf{S})$ ,  $\mathbf{C}_{2m,m}(\mathbf{S})$ , respectively, whose names are after the number and position of the stereogenic centers present in their side chains. As shown in Figure 3.6b,  $\mathbf{C}_{1p}(\mathbf{S})$  showed the lowest chiral amplification whereas  $\mathbf{C}_{1m}(\mathbf{S})$  and  $\mathbf{C}_{2m,m}(\mathbf{S})$  showed almost identical degree of chiral amplification to that of  $\mathbf{C}_3(\mathbf{S})$ , suggesting that the role of the side chain chirality at para- and meta-positions are totally different from one another. Because the side chains at meta-positions sterically hinders the rotation of the phenyl groups to which those side chains are attached, such anomalous difference between the side chain chirality at para- and meta-position might be the origin of MMP between the propeller-conformation and the stereogenic centers. The same trend was also observed for the soldiers. When the achiral TPA derivatives,  $\mathbf{A}_p$  and  $\mathbf{A}_m$ , whose a long alkyl at para- and meta-positions are replaced by a methyl group, respectively, are mixed with  $\mathbf{C}_3(\mathbf{S})$ ,  $\mathbf{A}_p$  showed the almost identical degree of chiral amplification with that of  $\mathbf{A}_{12}$ . On the other hand,  $\mathbf{A}_m$  showed the much lower degree of chiral amplification. More interestingly, a mixed system of  $\mathbf{A}_p$  and  $\mathbf{C}_3(\mathbf{S})$  surely showed the higher degree of chiral amplification than that with  $\mathbf{A}_{12}$  and  $\mathbf{C}_3(\mathbf{S})$ . 0.2 mol% of  $\mathbf{C}_3(\mathbf{S})$  forces to fully bias the helicity of supramolecular helices of  $\mathbf{A}_{12}$ , meaning that only one molecule of  $\mathbf{C}_3(\mathbf{S})$  molecule controls the supramolecular helices



with 500 molecules of  $A_{12}$  on average. This is the champion record for the sergeant-soldier system so far reported.

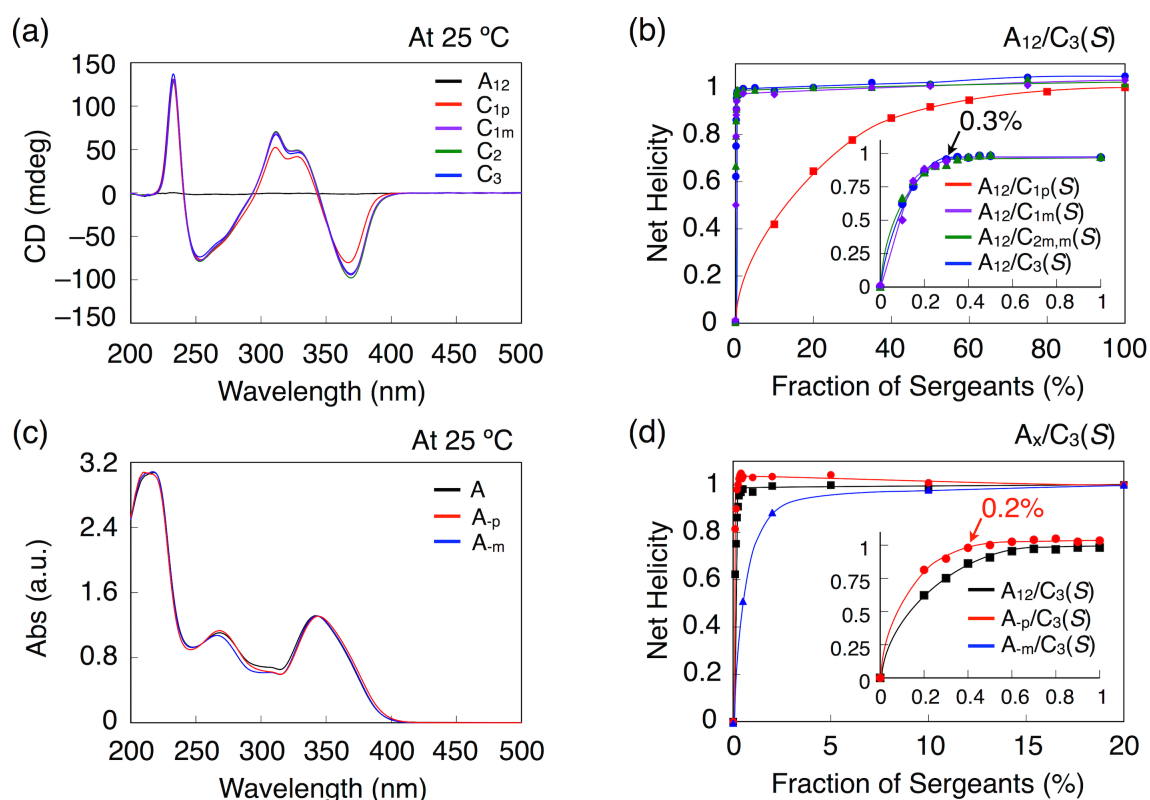


**Figure 3.6** (a) Full CD spectra for 30  $\mu\text{M}$   $A_{12}$ ,  $C_{1p}(S)$ ,  $C_{1m}(S)$ ,  $C_{2m,m}(S)$  and  $C_3(S)$  at 25  $^{\circ}\text{C}$  in cyclohexane. (b) Net helicity versus fraction of sergeants for 30  $\mu\text{M}$  mixture of  $A_{12}/C_{1p}(S)$ ,  $A_{12}/C_{1m}(S)$ ,  $A_{12}/C_{2m,m}(S)$  and  $A_{12}/C_3(S)$ . (c) Full UV/Vis absorption spectra for 30  $\mu\text{M}$   $A_{12}$ ,  $A_p$  and  $A_m$  at 25  $^{\circ}\text{C}$  in cyclohexane. (d) Net helicity versus fraction of sergeants for 30  $\mu\text{M}$  mixture of  $A_{12}/C_3(S)$ ,  $A_p/C_3(S)$  and  $A_m/C_3(S)$ .

### 3.5 Hierarchy of propeller-shaped chiral sergeants

It is noteworthy that the degree of chiral amplification can be compared over the various TPA derivatives because their helical conformations are almost identical to one another (Figure 3.2b and 3.6a,c), which is not necessarily realized by supramolecular helices with planar  $\pi$ -conjugated molecules such as perylene bisimide.<sup>27</sup> Furthermore, it is quite rare that the degree of chiral amplification drastically changes just by altering the position of the stereogenic centers. By utilizing these unique features, we finally demonstrated the hierarchy of the chiral TPA derivatives as sergeants. As shown in figure 3.7a, in the presence of 4 mol% of  $C_3(R)$ , the mixed system of  $A_{12}$  and  $C_{1p}(S)$  exhibited the constant CD intensity regardless of the fraction of  $C_{1p}(S)$ . Note that,  $C_{1p}(S)$  can behave as a sergeant in the mixed system with  $C_{1p}(S)$  and  $A_{12}$ . On the other hand,  $C_{1p}(S)$  behaves like a soldier in the presence of  $C_3(R)$ , suggesting the hierarchy of the sergeants and soldiers systems. The same thing hold true for the majority rule experiments of  $C_{1p}(R)/C_{1p}(S)$ . In the presence of 5 mol% of  $C_3(R)$ , the mixed system of  $C_{1p}(R)$  and  $C_{1p}(S)$  showed the constant CD signal independent of enantiomeric excess  $C_{1p}(R)/C_{1p}(S)$  (Figure 3.7b).

As shown in Figure 3.7c, when  $A_{12}$  dissolved in (*S*)-limonene, the resultant supramolecular helices displayed an optical activity (black line), which was corresponded with the supramolecular helix of  $C_3(S)$  in cyclohexane. It reveals that the handedness of racemic supramolecular helices was biased in the presence of chiral solvent, (*S*)-limonene. On the other hand,  $C_3(R)$  showed identical CD spectra either in cyclohexane or in (*S*)-limonene (purple line in Figure 3.7c), indicating that the handedness of the resultant supramolecular helix was determined by its intrinsic chirality regardless of the chirality of solvent. Indeed, the implementation of chiral

amplification was also occurred for the mixture of  $A_{12}$  and  $C_3(R)$  in (*S*)-limonene. As increasing the fraction of  $C_3(R)$ , the CD intensity for co-assembly of  $A_{12}/C_3(R)$  decrease and the CD spectra was finally displayed opposite spectra at 10 mol% of  $C_3(R)$  in (*S*)-limonene (Figure 3.7c,d). Consequently, we found that the strong sergeants could control the helicity of the other weak chiral analogues regardless of their ancient chirality. This is the first example of high amplification, which has not been convinced in conventional supramolecular helices.

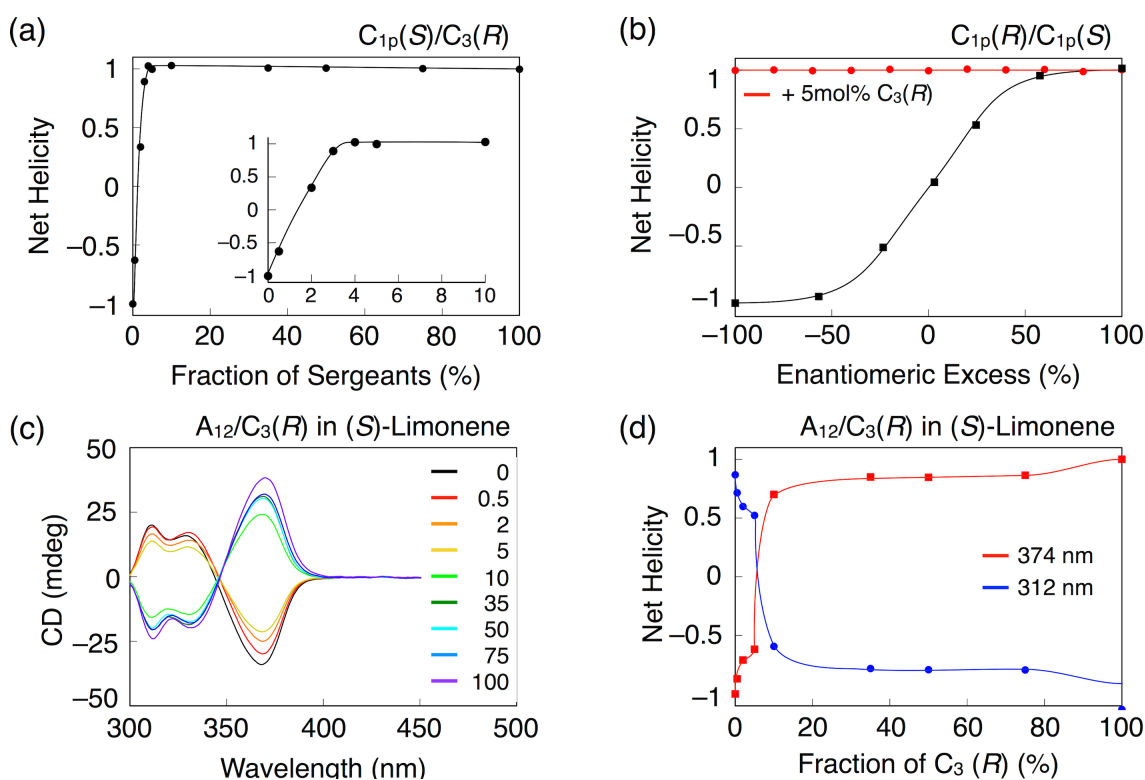


**Figure 3.7** (a) Net helicity versus fraction of sergeants for 30  $\mu$ M mixture of  $C_{1p}(S)/C_3(R)$  in cyclohexane. (b) Net helicity versus fraction of enantiomeric excess for 30  $\mu$ M mixtures of  $C_{1p}(R)/C_{1p}(S)$  in the presence of 5 mol%  $C_3(R)$  in cyclohexane. Black line displayed the experimental result of conventional majority rule of  $C_{1p}(R)/C_{1p}(S)$ . (c) Full CD spectra for 30  $\mu$ M mixture of  $A_{12}$  and  $C_3(R)$  at various fraction of  $C_3(R)$  in (*S*)-limonene. (d) Net Helicity versus fraction of sergeants for 30  $\mu$ M mixture of  $A_{12}/C_3(R)$  in (*S*)-limonene.

### 3.6 Conclusion

In conclusion, we have demonstrated that the unprecedented amplification of supramolecular chirality of TPA derivatives originated by efficient transferring chirality of side chains into the propeller chirality of aromatic core. By investigating the self-assembly behavior of each TPA compound, I clarified that the side chains at meta-positions of outer phenyls and its stereogenic center promote the formation of supramolecular nuclei and induce the world best chiral amplification with only 0.2 mol% of chiral sergeants. This unique system is not only promising for the growing field of supramolecular chirality but also interesting for investigating the origin of symmetry breaking of the biological system on the earth.

### 3.7 Experimental section

#### 3.7.1 Quantification of sergeants and soldiers data

For all sergeants and soldiers and mixed majority rules experiments,  $3.0 \times 10^{-5}$  M cyclohexane solutions of chiral sergeants and achiral soldiers were mixed in different feed ratios. The pre-mixed solution were heating up to 75 °C at molecular dissolved state and cooling to RT at  $-1 \text{ }^\circ\text{C min}^{-1}$ . The samples were aged overnight and measured.

To quantify the sergeants and soldiers data of  $A_{12}/C_3(S)$ , the  $g$ -values at 252 nm were converted into the dimensionless net helicity and fitted into a least-squares model developed by van der Schoot. Fitting of the data will yield the dimensionless energy penalties,  $\sigma$  and  $\omega$ , which are related to the HRP and the MMP via  $\sigma = \exp[-2\text{HRP}/RT]$  and  $\omega = \exp[-\text{MMP}/RT]$ , respectively. The contour plot of the sum of squared residuals shows a narrow region with a minimum at  $\sigma = 6.3 \cdot 10^{-8}$  and  $\omega = 0.68$  (Figure 3.8a) and the corresponding fit is shown in Figure 3.8b. At this point a combination of MMP and HRP results in the best fit of the data.

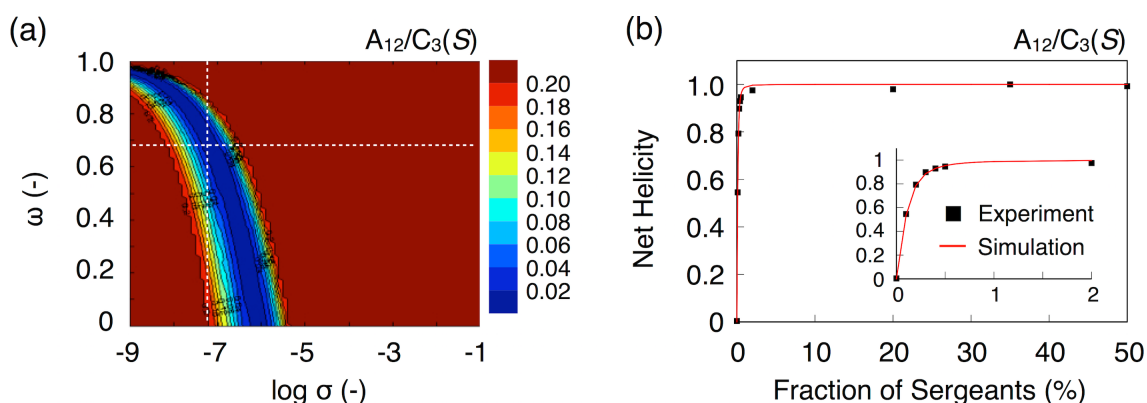


**Figure 3.8** (a) Contour plot of the sum of squared residuals obtained from fitting the sergeants and soldiers data with the minimum at which the dotted lines cross ( $\sigma = 6.3 \cdot 10^{-8}$  and  $\omega = 0.68$ ). (b) Simultaneous fit on both data sets at the minimum.

## 3.7.2 Supplementary figures for chiral amplification

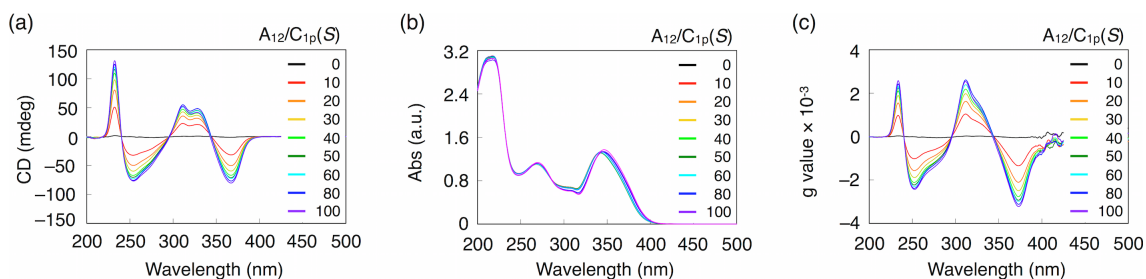


**Figure 3.9** (a) CD, (b) UV/Vis absorption and (c)  $g$ -value spectra for the  $A_{12}/C_{1p}(S)$  sergeants and soldiers experiment, in which each spectrum represents a specific mole fraction of  $C_{1p}(S)$  at a total concentration of  $30 \mu\text{M}$  at RT in cyclohexane.

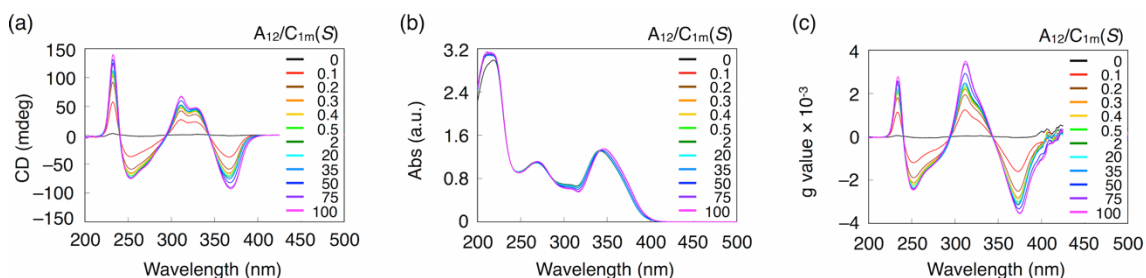


**Figure 3.10** (a) CD, (b) UV/Vis absorption and (c)  $g$ -value spectra for the  $A_{12}/C_{1m}(S)$  sergeant and soldiers experiment, in which each spectrum represents a specific mole fraction of  $C_{1m}(S)$  at a total concentration of  $30 \mu\text{M}$  at RT in cyclohexane.

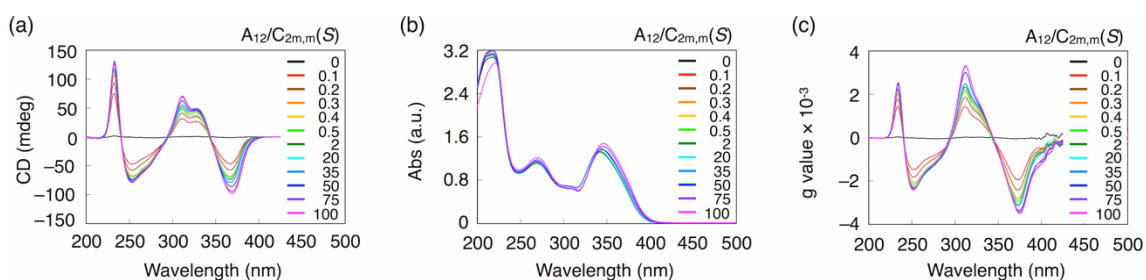


**Figure 3.11** (a) CD, (b) UV/Vis absorption and (c)  $g$ -value spectra for the  $A_{12}/C_{2m,m}(S)$  sergeants and soldiers experiment, in which each spectrum represents a specific mole fraction of  $C_{2m,m}(S)$  at a total concentration of  $30 \mu\text{M}$  at RT in cyclohexane.

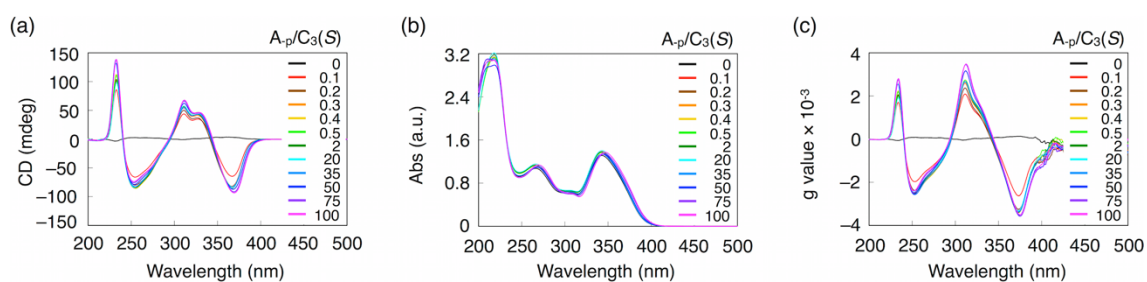


**Figure 3.12** (a) CD, (b) UV/Vis absorption and (c)  $g$ -value spectra for the  $30 \mu\text{M}$  mixtures of  $A_p/C_3(S)$  in sergeants and soldiers experiment, in which each spectrum represents a specific mole fraction of  $C_3(S)$  at a total concentration of  $30 \mu\text{M}$  at  $25^\circ\text{C}$  in cyclohexane.

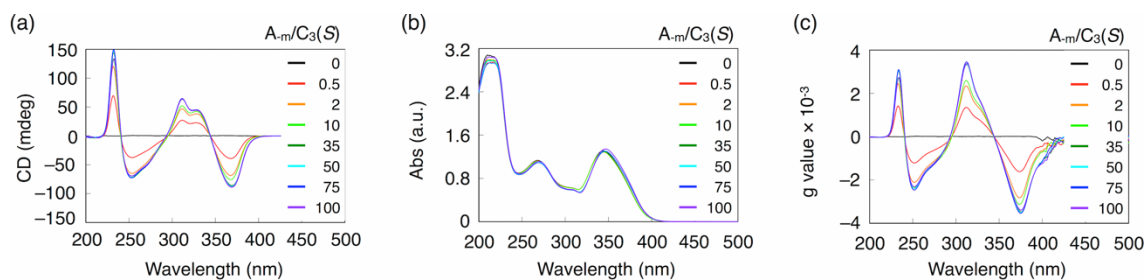


**Figure 3.13** (a) CD, (b) UV/Vis absorption and (c)  $g$ -value spectra for the mixtures of  $A_m/C_3(S)$  in sergeants and soldiers experiment, in which each spectrum represents a specific mole fraction of  $C_3(S)$  at a total concentration of  $30 \mu\text{M}$  at  $25^\circ\text{C}$  in cyclohexane.

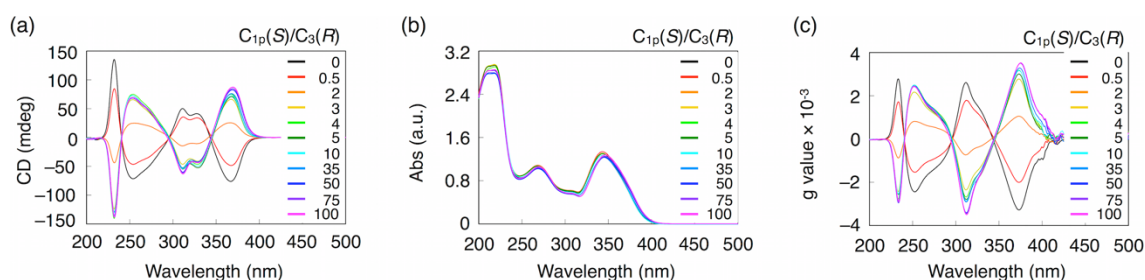


**Figure 3.14** (a) CD, (b) UV/Vis absorption and (c)  $g$ -value spectra for the mixtures of  $C_{1p}(S)/C_3(R)$  in mixed majority rule experiment, in which each spectrum represents a specific mole fraction of  $C_3(R)$  at a total concentration of  $30 \mu\text{M}$  at  $25^\circ\text{C}$  in cyclohexane.

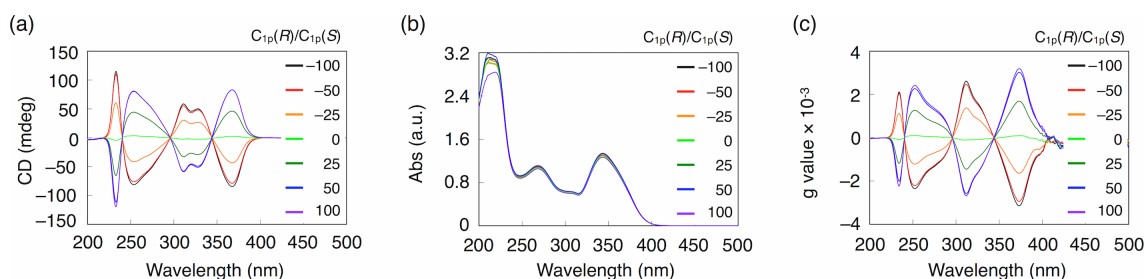


**Figure 3.15** (a) CD, (b) UV/Vis absorption and (c)  $g$ -value spectra for the mixtures of  $C_{1p}(R)/C_{1p}(S)$  in majority rule experiment, in which each spectrum represents a specific enantiomeric excess of  $C_{1p}(R)/C_{1p}(S)$  at a total concentration of  $30 \mu\text{M}$  at  $25^\circ\text{C}$  in cyclohexane.

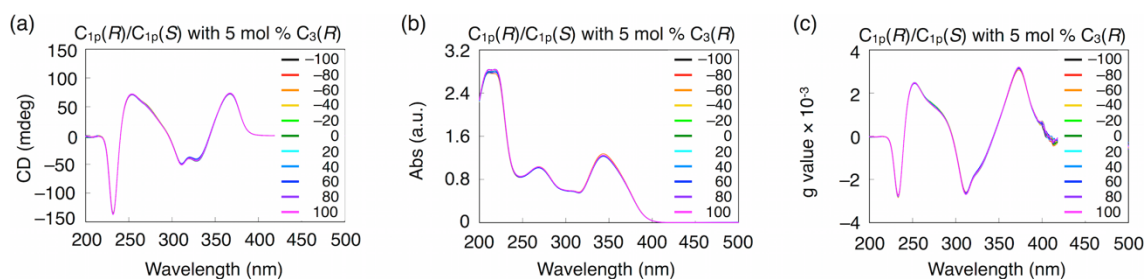


**Figure 3.16** (a) CD, (b) UV/Vis absorption and (c)  $g$ -value spectra for the mixtures of  $C_{1p}(R)/C_{1p}(S)$  with 5 mol %  $C_3(R)$  in majority rule experiment, in which each spectrum represents a specific enantiomeric excess of  $C_{1p}(R)/C_{1p}(S)$  at a total concentration of  $30 \mu\text{M}$  at  $25^\circ\text{C}$  in cyclohexane.



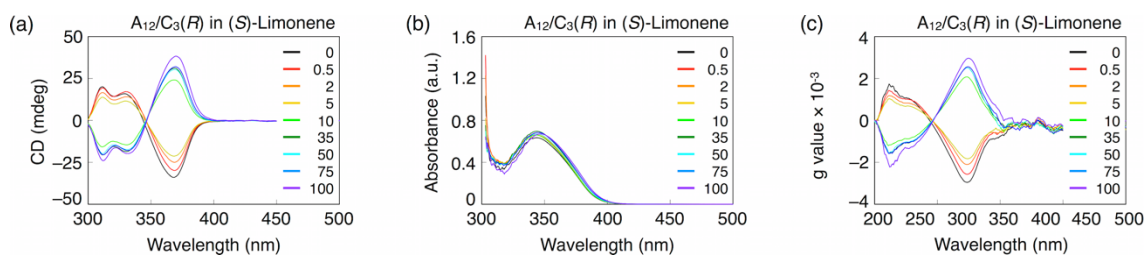


**Figure 3.17** (a) CD, (b) UV/Vis absorption and (c) g-value spectra for the mixtures of A<sub>12</sub>/C<sub>3</sub>(S) in sergeants and soldiers experiment, in which each spectrum represents a specific mole fraction of C<sub>3</sub>(S) at a total concentration of 30 μM at 25 °C in (S)-limonene.

### 3.8 References

- (1) Pijper, D.; Feringa, B. L. *Soft Matter* **2008**, *4*, 1349-1372
- (2) Cahill, K. *Phys. Rev. E* **2005**, *72*, 062901
- (3) Van Workum, K.; Douglas, J. F. *Phys. Rev. E* **2006**, *73*, 031502
- (4) Watson, J.; Crick, F. *Nature* **1956**, *177*, 473-475
- (5) Maeda, K.; Yashima, E. *Top. Curr. Chem.* **2006**, *265*, 47-88
- (6) Kornyshev, A.; Lee, D.; Leikin, S.; Wynveen, A. *Rev. Mod. Phys.* **2007**, *79*, 943-996
- (7) Yanagawa, H.; Ogawa, Y.; Furuta, H.; Tsuno, K. *J. Am. Chem. Soc.* **1989**, *111*, 4567-4570
- (8) Jin, W.; Fukushima, T.; Niki, M.; Kosaka, A.; Ishii, N.; Aida, T. *Proc. Natl. Acad. Sci. U.S.A.* **2005**, *102*, 10801-10806
- (9) Hisaki, I.; Sasaki, T.; Tohnai, N.; Miyata, M. *Chem. Eur. J.* **2012**, *18*, 10066-10073
- (10) Okamoto, Y.; Yashima, E.; *Angew. Chem. Int. Ed.* **1998**, *37*, 1020-1043.
- (11) Ito, Y.; Miyake, T.; Hatano, S.; Shima, R.; Ohara, T.; Sugimoto, M.; *J. Am. Chem. Soc.* **1998**, *120*, 11880-11893.
- (12) Barclay, T. G.; Constantopoulos, K.; Matisons, J. *Chem. Rev.* **2014**, *114*, 10217-10291.
- (13) Feringa, B. L.; van Delden, R. A. *Angew. Chem. Int. Ed.*, **1999**, *38*, 3418-3438
- (14) Palmans, A. R. A.; Meijer, E. W. *Angew. Chem. Int. Ed.* **2007**, *46*, 8948-8968.
- (15) Kang, J.; Miyajima, D.; Mori, T.; Inoue, Y.; Itoh, Y.; Aida, T. *Science* **2015**, *347*, 646-651
- (16) Grimme, S.; Antony, J.; Ehrlich, S.; Krieg, H.; *J. Chem. Phys.* **2010**, *132*, 154104
- (17) Grimme, S.; Ehrlich, S.; Goerigk, L.; *J. Comput. Chem.* **2011**, *32*, 1456-1465.
- (18) Buffeteau, T.; Ducasse, L.; Poniman, L.; Delsuc, N.; Huc, I. *Chem. Commun.* **2006**, 2714-2716.
- (19) Smulders, M. M. J.; Buffeteau, T.; Cavagnat, D.; Wolffs, M.; Schenning, A. P. H. J.; Meijer, E. W. *Chirality* **2008**, *20*, 1016-1022
- (20) Aparicio, F.; Nieto-Ortega, B.; Nájera, F.; Ramírez, F. J.; López Navarrete, J. T.;

- Casado, J.; Sánchez, L. *Angew. Chem. Int. Ed.* **2014**, *53*, 1373–1377.
- (21) Chernyshova, M. F.; Lushina, N. P. *Journal of Applied Spectroscopy* **1969**, *11*, 1330–1333.
- (22) Reva, I.; Lapinski, L.; Chattopadhyay, N.; Fausto, R. *Phys. Chem. Chem. Phys.* **2003**, *5*, 3844–3850.
- (23) Ishi-i, T.; Kuwahara, R.; Takata, A.; Jeong, Y.; Sakurai, K.; Mataka, S. *Chem. Eur. J.* **2006**, *12*, 763–776.
- (24) Palmans, A. R. A.; Vekemans, J. A. J. M.; Havinga, E. E.; Meijer, E. W. *Angew. Chem. Int. Ed.* **1997**, *36*, 2648–2651.
- (25) Smulders, M. M. J.; Schenning, A. P. H. J.; Meijer, E. W. *J. Am. Chem. Soc.* **2008**, *130*, 606–611.
- (26) Helmich, F.; Smulders, M. M. J.; Lee, C. C.; Schenning, A. P. H. J.; Meijer, E. W. *Angew. Chem. Int. Ed.* **2011**, *133*, 12238–12246.
- (27) Ghosh, S.; Li, X.-Q.; Stepanenko, V.; Würthner, F. *Chem. Eur. J.* **2008**, *14*, 11343–11357.



## **Chapter 4**

### **Self-assembly behavior of propeller-shaped TPA derivatives in diluted solution**



## 4.1 Introduction

Molecular self-assembly has attracted much attention of material scientists for the development of novel supramolecular nanostructures, starting from relatively small and simple building blocks.<sup>1-5</sup> With characteristic structures and properties of the resultant assembly, it also came into spotlight to elucidate the mechanisms of the self-assembly processes from monomers to polymer via noncovalent synthetic route.<sup>6-10</sup> Over the past few decades, many supramolecular building blocks were designed and investigated to elucidate the process of their supramolecular assembly.<sup>8,10-17</sup> Benzene tricarboxamide (BTA) is one of representative building blocks with simple structure and synthetic efficiency, which found to aggregate into 1D supramolecular polymers.<sup>18-22</sup> By controlling several parameters such as concentration, temperature, additive and tuning of peripheral unit, the found mechanism can be generally applicable for the self-assembly of various chemicals. In fact, these results facilitated the mechanism study for various molecular assemblies and provided us with benefit insight for understanding of structure-property relationship, which resulted in precise control of self-assembly process with more sophisticated design of building blocks such as seeded and chain growth supramolecular polymerization. However, these studies mainly focused on the self-assembly of planar-like  $\pi$ -conjugated compounds. Within this chapter, the self-assembly behavior of propeller-shaped TPA derivatives was investigated with temperature-dependent spectroscopic measurements. More particularly, by comparing the critical temperature in the self-assembly process of various TPA derivatives, the spatial effect of side chains at *meta*-position of paraffinic wedges will be discussed.

## 4.2 Effect of the length of alkyl chains

The supramolecular polymerization was mainly considered with the three major growth mechanisms, namely, isodesmic, ring-chain, and cooperative growth (Figure 4.1).<sup>8</sup> I will focus on the isodesmic and the cooperative mechanism, because the ring-chain mechanism is only valuable for linear oligomers and polymers are in equilibrium with their cyclic counterpart. The isodesmic polymerization is similar to the step-growth polymerization and is characterized by a high polydispersity, and the degree of polymerization strongly depends on the association constant of the linking supramolecular units. On the other hand, the cooperative mechanism of supramolecular polymerization is characterized by nonlinear growth with at least two different association constants in the assembly pathway. It is noteworthy that they exhibit a critical point in their self-assembly pathway, which is characterized by a rapid growth of supramolecular polymer.

Meijer and colleagues adapted nucleation-growth model, originally developed by Oosawa and Kasai for biological supramolecular polymers,<sup>26</sup> to describe the cooperative self-assembly of organic  $\pi$ -conjugated molecules into helical fibers.<sup>11</sup> To illustrate the temperature-dependent properties of cooperative supramolecular polymers, two temperature regimes will be illustrated as the nucleation and the elongation regime, which were separated by the elongation temperature. In this polymerization process, only a small portion of the monomers is active and able to polymerize above the elongation temperature. The other monomers are in an inactive state and unable to grow into long polymeric species. Importantly, the active and inactive states of the monomers are in thermal equilibrium, and the equilibrium strongly favors the inactive state, resulting in a cooperative supramolecular polymerization. When the temperature



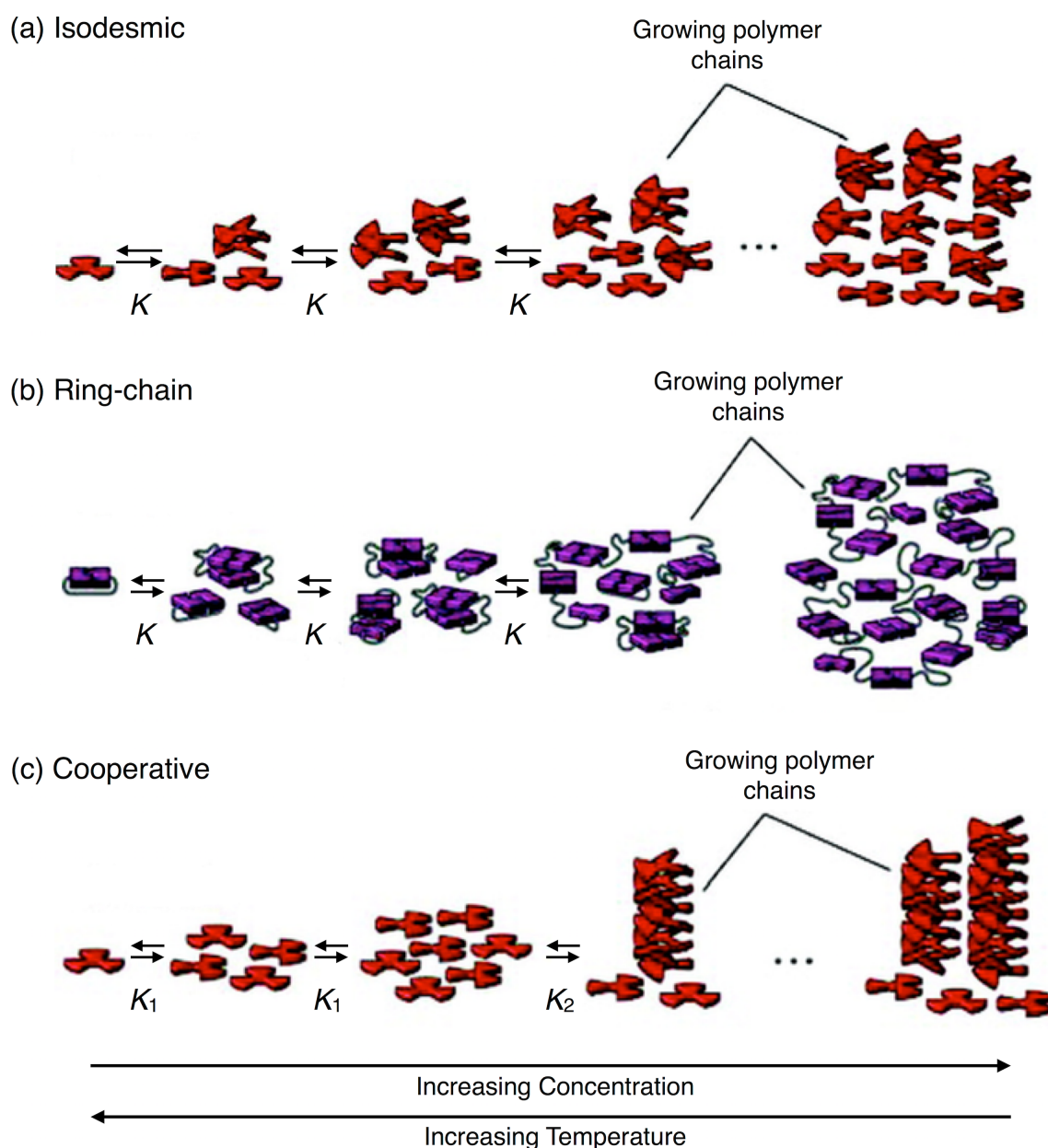


**Figure 4.1** Graphical representation of the three growth mechanisms by which a monomer can polymerize into a supramolecular polymer: (a) isodesmic supramolecular polymerization; (b) ring-chain mediated supramolecular polymerization; (c) cooperative supramolecular polymerization. In both of (a) and (b),  $K$  represents the intermolecular equilibrium constant, which is independent of the chain length. In contrast, (c) exhibits two equilibrium constants ( $K_1$  and  $K_2$ ).

of system cools down and approaches the elongation temperature, the growth of helical aggregates occurs.

By the benefit of high spectroscopic sensitivity, the self-assembly process can be investigated with temperature-dependent CD and UV/Vis spectroscopy measurements in dilute solution. To find basic assembly behavior, achiral TPA derivative **A**<sub>12</sub>, which was substituted to three dodecyl chains at the paraffinic wedges, was firstly investigated with temperature-dependent UV/Vis spectroscopy measurement for  $3.0 \times 10^{-5}$  M cyclohexane solution (Figure 4.2a). Upon cooling from 75 °C to 25 °C, an UV/Vis absorption spectra maximum slightly red-shifted by 1 nm and characteristic valley was generated at 315 nm. To study the self-assembly behavior of **A**<sub>12</sub> in detail, the absorbance at 315 nm was plotted as function of temperature from 75 °C at molecular dissolved state to 25 °C. As shown in Figure 4.2b, the absorbance suddenly decreased at 50 °C, suggesting that molecular behavior changed, which can probably be attributed to aggregation. This nonlinear change reveals that **A**<sub>12</sub> exhibits a cooperative self-assembly process. To elucidate the effect of the length of alkyl chain, other achiral TPA derivatives, which were substituted with octyl or hexadecyl chains, **A**<sub>8</sub> or **A**<sub>16</sub>, respectively, were also checked with their self-assembly behavior. Because of bad solubility derived from shorter alkyls, **A**<sub>4</sub> was not included in this study. Interestingly, the critical temperature for supramolecular polymerization decreases as increasing the length of linear alkyls. Basically, when the self-assembly occurs, the entropic loss of flexible alkyls emerges and increases with number of atoms in the alkyls, which results in the lower elongation temperature than the molecules substituted to shorter alkyl chain.<sup>27</sup> To illustrate the self-assembly behavior more clearly, the temperature-dependent CD spectroscopy measurement was performed for those achiral TPA

compounds. For the measurement of achiral compounds, which is optically inactive, 0.5 mol% of  $C_3(S)$  was added into  $3.0 \times 10^{-5}$  M of each achiral samples in cyclohexane. After aging the pre-mixed sample, those three achiral compounds showed clear Cotton effect and can be observed CD value at 25 °C. For all compounds  $A_8$ ,  $A_{12}$  and  $A_{16}$  at 75 °C, the CD signal was absent, which is indicating that all of them dispersed molecularly in cyclohexane. Upon cooling, the rise in Cotton effect with negative value at 252 nm and 367 nm, which is indicative of the formation of one-handed helical assembly as described in the chapter 3.4. To analyze this result in detail, the CD intensity at 252 nm was normalized with those value measured at 25 °C and plotted as function of temperature upon cooling (Figure 4.2d).<sup>18-19</sup> The critical temperature for each compound showed consistent value with those evaluated by the UV/Vis absorption spectroscopy measurement. It reveals that the chiral additive,  $C_3(S)$ , seldom influence on the self-assembly behavior of achiral TPA derivatives. However, it is noteworthy that the achiral analogues classified into two classes regarding the mechanism of in supramolecular polymerization. The sigmoidal cooling curve are obtained for  $A_8$ , indicating that isodesmic self-assembly process, while  $A_{12}$  and  $A_{16}$  showed cooperative process with nonsigmoidal curves.<sup>28</sup> This phenomenon could be related to the destabilization of molecular stacking triggered by the diminishment of intermolecular interaction between shorter alkyl chains.

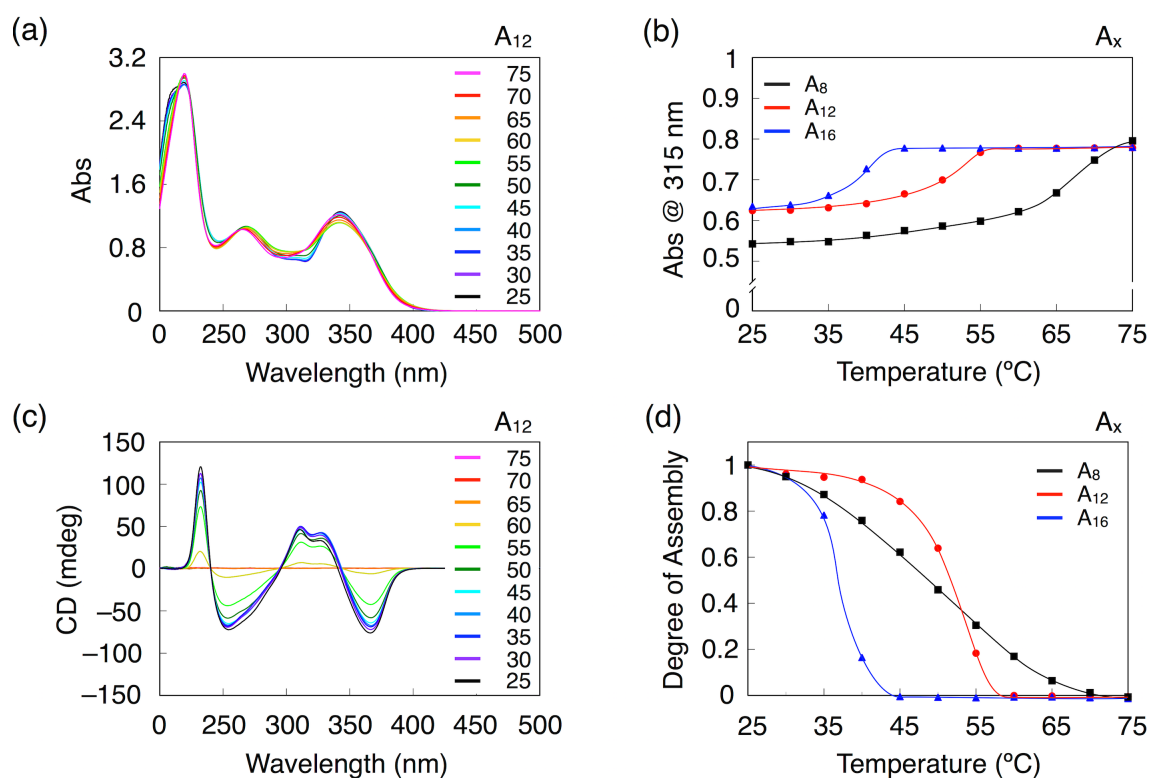


**Figure 4.2** (a) Full UV/Vis absorption spectra for 30  $\mu\text{M}$  of  $A_{12}$  in cyclohexane at temperatures between 75  $^{\circ}\text{C}$  and 25  $^{\circ}\text{C}$  with 10  $^{\circ}\text{C}$  intervals. (b) UV/Vis absorption at 315 nm as a function of temperature for solutions of  $A_{12}$  in cyclohexane. (c) Full CD spectra for 30  $\mu\text{M}$  of  $A_{12}$  in cyclohexane at temperatures between 75  $^{\circ}\text{C}$  and 25  $^{\circ}\text{C}$  with 10  $^{\circ}\text{C}$  intervals. (d) Degree of assembly as a function of temperature for 30  $\mu\text{M}$  solutions of  $A_{12}$  in cyclohexane. The value was obtained from CD intensity at 252 nm.

### 4.3 Effect of the position of long alkyl chains

As described above, the self-assembly behavior of TPA derivatives could be affected by the length of alkyl chain in peripheral paraffinic wedges. On the other hand, from the results of the sergeants and soldier experiments with the different types of sergeants and soldiers (Figure 3.6b,d), it is clear that the degree of chiral amplification drastically decreases when TPA possesses the stereogenic centers only at the para-position of the paraffinic wedges. In other word, the observed high MMP value is originated in the stereogenic centers at meta-position. The similar special effect of meta-position is also confirmed by the self-assembling behaviors of achiral TPA derivatives. The experimental procedure is identical with the temperature-dependent spectroscopy measurement of fully alkylated TPA analogues, which was discussed above.

Upon cooling the solution, the cooling curves for each compound was also found to exhibit a nonsigmoidal shape, which well corresponded with a cooperative self-assembly process. The critical temperature, at which supramolecular helices started to be formed on cooling process, drastically decreased when one of the dodecyl chains at the meta-positions ( $\mathbf{A}_m$ ) was replaced with a methyl group. On the other hand, the critical temperature of  $\mathbf{A}_p$ , which was equipped with a short methoxy group at the para-position instead of a dodecyl chain, slightly increased than  $\mathbf{A}_{12}$ . In general, the critical temperature could decrease as the length of side chains increases because the entropic loss accompanied by the formation of supramolecular aggregate.<sup>27</sup> Hence, it is natural that  $\mathbf{A}_p$  shows higher critical temperature than that of  $\mathbf{A}_{12}$ . However, with the conventional notion on the supramolecular system, it is hard to explain the reason why  $\mathbf{A}_m$  shows the lower critical temperature than that of  $\mathbf{A}_{12}$ .

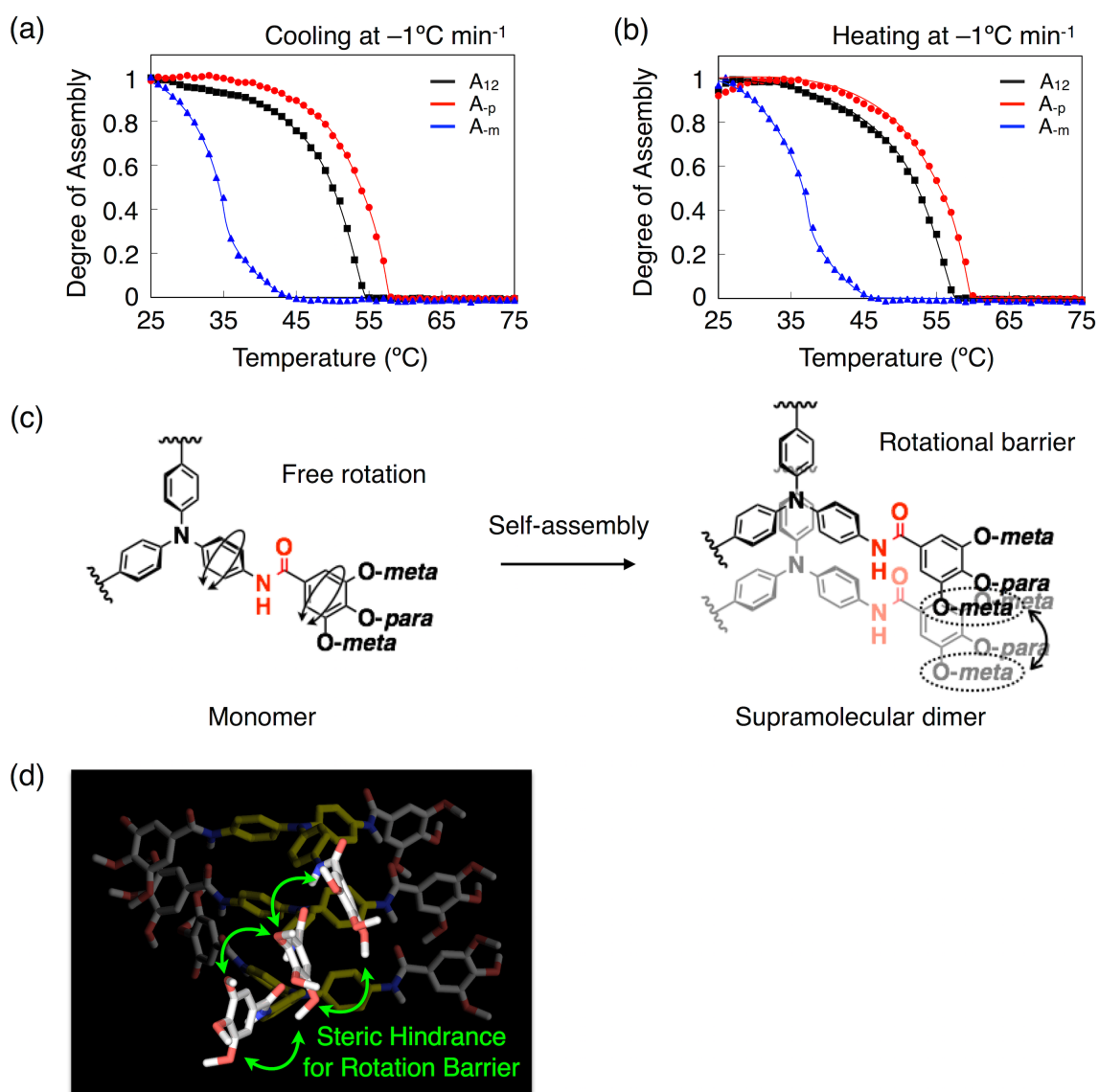


**Figure 4.3** Degree of assembly versus temperature for  $30\ \mu\text{M}$  achiral TPA compounds,  $A_{12}$ ,  $A_p$  and  $A_m$  upon (a) cooling and (b) heating, respectively. Change in CD effect at 252 nm as a function of temperature with cooling rate at  $-1\ ^{\circ}\text{C min}^{-1}$ . (c, d) Schematic illustration for TPA conformation at the moment of supramolecular nucleation. The side chains at the meta-positions restricted rotation of outer phenyl intermolecularly in the assembly.

To illustrate this contradictory phenomenon, it is valuable to look into the molecular behavior near the elongation temperature. According to the nucleation-elongation model developed by van der Schoot, free monomers are readily elongated from nuclei and form supramolecular polymer below the elongation temperature.<sup>8, 11-29</sup> It is noteworthy that the presence of a nucleus was a prerequisite for elongation process. It indicates that the elongation temperature reflects the stability of supramolecular nuclei. In the nuclei, molecules should adopt an appropriate conformation that facilitates the formation of helical supramolecular polymer via hydrogen bonds. As shown in VCD measurement and DFT calculation in Chapter 3, the aromatic units in TPA derivatives adopted an optimal propeller conformation in the helical assembly (Figure 3.1, 3.3). However, the molecular stacking in supramolecular nuclei was getting less stable as decreasing the rotation barrier of the outer phenyls, which was derived from the lack of long alkyls at the meta-position of outer phenyls. As a result, **A<sub>m</sub>** displayed the lower elongation temperature than the other achiral analogues, which possessed the long alkyls at the both of meta-position (Figure 4.3a). In other words, when the formation of supramolecular nuclei at the elongation temperature occurs, the side chains at the meta-position get closer to those of vicinal stacks and intermolecularly crush to one another. Concomitantly, the free rotation of benzenes in both the inner and outer phenyl blades would be restrained by ensuring the formation of hydrogen bonding. In conclusion, the formation of nuclei was strongly facilitated by the intermolecular interaction of the side chains at the meta-positions in peripheral paraffinic wedges.

#### 4.4 Effect of the position of chiral chains

It is well known that branched chiral chains lead to less stable stacks compared to linear chains. Because of steric hindrances, the branching could destabilize the 1D supramolecular polymer compared to linear side chains.<sup>18,30,31</sup> For example, when  $C_3$ -symmetrical trialkylbenzene-1,3,5-tricarboxamides were substituted to branched chiral side chains such as (*R*)-3,7-dimethyloctyl, the molecules showed lower elongation temperature than their achiral analogues. However, the chiral sergeant  $C_3(S)$  showed higher elongation temperature than the achiral analogue  $A_{12}$ , indicating that the supramolecular nucleation of  $C_3(S)$  is more stable in spite of its nine branched chiral alkyl groups. To the best of our knowledge, this is the first example that the branching promotes to aggregate at higher temperature.

The nucleation process was further facilitated by adding asymmetric elements into the side chain at the meta-position, which results in the higher elongation temperature of  $C_{1m}(S)$  than  $C_{1p}(S)$  and achiral analogues. Both of chiral TPA derivatives have same number of chiral side chain, but the elongation of self-assembly occurs at different temperatures. In addition, although  $C_{1m}(S)$  has a chiral side chain at one of the meta-positions, their aggregation was found at higher temperature compared to  $C_3(S)$ , which was equipped with three chiral side chains at both of the meta- and para-positions. The elongation temperature of  $C_{2m,m}(S)$  further increased above that of  $C_{1m}(S)$  as the number of chiral side chains at the meta-position increased. It indicates that the stability of molecular stacks is not simply related to the number of chiral side chains present in a molecule.

Principally, the aromatic propeller of TPA core presented the racemate of P- and M-helicity with no preferable helicity. However, by intermolecularly colliding with



the chiral side chains at the meta-positions, the propeller structure was easily biased to more favorable helicity. It allowed the chiral monomer to smoothly access on the polymerized stack of the corresponding preferred helicity with entropic profit. Although the point chirality at the side chains is expected to give insignificant effect on the far-off TPA core, it would indirectly contribute to control the chirality of TPA propeller by efficient transfer of point chirality through intermolecular interaction during the assembly.

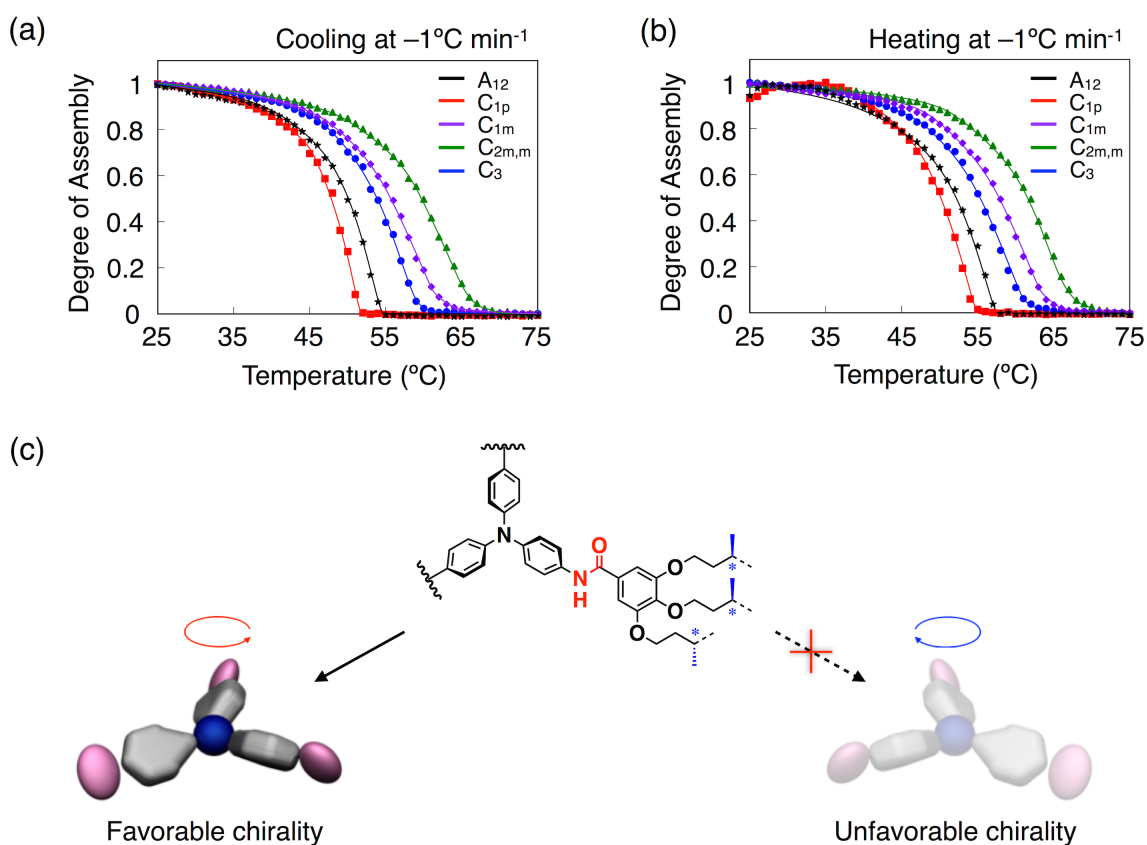


**Figure 4.4** Degree of assembly versus temperature for  $30\ \mu\text{M}$  chiral TPA compounds,  $C_{1p}(S)$ ,  $C_{1m}(S)$ ,  $C_{2m,m}(S)$ ,  $C_3(S)$  and  $A_{12}$  (for comparison) upon (a) cooling and (b) heating, respectively. Change in CD effect at  $252\ \text{nm}$  as a function of temperature with cooling rate at  $-1\ ^{\circ}\text{C min}^{-1}$ . (c) Schematic illustration for the facilitation of chiral TPA compounds due to a smooth access on the polymerized stack of corresponding preferred helicity with entropic profit.

## 4.5 Conclusion

With temperature-dependent spectroscopy measurement, I was able to investigate the self-assembly behavior of TPA derivatives and proposed the process of supramolecular polymerization based on unique feature of propeller conformation presented in molecules. Except for **A<sub>8</sub>**, which have linear octyl chains, all compounds self-assembled via cooperative process. According to nucleation-elongation model for cooperative supramolecular polymerization, the spatial effect of side chains was realized by comparing the elongation temperature of TPA analogues. In the assembled state, I assumed that the rotation of both inner and outer phenyl blades is restricted by intermolecular interactions of long alkyls at the meta-position in peripheral paraffinic wedges. In addition, chiral side chains could support the smooth access of TPA propeller on the polymerized stack of preferable helicity with entropic benefit. As a result, the chiral TPA compounds, which possess branched chiral chains, exhibited higher elongation temperature than achiral analogues. Importantly, this phenomenon has not been realized in the assembly of planar-shaped aromatic molecules. The unique self-assembly of TPA derivatives could give a fresh insight into the development of molecular assemblies based on propeller-shaped building blocks.

## **4.6 Experimental section**

### **Temperature-dependent Circular Dichroism (CD) and UV/Vis Absorption measurement**

The enantiomerically pure chiral compounds were dissolved at  $3.0 \times 10^{-5}$  M in cyclohexane. For the measurement of achiral compounds, which is optically inactive, 0.5 mol% of **C<sub>3</sub>(S)** was added into  $3.0 \times 10^{-5}$  M of each achiral samples in cyclohexane. The pre-mixed solutions were heated up to 75 °C at molecular dissolved state and cooled to RT at  $-1$  °C min<sup>-1</sup>. After 1 h, the samples were aged overnight and measured. The CD intensity at 252 nm were measured upon cooling from the molecularly dissolved state at 75 °C to 25 °C at  $1$  °C min<sup>-1</sup> and upon heating in the reverse order. The elongation temperatures for all compounds were consistent with those in UV/Vis absorption spectra.

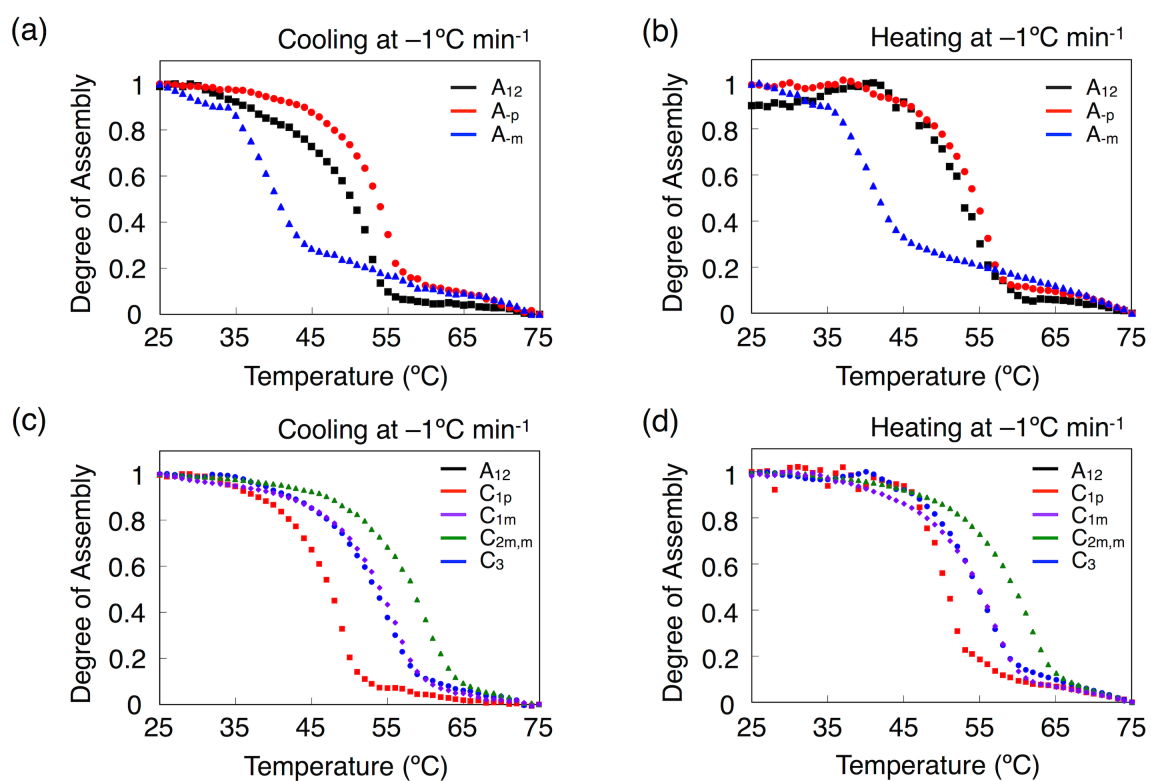


**Figure 4.5.** Degree of assembly versus temperature for 30  $\mu\text{M}$  of achiral TPA compounds,  $\text{A}_{12}$ ,  $\text{A}_p$  and  $\text{A}_m$ , and chiral TPA compounds,  $\text{C}_{1p}(\text{S})$ ,  $\text{C}_{1m}(\text{S})$ ,  $\text{C}_{2m,m}(\text{S})$  and  $\text{C}_3(\text{S})$ , upon (a, c) cooling and (b, d) heating, respectively. Change in absorbance at 252 nm as a function of temperature with cooling rate at  $-1\text{ }^\circ\text{C min}^{-1}$ .

## 4.7 References

- (1) Lee, C. C.; Grenier, C.; Meijer, E. W.; Schenning, A. P. H. J. *Chem. Soc. Rev.* **2009**, *38*, 671–683
- (2) Maggini, L.; Bonifazi, D. *Chem. Soc. Rev.* **2012**, *41*, 211–241
- (3) Barclay, T. G.; Constantopoulos, K.; Matisons, J. *Chem. Rev.* **2014**, *114*, 10217–10291
- (4) Ciferri, A. *Chem. Rev.* **2016**, *116*, 1353–1374.
- (5) De Santis, E.; Ryadnov, M. G. *Chem. Soc. Rev.* **2015**, *44*, 8288–8300.
- (6) Service, R. F. *Science* **2005**, *309*, 95.
- (7) Knowles, T. P. J.; Waudby, C. A.; Devlin, G. L.; Cohen, S. I. A.; Aguzzi, A.; Vendruscolo, M.; Terentjev, E. M.; Welland, M. E.; Dobson, C. M. *Science* **2009**, *326*, 1533–1537.
- (8) De Greef, T. F. A.; Smulders, M. M. J.; Wolffs, M.; Schenning, A. P. H. J.; Sijbesma, R. P.; Meijer, E. W. *Chem. Rev.* **2009**, *109*, 5687–5754
- (9) Markvoort, A. J.; Eikelder, Ten, H.; Hilbers, P. *Nature* **2011**.
- (10) Würthner, F.; Kaiser, T. E.; Saha-Möller, C. R. *Angew. Chem. Int. Ed.* **2011**, *50*, 3376–3410.
- (11) Jonkheijm, P.; Schoot, P. V. D.; Albertus P. H. J.; Schenning, A. P. H. J.; Meijer, E. W. *Science* **2006**, *313*, 80–83
- (12) Wang, F.; Gillissen, M. A. J.; Stals, P. J. M.; Palmans, A. R. A.; Meijer, E. W. *Chem. Eur. J.* **2012**, *18*, 11761–11770.
- (13) Schenning, A.; De Greef, T.; Meijer, E. W. *Nature* **2012**, *481*, 491–497
- (14) Ogi, S.; Sugiyasu, K.; Manna, S.; Samitsu, S.; Takeuchi, M. *Nat. Chem.* **2014**, *6*, 188–195
- (15) Krieg, E.; Weissman, H.; Shimoni, E. *J. Am. Chem. Soc.*, **2014**, *136*, 9443–9452
- (16) Rest, C.; Kandanelli, R.; Fernández, G. *Chem. Soc. Rev.* **2015**, *44*, 2543–2572.
- (17) Gershberg, J.; Fennel, F.; Rehm, T. H.; Lochbrunner, S.; Würthner, F. *Chem. Sci.* **2016**. DOI: 10.1039/c5sc03759j
- (18) Smulders, M. M. J.; Schenning, A. P. H. J.; Meijer, E. W. *J. Am. Chem. Soc.* **2008**, *130*, 606–611
- (19) Smulders, M. M. J.; Stals, P. J. M.; Mes, T.; Paffen, T. F. E.; Schenning, A. P.

- H. J.; Palmans, A. R. A.; Meijer, E. W. *J. Am. Chem. Soc.* **2009**, *132*, 620–626
- (20) Smulders, M. M. J.; Nieuwenhuizen, M. M. L.; Grossman, M.; Filot, I. A. W.; Lee, C. C.; De Greef, T. F. A.; Schenning, A. P. H. J.; Palmans, A. R. A.; Meijer, E. W. *Macromolecules* **2011**, *44*, 6581–6587.
- (21) Stals, P. J. M.; Korevaar, P. A.; Gillissen, M. A. J.; De Greef, T. F. A.; Fitié, C. F. C.; Sijbesma, R. P.; Palmans, A. R. A.; Meijer, E. W. *Angew. Chem. Int. Ed.* **2012**, *51*, 11297–11301.
- (22) Albertazzi, L.; van der Zwaag, D.; Leenders, C. M. A.; Fitzner, R.; van der Hofstad, R. W.; Meijer, E. W. *Science* **2014**, *344*, 491–495.
- (23) Ogi, S.; Stepanenko, V.; Sugiyasu, K.; Takeuchi, M.; Würthner, F. *J. Am. Chem. Soc.* **2015**, *137*, 3300–3307
- (24) Kang, J.; Miyajima, D.; Mori, T.; Inoue, Y.; Itoh, Y.; Aida, T. *Science* **2015**, *347*, 646–651.
- (25) van der Zwaag, D.; De Greef, T. F. A.; Meijer, E. W. *Angew. Chem. Int. Ed.* **2015**, *54*, 8334–8336.
- (26) Oosawa, F.; Kasai, M. *J. Mol. Biol.* **1962**, *4*, 10–21
- (27) Inoue, S.; Minemawari, H.; Tsutsumi, J.; Chikamatsu, M.; Yamada, T.; Horiuchi, S.; Tanaka, M.; Kumai, R.; Yoneya, M.; Hasegawa, T. *Chem. Mater.* **2015**, *27*, 3809–3812.
- (28) Smulders, M. M. J.; Nieuwenhuizen, M. M. L.; De Greef, T. F. A.; van der Schoot, P.; Schenning, A. P. H. J.; Meijer, E. W. *Chem. Eur. J.* **2010**, *16*, 362–367.
- (29) van der Schoot, P. Theory of Supramolecular Polymerization. In *Supramolecular Polymers*, 2nd ed.; Ciferri, A., Ed.; Taylor & Francis: London, U.K., **2005**.
- (30) Pisula, W.; Zorn, M.; Chang, J. Y.; Müllen, K.; Zentel, R. *Macromol Rapid Commun* **2009**, *30*, 1179–1202.
- (31) Lee, C. C.; Grenier, C.; Meijer, E. W.; Schenning, A. P. H. J. *Chem. Soc. Rev.* **2009**, *38*, 671–683.

## **Chapter 5**

### **LC assembly of propeller-shaped TPA derivatives**





## 5.1 Introduction

Controlling the organization of functional molecules via self-assembly has been an attractive subject for developing organic materials and devices.<sup>1-3</sup> Therefore  $\pi$ -conjugated liquid crystals (LCs) have attracted much attention in organic electronics because they exhibit self-organization, thermal stabilities and ease of processing through supramolecular interaction.<sup>3-6</sup> Those characteristic features were derived from their ordered phase and dynamicity.<sup>7</sup> First, ordered phase is a key factor for charge transport through the co-facial coupling of  $\pi$ -electrons, resulting from strong intermolecular interactions along superimposed aromatic cores. By controlling ordered assembly in the bulk and at interfaces, the resulting LCs could be fabricated at all length scales from molecular to macroscopic distances (Figure 5.1a). In addition, LCs have a self-healing ability for structural defects such as grain boundaries due to their fluid-like flow behavior. Upon simple thermal annealing, large single domains spontaneously formed over millimeter scale with millimeter thickness in LC mesophase.<sup>8,9</sup> More particularly, molecular orientation can be controlled by the manipulation of a concentration or temperature gradient,<sup>10,11</sup> external e-field,<sup>12,13</sup> or surface alignment layers.<sup>12-17</sup>

As substituted by appropriate solubilizing groups in  $\pi$ -conjugated aromatic segment peripherally, resulting LC materials formed 1D or 2D morphology depended on molecular shape (Figure 5.1b). The rod-like molecules<sup>18-19</sup> could form nematic and smectic phases and demonstrate a 2D charge transport in directions perpendicular to the molecular axis. On the other hand, the disk-like molecules<sup>20</sup> exhibit columnar assembly and promote 1D charge transport along columnar axis. Compared to rod-like molecules, the large orbital overlap was emerged between stacked disc-like molecules

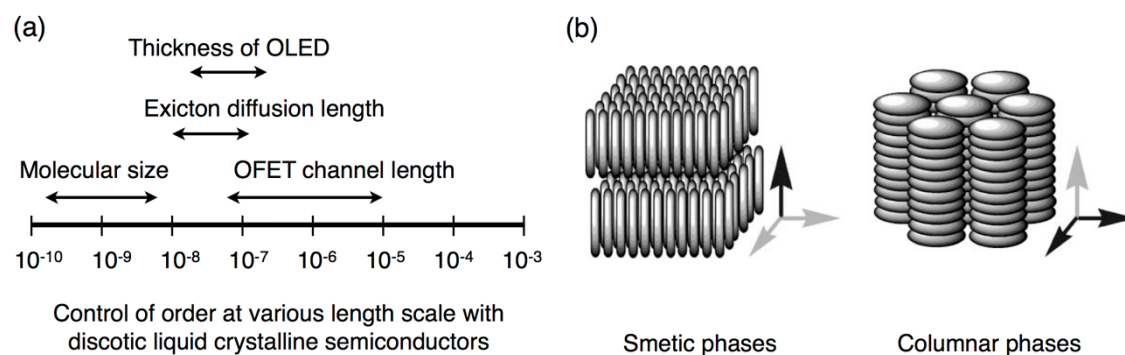


**Figure 5.1** (a) Typical length scales encountered in organic electronics and control of order achievable with LC semiconductors. (b) Schematic representation of rod-like (left) and disc-like (right) LC molecules.

and promoted more efficient charge transport along the columnar axis.<sup>7,21</sup> To develop optoelectronic devices based on 1D columnar assembly, planar  $\pi$ -conjugated aromatics such as triphenylene,<sup>22,23</sup> phthalocyanine<sup>24,25</sup> and hexabenzocoronene<sup>26,27</sup> have been utilized for core area in discotic molecules. However, those molecules suffer from some limitations, including high viscosity due to the bulky alkyl chains and high isotropic melting temperatures of discotic LCs as a result of the strong  $\pi$ - $\pi$  interaction between the planar-like aromatic cores.

On the other hand, non-planar  $\pi$ -conjugated motif was rarely utilized in spite of their unique properties such as macroscopic polarization and weak intermolecular interaction. Triphenylamine (TPA) is one of famous nonplanar aromatics with good hole transporting ability. As described in Chapter 1.2, there are only a few examples of TPA-based LC materials and their structure-property relationship is rarely discussed.<sup>17,28,29</sup> A systematic study on the self-assembly of triaryl amines in LC mesophase is supposed to provide us with a beneficial insight for their implementation as functional materials. Within this chapter, I describe hexagonal columnar assembly of

propeller-shaped TPA derivatives and their thermal behavior in LC mesophase by substituting to their peripheral paraffinic wedges, which result in their characteristic mesomorphic properties.

## 5.2 Hexagonal columnar assembly in LC mesophase

For bulk samples, the phase transitions and thermal behaviors of propeller-shaped TPA derivatives were summarized in Table 5.1. DSC and XRD analysis of fully alkylated TPA analogues, except for **A<sub>4</sub>**, showed an LC mesophase with hexagonal columnar assemblies in a wide temperature range. For example, DSC analysis of **A<sub>12</sub>** on second heating displayed that LC mesophase arised at  $-6\text{ }^{\circ}\text{C}$  and then disappeared at  $154\text{ }^{\circ}\text{C}$  to form an isotropic melt (Figure 5.2a). At  $140\text{ }^{\circ}\text{C}$ , resulting fluid LC materials showed a typical X-ray diffraction (XRD) pattern of a hexagonal columnar ( $\text{Col}_h$ ) geometry (Figure 5.2b). The diffraction peaks can be indexed as the (100), (110), and (200) reflections of a  $\text{Col}_h$  mesophase with d-spacings of 30.9, 17.8, and  $15.4\text{ \AA}$ . As a result, intercolumnar distance of the LC mesophase was evaluated as 3.56 nm. Upon cooling, the intensity of XRD spectra was decreased, but the diffraction peaks still displayed  $\text{Col}_h$  mesophase even at room temperature, suggesting that the columnar structure maintained in the whole temperature range of the LC mesophase.

By variable-temperature infrared spectroscopy, I successfully confirmed that hydrogen bondings supported the columnar assembly among superimposed molecular stacks through 3-folded amide units present in a molecule (Figure 5.2c). The characteristic vibrational bands of amide groups on the molecule shifted discontinuously to lower wavenumbers at the isotropic melt-to-LC phase transition of the molecules.<sup>30</sup>

In comparison with the other TPA analogues, as the length and the volume of side chains were reduced, the intercolumnar distance in the hexagonal columnar mesophase decreased. For example, as alkyl chain length of **A<sub>16</sub>**, **A<sub>12</sub>** and **A<sub>8</sub>** reduced from hexadecyl, dodecyl to octyl, the intercolumnar distances of their LC mesophases

**Table 5.1** Phase transition profiles and intercolumnar distance of propeller-shaped TPA derivatives.

Compounds	Transition Temperature (°C)				Intercolumnar Distance (nm)			
<b>A<sub>4</sub></b>	Cr	$\xrightleftharpoons[136]{157}$	Iso		-			
<b>A<sub>8</sub></b>	Cr	$\xrightleftharpoons[nd]{nd}$	Col <sub>h</sub>	$\xrightleftharpoons[183]{184}$	Iso	3.20 nm		
<b>A<sub>12</sub></b>	Cr	$\xrightleftharpoons[-15]{-6}$	Col <sub>h</sub>	$\xrightleftharpoons[156]{159}$	Iso	3.56 nm		
<b>A<sub>16</sub></b>	Cr	$\xrightleftharpoons[32]{nd}$	Col <sub>h</sub>	$\xrightleftharpoons[147]{148}$	Iso	3.84 nm		
<b>A<sub>m</sub></b>	Cr	$\xrightleftharpoons[-21]{-19}$	Col <sub>h</sub>	$\xrightleftharpoons[165]{167}$	Iso	3.25 nm		
<b>A<sub>p</sub></b>	Cr	$\xrightleftharpoons[131]{99}$	Col <sub>h</sub>	$\xrightleftharpoons[143]{141}$	Iso	3.25 nm		
<b>C<sub>1m(S)</sub></b>	Cr	$\xrightleftharpoons[nd]{nd}$	Col <sub>h</sub>	$\xrightleftharpoons[151]{151}$	Iso	3.44 nm		
<b>C<sub>1p(S)</sub></b>	Cr	$\xrightleftharpoons[nd]{nd}$	Col <sub>h</sub>	$\xrightleftharpoons[154]{155}$	Iso	3.45 nm		
<b>C<sub>2m,m(S)</sub></b>	Cr	$\xrightleftharpoons[nd]{nd}$	Col <sub>h</sub>	$\xrightleftharpoons[151]{153}$	Iso	3.31 nm		
<b>C<sub>3(S)</sub></b>	Cr	$\xrightleftharpoons[nd]{nd}$	G	$\xrightleftharpoons[141]{144}$	Col <sub>h</sub>	$\xrightleftharpoons[150]{151}$	Iso	3.23 nm

<sup>a</sup> Cr, Col<sub>h</sub>, G, and Iso denote crystalline, hexagonal columnar, glass, and isotropic phases, respectively.

<sup>b</sup> Intercolumnar Distance of the LC mesophases.

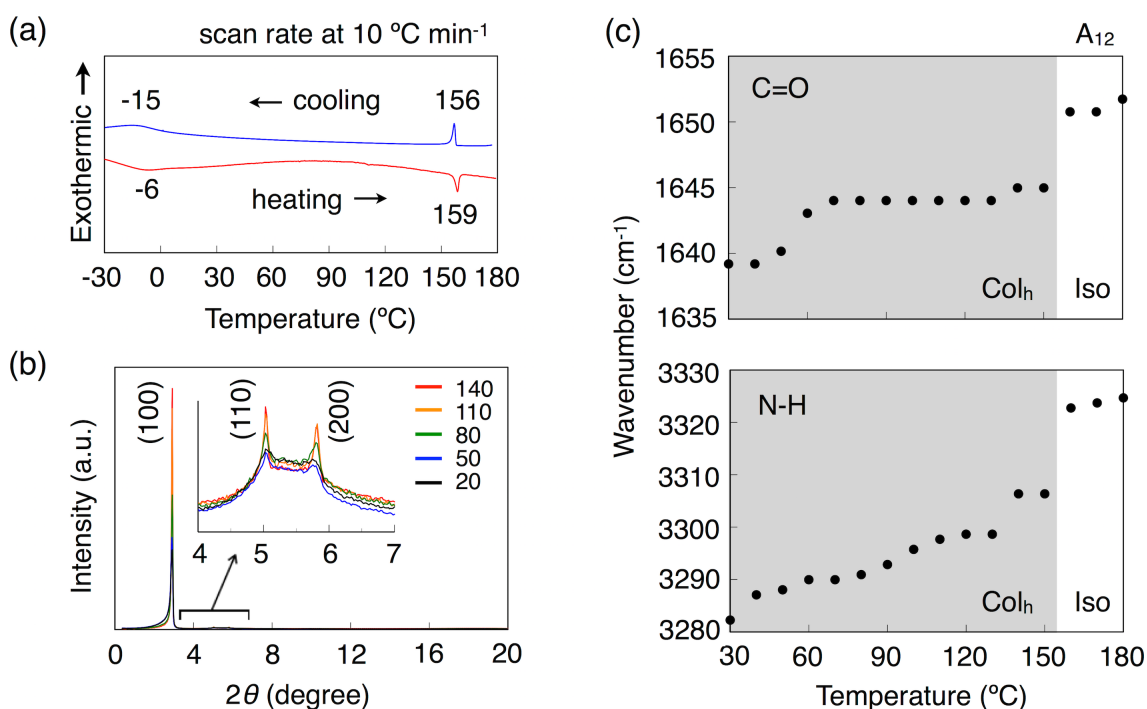


**Figure 5.2** (a) DSC traces on second heating/cooling of **3** at a scan rate of 10 °C min<sup>-1</sup>. (b) XRD patterns of **A**<sub>12</sub> depend on temperature upon cooling from its isotropic melt to Col<sub>h</sub> mesophase. Inset shows a magnified XRD pattern at 2θ = 4°~7°. (c) IR spectral change profiles of the N-H and C=O stretching vibrational bands of **A**<sub>12</sub> on cooling from 180 to 30 °C, where the white- and blue-colored regions represent temperature ranges for the isotropic melt and hexagonal columnar (Col<sub>h</sub>) meso-phase, respectively.

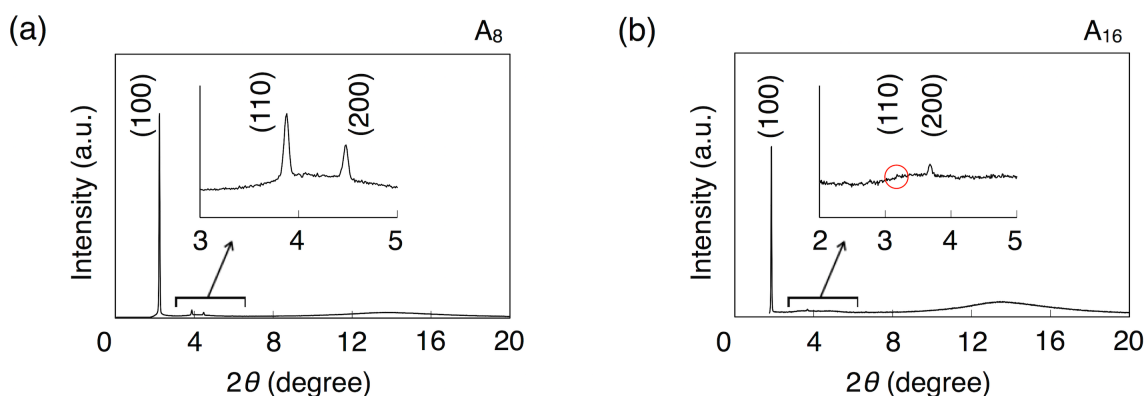


**Figure 5.3** XRD patterns for (a) **A**<sub>8</sub> and (b) **A**<sub>16</sub> at 120 °C. Inset shows a magnified XRD pattern at 2θ = 3°~5° and 2°~5°, respectively.

continuously decrease from 3.84 nm, 3.56 nm into 3.20 nm, respectively. However, the XRD pattern of  $A_{16}$  slightly mismatched with the index of (110) including in weak intensity, while  $A_8$  displayed clear diffraction peaks with strong intensity, which was well corresponded to  $Col_h$  geometry (Figure 5.3). It indicates that longer alkyl chain destabilized columnar assembly due to their high mobility with entropic gain.<sup>31,32</sup> When one of dodecyl chains reduced from peripheral wedges, the vicinal column was getting closer with diminishing the volume of dendritic chains. As a result,  $A_m$  and  $A_p$  exhibit shorter intercolumnar distance than  $A_{12}$ . The chiral analogues in LC mesophase were also found to reduce intermolecular distances as long alkyls substituted to shorter chiral chains.

### 5.3 Thermal behavior in LC mesophase

Propeller-shaped TPA compounds showed hexagonal columnar geometry in LC mesophase, while only  $\mathbf{A}_4$  exhibited simple isotropic melt-to-crystalline phase transition. It could be explained that substitution with short alkyl chains did not implicate in the phase segregation of isolated alkyl chain layers, which restrict formation of LC mesophase.<sup>32</sup> On the other hand, the longer alkyl chains apparently contribute to the change of phase-transition temperature with their thermal motion.

In contrast to XRD analysis, DSC analysis is highly dependent on the structure of peripheral paraffinic wedges. In comparison with these analogues, as the length of alkyl chains was shortened, the transition temperature from isotropic melt to LC mesophase became higher (Figure 5.4a). It revealed that the strength of columnar assemblies had risen by the enhanced crystallinity of shorter side chains with entropic benefit. For example,  $\mathbf{A}_{16}$  transforms from the LC mesophase into isotropic melt at 148 °C, while  $\mathbf{A}_{12}$  and  $\mathbf{A}_8$  melt at 159 °C and 184 °C, respectively. Interestingly, although the same number of long alkyl chains substituted to methyl group,  $\mathbf{A}_m$  and  $\mathbf{A}_p$  also showed different phase-transition temperatures.  $\mathbf{A}_m$ , which lacks long alkyls at one of the meta-positions, showed higher melting temperature than that of  $\mathbf{A}_{12}$ , while  $\mathbf{A}_p$  reached isotropic melt at lower temperature (Figure 5.4b). This phenomenon is of opposite trend with temperature-dependent spectroscopy study in diluted solution. It is noteworthy that the molecular behavior in the LC mesophase discriminates from the supramolecular equilibrium states such as elongation, nucleation and disassembly at elongation temperature in diluted solution. Below the melting temperature, all molecules formed columnar assemblies through hydrogen bonding of amide units and interdigitation of peripheral alkyls. It indicates that melting temperature reflects the



stability of columnar assembly in the LC mesophase. Upon heating, the side chains at the meta-position could be allowed to clash with one another intermolecularly for free rotation of outer phenyls. As a result, the lack of long alkyls at the meta-position enhanced the crystallinity and exhibited higher melting temperature of the LC mesophase. On the other hand, the branching in the chiral side chain triggers steric hindrances and the intermolecular interaction on columnar assembly was weakened, which resulted in lower melting temperature of TPA analogues with chiral side chain (Figure 5.4c). However, it is noteworthy that  $C_{1p}$  exhibits slightly higher melting temperature than the other chiral analogues due to the linear alkyls at meta-position. It indicates that the steric hindrance at meta-position is crucial for phase transition of propeller-shaped TPA derivatives in LC mesophase.

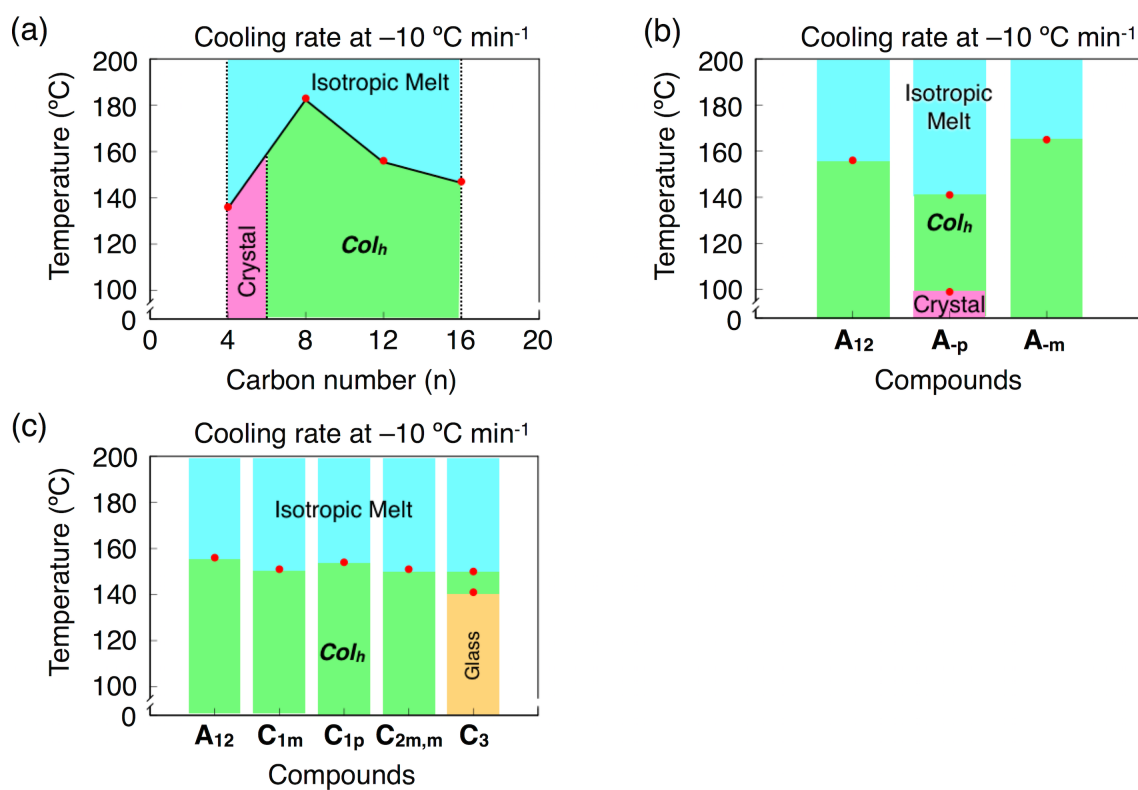


**Figure 5.4** Changes in phase-transition temperature of (a)  $A_4$ ,  $A_8$ ,  $A_{12}$  and  $A_{16}$ ; (b)  $A_{12}$ ,  $A_{-p}$  and  $A_{-m}$ ; (c)  $C_{1m}(S)$ ,  $C_{1p}(S)$ ,  $C_{2m,m}(S)$ , and  $C_3(S)$ : determined using DSC measurements on the second cooling at a scan rate of  $10\text{ °C min}^{-1}$ .

## 5.4 Homeotropic alignment of TPA derivatives in LC mesophase

Controlling the macroscopic orientation of discotic LC materials is an important issue for the development of electronic devices. For example, edge-on orientation of the hexagonal columns parallel to the substrate is suitable for field effect transistors (FETs), while homeotropic alignment with a face-on orientation of columns is required for photovoltaic and light-emitting applications.<sup>23,34</sup> To manipulate the both orientations, various techniques have been developed and applied to fluidic LC materials. Miyajima et al. reported that the amide-appended side-chain motif offered as E-field responsive handle for controlling large-area orientation of hexagonal columnar LC materials. Interestingly, the e-field responsiveness of discotic LC molecules was well emerged regardless of the structures of  $\pi$ -conjugated aromatic core and branched paraffinic tails, assembly and lattice dimensions. By taking this advantage of amide handle, the macroscopic alignment of TPA derivatives was investigated.

In POM measurement under crossed polarizers at 150 °C,  $A_{12}$  showed a characteristic fan texture corresponding with hexagonal columnar LC assembly, which is consistent with XRD analysis (Figure 5.5a). To confirm the orientation of hexagonal columnar LC mesophase, the LC compounds placed in the sandwich-typed glass cell composed of patterned ITO electrodes with designated electrode gaps of 5  $\mu\text{m}$ . When an electric field was applied as 20  $V_{pp} \mu\text{m}^{-1}$  at 150 °C, the fan texture was gradually eliminated and the dark field only was displayed in a part of sandwiched ITO electrodes, indicating that the columns of  $A_{12}$  aligned homeotropically to the surface of electrodes (Figure 5.5a). Interestingly, the homeotropic alignment was sustained for a long time after removing electric field and the random orientation with the birefringent texture was recovered by heating up to isotropic melt state and cooling to the LC

mesophase, subsequently. When the same experiment was performed for TPA analogues  $A_8$  and  $A_{16}$  at 180 °C and 140 °C, respectively, both of them also responded to the applied electric field and maintained a homeotropic alignment for a long time (Figure 5.5b,c). It indicates that the columnar assembly of TPA-based LC can be manipulated regardless of substituted alkyl chain length. With this easy control of the columnar orientation, a systematic study on the self-assembly of triaryl amines in LC mesophase provides us with a useful insight for their implementation as functional materials.

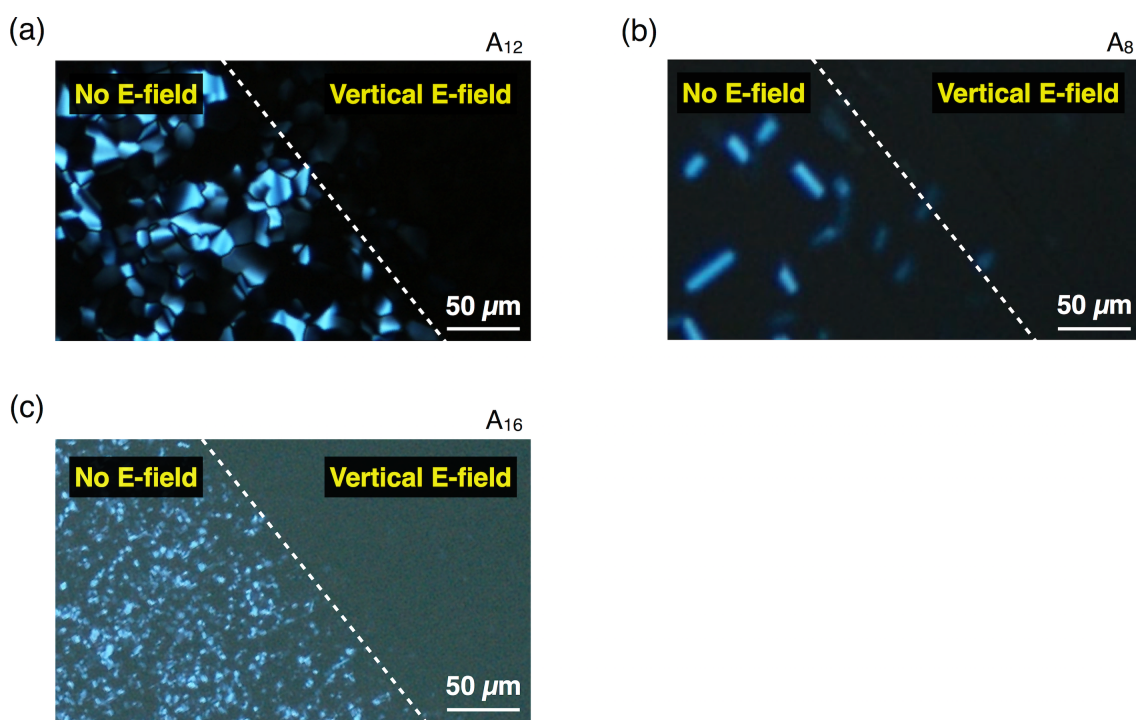


**Figure 5.5** POM images of (a)  $A_{12}$  at 150 °C, (b)  $A_8$  at 175 °C and (c)  $A_{16}$  at 140 °C, respectively. All columnar LC compounds were sandwiched by glass plates with patterned ITO electrodes (5- $\mu\text{m}$  separation) under applied electric field of 20  $V_{pp} \mu\text{m}^{-1}$ .

## **5.5 Conclusion**

In summary, I have investigated the self-assembly of TPA derivatives with a variation of their peripheral groups in the bulk. By the mean of DSC, XRD and POM analysis, the TPA compounds in an LC mesophase were found to form hexagonal assembly, which are supported by hydrogen bonded amide group and branched paraffinic wedges, in a wide temperature range. As comparing the thermal behavior of TPA-based LC molecules, I obtained a fresh insight into the relationship between propeller conformation and self-assembly. First, the critical temperature from the LC mesophase into isotropic melt is getting higher with diminishing their alkyl chain length with entropic benefit in columnar assembly. When one of the long alkyls was replaced with a methyl group, the critical temperature was differentiated by the substituted position, indicating that the rotational intermolecular restriction was strongly related to thermal stability of the LC mesophase. Furthermore, I successfully could manipulate the orientation of hexagonal columns by using external E-field. With considering the structure-property relationship, a systematical study on the columnar assembly of TPA-based LC compounds provides us with useful insight for design of soft materials for optoelectronics based on propeller-shape conformation.

## **5.6 Experimental Section**

### **5.6.1. Differential scanning calorimetry (DSC) Analysis**

Differential scanning calorimetry (DSC) was performed on a Mettler–Toledo model DSC 822e differential scanning calorimeter, where temperature and enthalpy were calibrated with In (430 K, 3.3 J mol<sup>-1</sup>) and Zn (692.7 K, 12 J mol<sup>-1</sup>) standard samples using sealed Al sample pans. Cooling and heating profiles were recorded and analyzed using the Mettler–Toledo STARe software system.

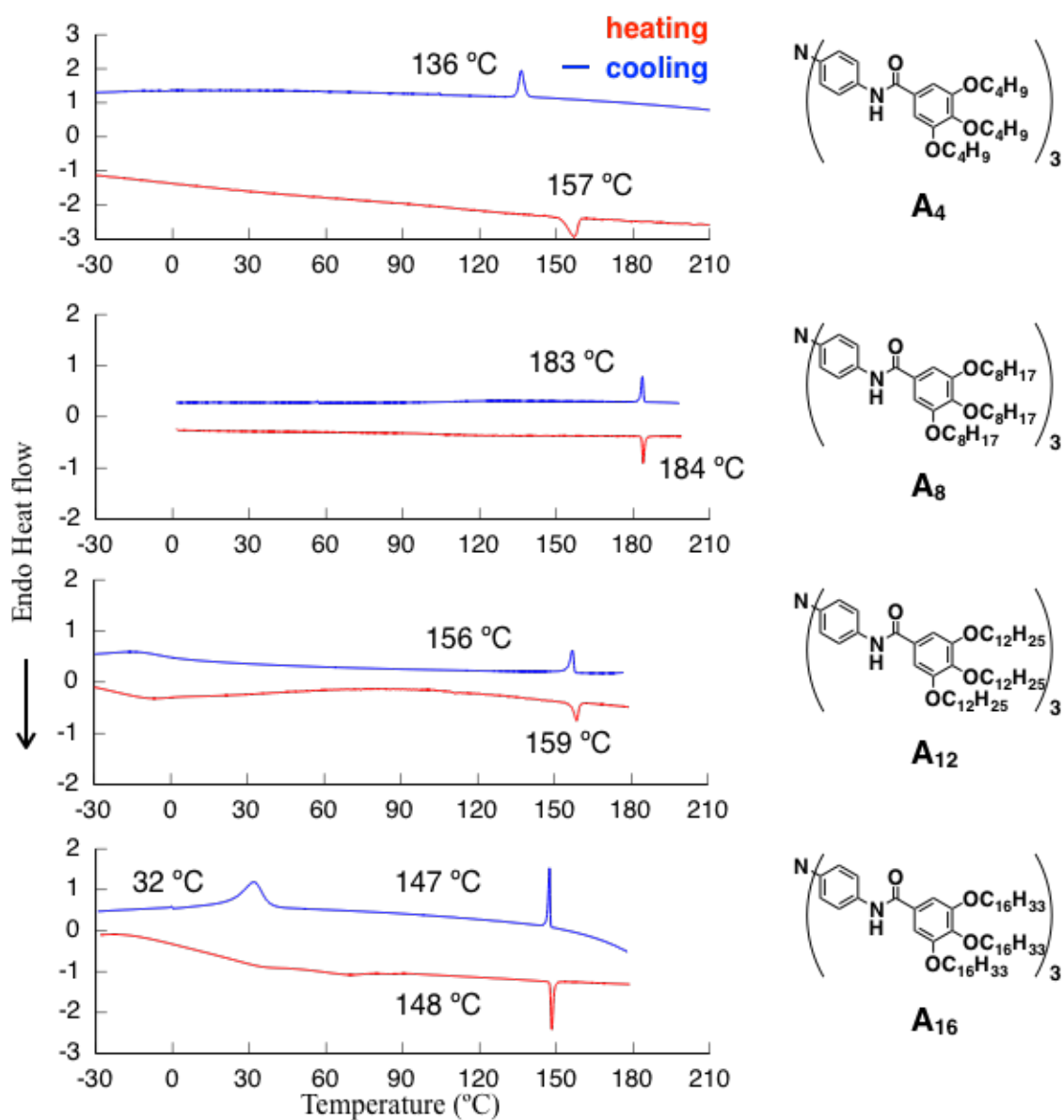


**Figure 5.6** DSC traces on the second heating and cooling of A<sub>4</sub>, A<sub>8</sub>, A<sub>12</sub>, and A<sub>16</sub> at a scan rate of 10 °C min<sup>-1</sup>.

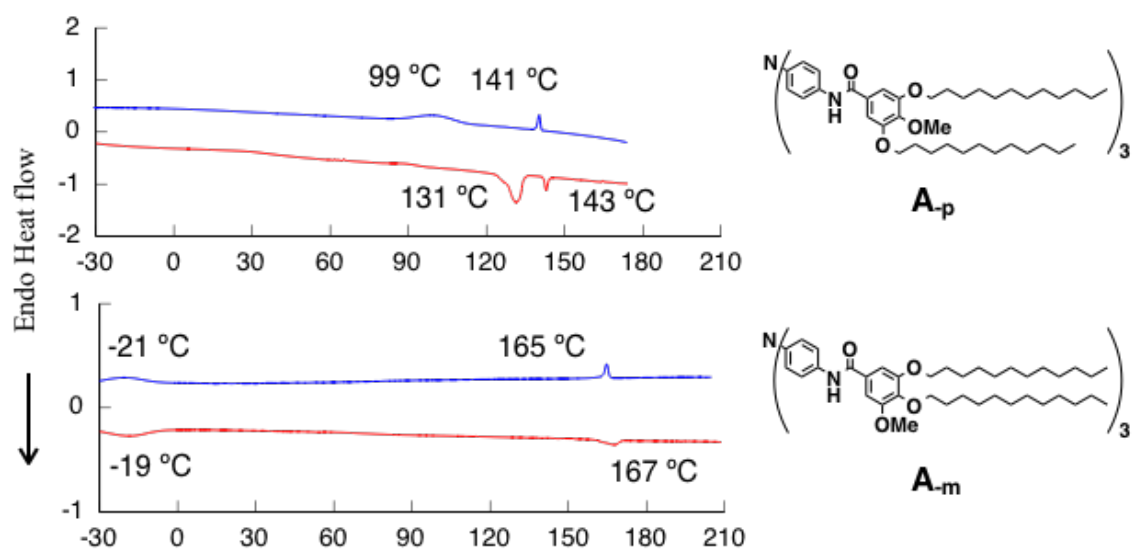


**Figure 5.6 (cont.)** DSC traces on the second heating and cooling of **A-p**, and **A-m** at a scan rate of  $10\text{ }^{\circ}\text{C min}^{-1}$ .



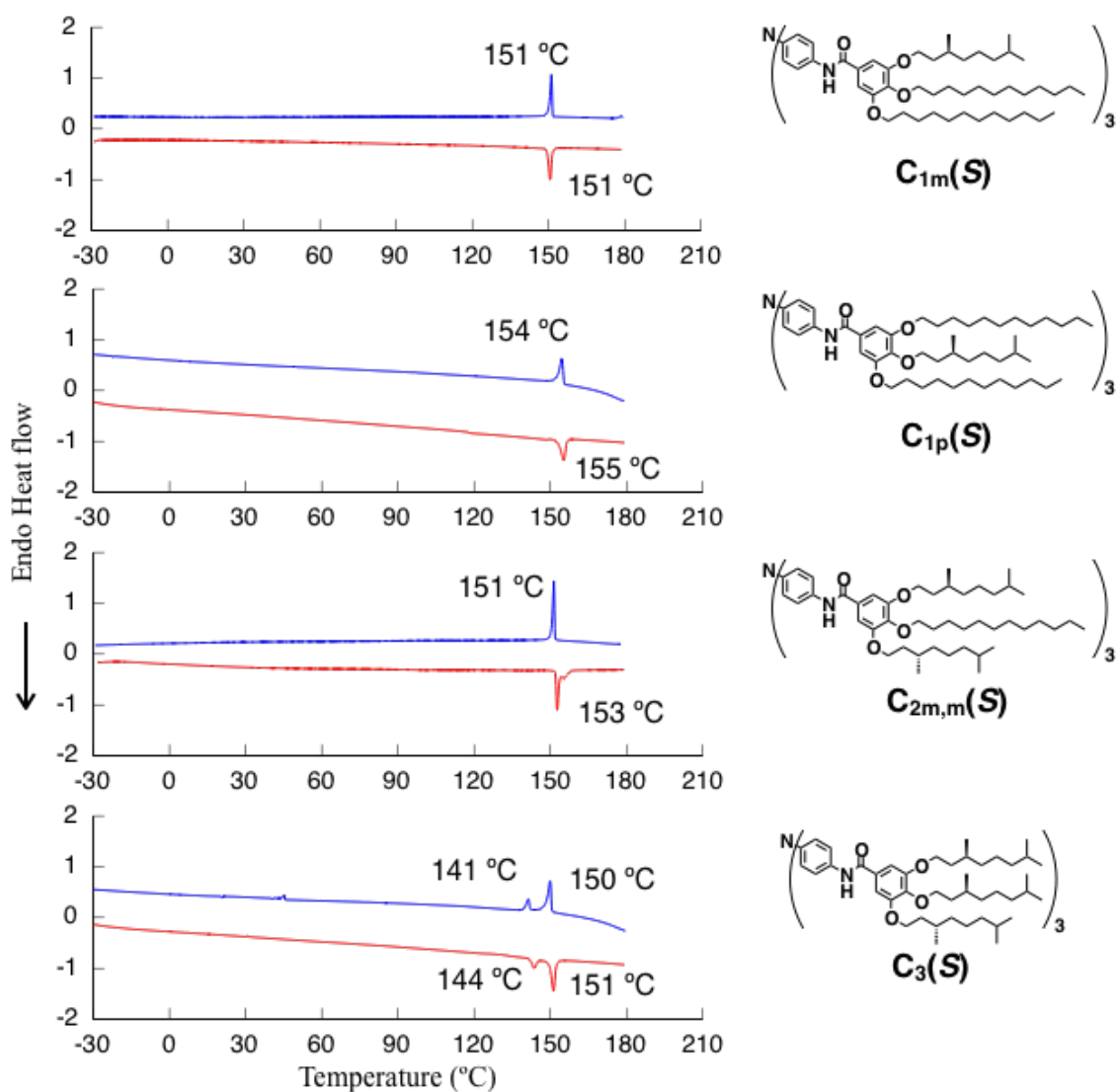


**Figure 5.6 (cont.)** DSC traces on the second heating and cooling of C<sub>1m</sub>(S), C<sub>1p</sub>(S), C<sub>2m,m</sub>(S), and C<sub>3</sub>(S) at a scan rate of 10 °C min<sup>-1</sup>.

### 5.6.2. X-ray diffraction (XRD) analysis

X-ray diffraction (XRD) analysis was performed on a Cu substrate using a Rigaku model Ultima III X-ray diffractometer with a monochromated CuK $\alpha$  radiation source. High-resolution XRD analysis of TPA derivatives was carried out at 120 °C using a synchrotron radiation X-ray beam with a wavelength of 1.08 Å on BL02B2 at SPring-8 (Hyogo, Japan). A large Debye-Scherrer camera with a camera length of 286.48 mm was used with an imaging plate as a detector, where the diffraction pattern was obtained with a 0.01 ° step in  $2\theta$ . The exposure time to the X-ray beam was 20 min.

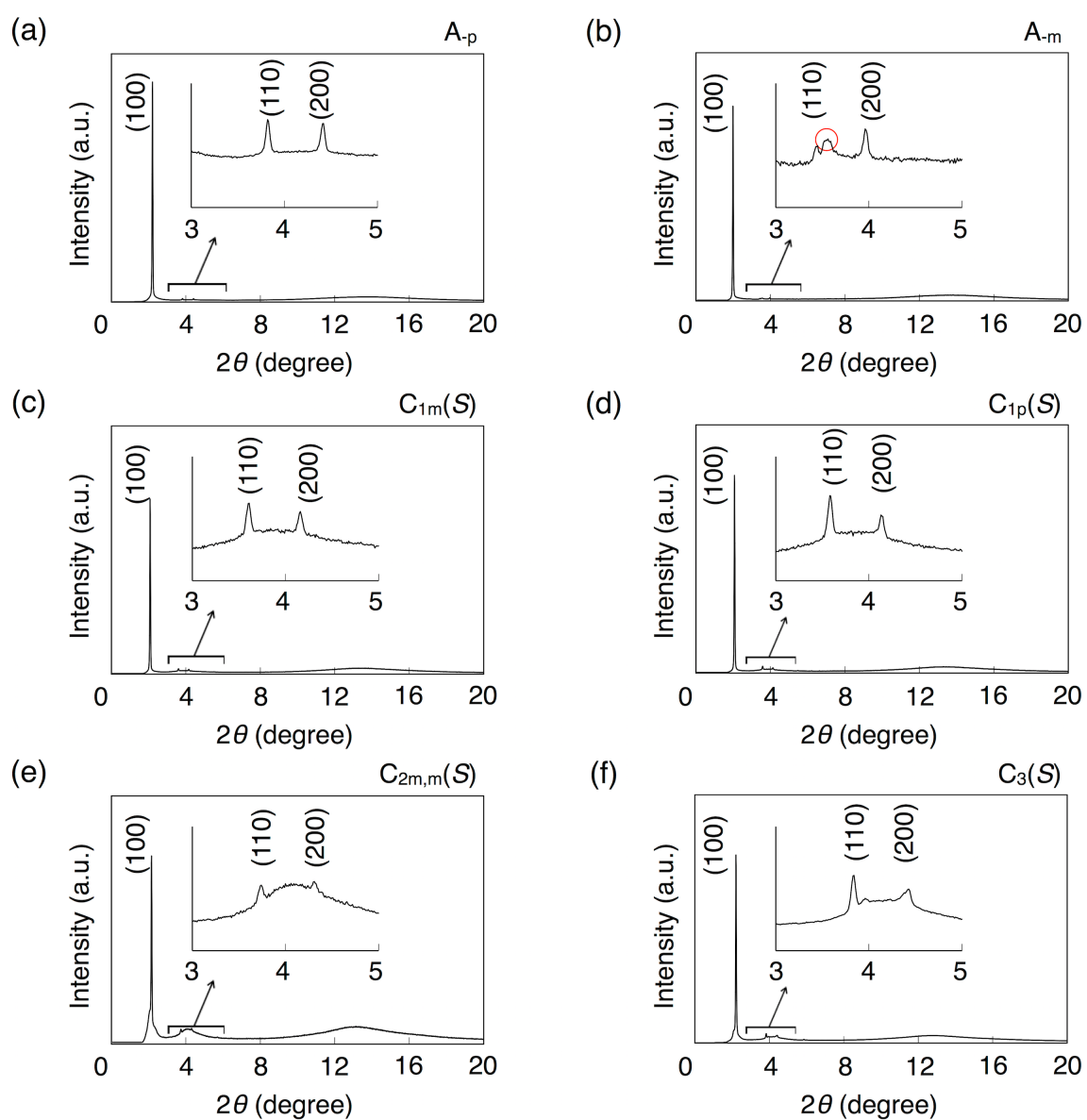


**Figure 5.7** XRD patterns for (a)  $A_p$ , (b)  $A_m$ , (c)  $C_{1m}(S)$ , (d)  $C_{1p}(S)$ , (e)  $C_{2m,m}(S)$  and (f)  $C_3(S)$ . All compounds were measured at 120 °C except for  $C_3(S)$  at 155 °C. Inset shows a magnified XRD pattern at  $2\theta = 3^\circ \sim 5^\circ$ . An unidentified peak is marked with red circle.

### 5.6.3. Polarized optical microscopy (POM) analysis

Polarized optical microscopy (POM) was performed on an OLYMPUS model BX-51 polarized optical microscope equipped with a Mettler FP-82HT hot stage.

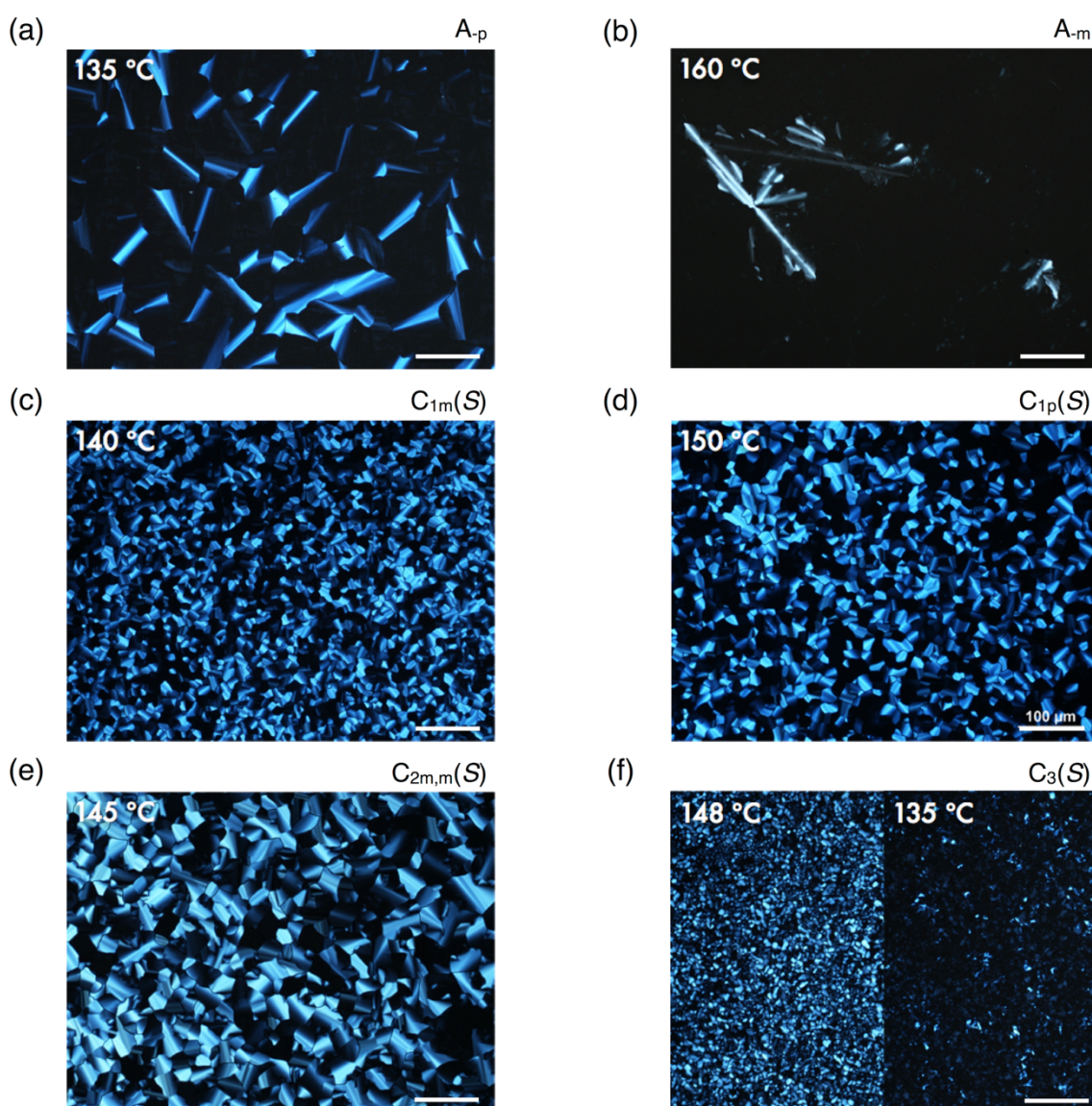


**Figure 5.8** POM image of (a)  $A_p$ , (b)  $A_m$ , (c)  $C_{1m}(S)$ , (d)  $C_{1p}(S)$ , (e)  $C_{2m,m}(S)$  and (f)  $C_3(S)$ , respectively, at the temperature noted in the top left of image. All columnar LC compounds were sandwiched by glass plates with 5- $\mu\text{m}$  separation.

## 5.7 References

- (1) Goodby, J. W.; *Curr. Opin. Solid State Mater. Sci.* **1999**, *4*, 361-368
- (2) Kato, T.; *Science* **2002**, *295*, 2414-2418
- (3) Percec, V.; Glodde, M.; Bera, T. K.; Miura, Y.; Shiyanovskaya, I.; Singer, K. D.; Balagurusamy, V. S. K.; Heiney, P. A.; Schnell, I.; Rapp, A.; Spiess, H.-W.; Hudson, S. D.; Duan, H. *Nature* **2002**, *419*, 384-387
- (4) Schmidt-Mende, L.; Fechtenkötter, A.; Müllen, K.; Moons, E.; Friend, R. H.; MacKenzie, J. D. *Science* **2001**, *293*, 1119-1122
- (5) Hoogboom, J.; Behdani, M.; Elemans, J. A. A. W.; Devillers, M. A. C.; De Gelder, R.; Rowan, A. E.; Rasing, T.; Nolte, R. J. M. *Angew. Chem. Int. Ed. Engl.* **2003**, *42*, 1812-1815
- (6) Hoogboom, J.; Elemans, J. A.; Rasing, T.; Rowan, A. E.; Nolte, R. J. *Polym. Int.* **2007**, *56*, 1186-1191.
- (7) Sergeev, S.; Pisula, W.; Geerts, Y. H. *Chem. Soc. Rev.* **2007**, *36*, 1902-1929
- (8) De Cupere, V.; Tant, J.; Viville, P.; Lazzaroni, R.; Osikowicz, W.; Salaneck, W. R.; Geerts, Y. H. *Langmuir* **2006**, *22*, 7798-7806
- (9) van Breemen, A. J. J. M.; Herwig, P. T.; Chlon, C. H. T.; Sweelssen, J.; Schoo, H. F. M.; Setayesh, S.; Hardeman, W. M.; Martin, C. A.; de Leeuw, D. M.; Valetton, J. J. P.; Bastiaansen, C. W. M.; Broer, D. J.; Popa-Merticaru, A. R.; Meskers, S. C. J. *J. Am. Chem. Soc.* **2006**, *128*, 2336-2345
- (10) Tracz, A.; Jeszka, J. K.; Watson, M. D.; Pisula, W.; Müllen, K.; Pakula, T. *J. Am. Chem. Soc.* **2003**, *125*, 1682-1683
- (11) Pisula, W.; Menon, A.; Stepputat, M.; Lieberwirth, I.; Kolb, U.; Tracz, A.; Sirringhaus, H.; Pakula, T.; Müllen, K. *Advanced Materials* **2005**, *17*, 684-689
- (12) Miyajima, D.; Tashiro, K.; Araoka, F.; Takezoe, H.; Kim, J.; Kato, K.; Takata, M.; Aida, T. *J. Am. Chem. Soc.* **2009**, *131*, 44-45
- (13) Miyajima, D.; Araoka, F.; Takezoe, H.; Kim, J.; Kato, K.; Takata, M.; Aida, T. *Angew. Chem. Int. Ed.* **2011**, *50*, 7865-7869.
- (14) Zimmermann, S.; Wendorff, J. H.; Weder, C. *Chem. Mater.* **2002**, *14*, 2218-2223.
- (15) van de Craats, A. M.; Stutzmann, N.; Bunk, O.; Nielsen, M. M.; Watson, M.;

- Müllen, K.; Chanzy, H. D.; Siringhaus, H.; Friend, R. H. *Adv. Mater.* **2003**, *15*, 495–499
- (16) Bunk, O.; Nielsen, M. M.; Sølling, T. I.; Van De Craats, A. M.; Stutzmann, N. *J. Am. Chem. Soc.* **2003**, *125*, 2252–2258
- (17) Choudhury, T. D.; Rao, N. V. S.; Tenent, R.; Blackburn, J.; Gregg, B.; Smalyukh, I. I. *J. Phys. Chem. B* **2011**, *115*, 609–617
- (18) Funahashi, M.; Hanna, J.-I. *Appl. Phys. Lett.* **2000**, *76*, 2574–2576
- (19) O'Neill, M.; Kelly, S. M. *Adv. Mater.* **2003**, *15*, 1135–1146
- (20) Simpson, C. D.; Wu, J.; Watson, M. D.; Mullen, K. *J. Mater. Chem.* **2004**, *14*, 494–504
- (21) Warman, J. M.; de Haas, M. P.; Dicker, G.; Grozema, F. C.; Pirus, J.; Debije, M. *G. Chem. Mater.* **2004**, *16*, 4600–4609
- (22) Laschat, S.; Baro, A.; Steinke, N.; Giesselmann, F.; Hägele, C.; Scalia, G.; Judele, R.; Kapatsina, E.; Sauer, S.; Schreivogel, A.; Tosoni, M. *Angew. Chem. Int. Ed.* **2007**, *46*, 4832–4887
- (23) Adam, D.; Schuhmacher, P.; Simmerer, J.; Häussling, L.; Siemensmeyer, K.; Etzbachi, K. H.; Ringsdorf, H.; Haarer, D. *Nature* **1994**, *371*, 141–143
- (24) Van der Pol, J. F.; Neeleman, E.; Zwikker, J. W.; Nolte, R. J. M.; Drenth, W.; Aerts, J.; Visser, R.; Picken, S. J. *Liq. Cryst.* **2006**, *6*, 577–592
- (25) Sergeev, S.; Pouzet, E.; Debever, O.; Levin, J.; Gierschner, J.; Cornil, J.; Aspe, R. G.; Geerts, Y. H. *J. Mater. Chem.* **2007**, *17*, 1777–1784
- (26) Herwig, P.; Kayser, C. W.; Müllen, K.; Spiess, H. W. *Adv. Mater.* **1996**, *8*, 510–513.
- (27) Feng, X.; Pisula, W.; Kudernac, T.; Wu, D.; Zhi, L.; De Feyter, S.; Müllen, K. *J. Am. Chem. Soc.* **2009**, *131*, 4439–4448.
- (28) Wang, Y.-J.; Sheu, H.-S.; Lai, C. K. *Tetrahedron* **2007**, *63*, 1695–1705
- (29) Domoto, Y.; Busseron, E.; Maaloum, M.; Moulin, E.; Giuseppone, N. *Chem. Eur. J.* **2014**, *21*, 1938–1948
- (30) Miyajima, D.; Araoka, F.; Takezoe, H.; Kim, J.; Kato, K.; Takata, M.; Aida, T. *J. Am. Chem. Soc.* **2010**, *132*, 8530–8531.
- (31) Inoue, S.; Minemawari, H.; Tsutsumi, J.; Chikamatsu, M.; Yamada, T.; Horiuchi, S.; Tanaka, M.; Kumai, R.; Yoneya, M.; Hasegawa, T. *Chem. Mater.*

- 2015**, 27, 3809–3812.
- (32) Mei, J.; Bao, Z. *Chem. Mater.* **2014**, 26, 604–615.
- (33) Pisula, W.; Tomovic, Z.; Hamaoui, El, B.; Watson, M. D.; Pakula, T.; Müllen, K. *Adv. Func. Mater.* **2005**, 15, 893–904.
- (34) Miyajima, D.; Araoka, F.; Takezoe, H.; Kim, J.; Kato, K.; Takata, M.; Aida, T. *Science* **2012**, 336, 209–213.





## **Chapter 6**

### **Summary and perspective**



## 6.1 Summary and perspective

To develop novel materials with better functional property and improved practical accessibility, many material scientists have designed and investigated various chemicals. Among them, supramolecular building blocks have attracted international attention to their unique feature that integrates order and dynamics to accomplish self-organization. Especially,  $\pi$ -conjugated aromatic molecules have been utilized as essential component of supramolecular building blocks. They could form strongly ordered structures derived from their strong  $\pi$ - $\pi$  interaction, which also allowed for extending their electronic properties. As a result, various types of  $\pi$ -conjugated molecules have been reported and implemented in organic electric devices. However, nonplanar  $\pi$ -conjugated molecules have attracted less attention from supramolecular chemists in spite of their unique features such as macroscopic polarization and intrinsic chirality. TPA is a propeller-shaped molecule, which have emerged a good hole transporting material. They were mostly utilized in solid state, but the self-assembly behavior and their associated properties were rarely investigated. Along this line, I designed new supramolecular building blocks based on TPA core and could elucidate the relationship between propeller conformation and their unique self-assembly behavior.

First, I found high amplification of supramolecular chirality derived from propeller conformation of TPA, which serves as an extra chiral source with the stereogenic centers in their side chains. As a result, one molecules of a chiral TPA compound can manipulate the helical orientation of 500 molecules of achiral analogues. Furthermore, the hierarchy of chiral molecules was emerged by tuning the peripheral chiral side chains. This unique feature of propeller-shaped TPA compounds provides us

with fresh insight for exploring the origin of symmetry breaking as well as realizing the practical application of single-handed supramolecular helix. For instance, this system can be applicable for asymmetric catalysis, which has been proved in the hybrid catalyst with covalent helical polymers and metals.<sup>1-6</sup> In 2013, Raynal and co-workers reported the asymmetric hydrogenation utilizing the sergeants and soldiers system for supramolecular helices of phosphine-appended BTA derivatives.<sup>7</sup> However, the resultant selectivity of product was low (31%ee) in chiral amplified system and totally lost in highly polar solvent, CH<sub>2</sub>Cl<sub>2</sub>. In addition, because the phosphine ligand attached one of three-arms in BTA, the degree of chiral amplification could decrease in the resultant assembly. In biological system, highly ordered biomolecules with single helicity was selectively produced by efficient asymmetric catalysis together with the complex of a metal and proteins,<sup>8-10</sup> or DNA.<sup>11,12</sup> Because the helical structure of DNA and proteins was derived from the formation of supramolecular assemblies, it is desirable to develop and investigate the asymmetric catalysis in artificial supramolecular helices and their sergeants and soldiers system. It is noteworthy that the high degree of chiral amplification is exhibited in the presence of even one chiral side chain at meta-position of outer phenyls present in a my TPA compound. It means that the other side chain can be functionalized with the binding site for a metal. Especially, the para-position is valuable to append other functional group due to no steric hindrance for the rotation of outer phenyls. This structural merit supposes to enhance the efficiency and the selectivity of asymmetric reactions. Furthermore, if such high amplification of supramolecular chirality can be also realized in aqueous media by substituting with hydrophilic side chain, it provides us with profit insight for studying asymmetric biological system.

Second, to elucidate the effect of propeller conformation for TPA assembly, I performed a systematic study on the process of supramolecular polymerization by tuning peripheral alkyl units. With the temperature-dependent spectroscopy measurement, I could discuss the role of long alkyl chain in the self-assembly of propeller-shaped compounds. As tuning the position of long alkyl substitution, the critical temperature of supramolecular polymerization was varied largely. It is related to the restriction of the propeller rotation via intermolecular interactions of long alkyls at meta-position. In addition, the propeller conformation could provide extra entropy benefit, which is not the case for planar-shaped molecules, for easy access of molecular assembly with branched chiral chains. This unique assembly behavior was also realized in the bulk. TPA derivatives exhibited hexagonal columnar geometry, which was supported by aromatic appended amide units and peripheral paraffinic wedges. Interestingly, the transition temperature from LC mesophase into isotropic melt showed an opposite trend with the process of supramolecular polymerization in cyclohexane. It is also related to the rotation freedom of propeller units, which results in the higher melting temperature with the lack of long alkyls at meta-position. Furthermore, these liquid crystalline TPA exhibited electric field responsiveness, indicating that they formed highly ordered columns and their orientations could be easily manipulated by external stimuli. Recently, the processability of organic materials for electronic and semiconducting application has attracted considerable attention, because it may enable flexible and large-area fabrication with low cost production.<sup>13-15</sup> For example, organic semiconductors in small molecular level such as 6,13-Bis(triisopropylsilylethynyl) pentacene<sup>16,17</sup> or benzothieno-[3,2-*b*][1]benzothiophene (BTBT) derivatives<sup>18-20</sup> can be processed by using print production technologies. To achieve suitable solubilities and

thermal stabilities with desired properties, it necessarily investigates the relationship of molecular structure and their associated properties in the assembly. In general, alkyl chain substitution leads to improve the solubility of organic materials<sup>21,22</sup> and supports to formation of ordered 1D or 2D structures. However, I realized that exceptional melting temperature increase with alkyl chain substitution, which derived from dynamic propeller conformation of TPA compounds. Considering the structure-property relationship in the development of organic materials, these studies are supposed to provide us with beneficial insight for the design of organic devices with better optoelectronic properties.

## 6.2 References

- (1) Reggelin, M.; Schultz, M.; Holbach, M.; *Angew. Chem., Int. Ed.* **2002**, *41*, 1614–1617.
- (2) Reggelin, M.; Doerr, S.; Klussmann, M.; Schultz, M.; Holbach, M.; *Proc. Natl. Acad. Sci., U. S. A.* **2004**, *101*, 5461–5466.
- (3) Roelfes, G.; Feringa, B. L.; *Angew. Chem. Int. Ed.* **2005**, *44*, 3230–3232.
- (4) Davie, E. A. C.; Mennen, S. M.; Xu, Y.; Miller, S. J.; *Chem. Rev.* **2007**, *107*, 5759–5812.
- (5) Yamamoto, T.; Suginome, M.; *Angew. Chem. Int. Ed.* **2009**, *48*, 539–542.
- (6) Miyabe, T.; Hase, Y.; Iida, H.; Maeda, K.; Yashima, E.; *Chirality* **2009**, *21*, 44–50.
- (7) Raynal, M.; Portier, F.; van Leeuwen, P. W. N. M.; Bouteiller, L.; *J. Am. Chem. Soc.* **2013**, *135*, 17687–17690.
- (8) Ward, T. R. *Acc. Chem. Res.* **2011**, *44*, 47–57 and references therein.
- (9) Bos, J.; Fusetti, F.; Driessen, A. J. M.; Roelfes, G. *Angew. Chem. Int. Ed.* **2012**, *51*, 7472–7475.
- (10) Hyster, T. K.; Knörr, L.; Ward, T. R.; Rovis, T. *Science* **2012**, *338*, 500–503.
- (11) Boersma, A. J.; Megens, R. P.; Feringa, B. L.; Roelfes, G. *Chem. Soc. Rev.* **2010**, *39*, 2083–2092 and references therein.
- (12) Park, S.; Sugiyama, H. *Molecules* **2012**, *17*, 12792–12803 and references therein.
- (13) Kang, B.; Lee, W. H.; Cho, K. *ACS Appl. Mater. Interfaces* **2013**, *5*, 2302–2315.
- (14) Carlson, A.; Bowen, A. M.; Huang, Y.; Nuzzo, R. G.; Rogers, J. A. *Adv. Mater.* **2012**, *24*, 5284–5318.
- (15) Berggren, M.; Nilsson, D.; Robinson, N. D. *Nat. Mater.* **2007**, *6*, 3–5.
- (16) Park, S. K.; Jackson, T. N.; Anthony, J. E.; Mourey, D. A. *Appl. Phys. Lett.* **2007**, *91*, 063514.
- (17) Kjellander, B. K. C.; Smaal, W. T. T.; Anthony, J. E.; Gelinck, G. H. *Adv. Mater.* **2010**, *22*, 4612–4616.
- (18) Ebata, H.; Izawa, T.; Miyazaki, E.; Takimiya, K.; Ikeda, M.; Kuwabara, H.; Yui, T. *J. Am. Chem. Soc.* **2007**, *129*, 15732–15733.

- (19) Izawa, T.; Miyazaki, E.; Takimiya, K. *Adv. Mater.* **2008**, *20*, 3388–3392.
- (20) Minemawari, H.; Yamada, T.; Matsui, H.; Tsutsumi, J.; Haas, S.; Chiba, R.; Kumai, R.; Hasegawa, T. *Nature* **2011**, *475*, 364–367.
- (21) Allard, S.; Forster, M.; Souharce, B.; Thiem, H.; Scherf, U. *Angew. Chem. Int. Ed.* **2008**, *47*, 4070–4098.
- (22) Mei, J.; Bao, Z. *Chem. Mater.* **2014**, *26*, 604–615.







## Curriculum Vitae



Taehoon Kim was born in Donghae-si, Republic of Korea on May 1th, 1984. He received his Bachelor of Science degree (2007) in chemistry from Yonsei University, Korea. After completing the compulsory military service in Chemical Corps of Republic of Korea Army as a platoon commander, he started in 2010 with his study in Chemistry at Seoul National University, Korea. In Feb 2013, he graduated with a major in Organic Chemistry under the supervision of Prof. M. Lee and Prof. C.-M. Park. As a Ph.D student began the author of this thesis in in April 2013. The author of this thesis started his PhD-research in April 2013 in the Department of Chemistry and Biotechnology at the University of Tokyo under the guidance of prof.dr. T. Aida and dr. D. Miyajima. The results from the investigations conducted in his Ph.D course, are described in this thesis. His main research interests include self-assembling molecules, supramolecular chirality and controlled supramolecular structures.



## **Acknowledgements**

First I want to express my sincere gratitude to advisor, Professor Takuzo Aida. His enthusiasm always motivated me to think harder and to research better. I ensure that my communication and discussion skills could not be enhanced without his subsequent request for giving questions. I am also deeply grateful to the other members of this thesis committee: Professor Kazuaki Kudo, Associate Professor Masafumi Yoshio, Lecturer Hiroshi Sato and Dr. Yasuhiro Ishida (RIKEN). Their profitable advices and comments make my thesis become more valuable. I extend my gratitude to Dr. Daigo Miyajima for supervising me in daily contacts. His willingness and support has ensured that I never lost courage, while his questions often threatened me to get a cliff parade due to my shallow knowledge and narrow observation.

Grateful acknowledgement is also made to Dr. Tadashi Mori, Associate Professor in Osako University. He provided the chance to visualize the molecular assembly model using density functional theory (DFT) computational study.

As a student trainee in Emergent Soft Matter Function Research Group, RIKEN Center for Emergent Matter Science, I have had the privilege to accompany intelligent colleagues for studying supramolecular system. Although some of them are younger than me, I can learn many things from their profound knowledge for basics as well as cautious attitude for experiments. Jiheong Kang and Dr. Venkata Rao Kotagiri, who are my best question-answerers, have provided some key point for my experiments and saved me from many booby traps. I could enjoy productive discussion with Giulio Ragazzon in last 6 months, who made me change the prejudice about Italian. Although

---

their research topics were far from mine, Hiroki Arazoe and Yuki Omata always responded to my request kindly and provided many favor for using instruments. And I want to thank Atsuko Nihonyanagi for synthetic support.

In addition to our group member, there are more people who have contributed to this thesis. Above all, the past and present members of Aida Laboratory pointed out missing points and gave valuable comment. I really appreciate not only their effort for my research but also consideration for a foreign student. More particularly, I feel deep appreciation to senior Korea students such as Dr. Joonil Cho, Dr. Jay Jeongho Lee, Dr. Younsoo Kim, who support to adapt research life in Japan quickly by introducing valuable information and encouraging me during my Ph.D course. Also, I received many scientific advices and administrative helps from Kohei Sato, Takahiro Fukino, Noriyuki Uchida, Michio Matsumoto, Hiroshi Yamagishi, Yoshiki Shibuya and Yusuke Saito.

Although they are not directly involved in my research, I ensure that I got a lot of supports and encouragements from Professor Myongsoo Lee, Professor Zhegang Huang, Professor Bohm-Jung Yang, Dr. Yongju Kim and Hyeokyoung Choi. Also, I want to thank the group members of Korean chemists in the University of Tokyo for sharing their experiences and thoughts. Additionally, I will never forget the good memories with AGIT family; Siyoong Seo, Shinhye Park, Misun Hong and Jiheong Kang. I hope that all of them get a great success as a global research leader.

I also thank the Fellowship of Japan Society for the Promotion of Science (JSPS) for Young Scientists for financial support.

Finally, I would like to express profound gratitude for my family. Although I've not explained to them what I now work and consider in all those years at the lab,

they have always supported me and prayed for my happiness unconditionally.

Taehoon Kim

A handwritten signature in black ink, appearing to read 'Taehoon Kim', with a stylized, cursive script.

*Aida Laboratory*

*Department of Chemistry and Biotechnology*

*School of Engineering*

*The University of Tokyo*

*February 2016*